공학박사학위논문

디젤 엔진의 성능과 배기 최적화를 위한 연소 디자인 연구

Design of Combustion for Optimized Performance and Emissions in a Diesel Engine

2021 년 8 월

서울대학교 대학원

기계공학부

이 용 주

디젤 엔진의 성능과 배기 최적화를 위한 연소 디자인 연구

Design of Combustion for Optimized Performance and Emissions in a Diesel Engine

지도교수 민 경 덕

이 논문을 공학박사 학위논문으로 제출함

2021 년 4 월

서울대학교 대학원

기계항공공학부

이 용 주

이용주의 공학박사 학위논문을 인준함

2021 년 6 월

위 원 장 : 송 한 호

부위원장 : 민 경 덕

위 원 : 도 형 록

위 원 : 황 원 태

위 원 : 최 회 명

Acknowledgement

The work of my Ph. D thesis would not be happened without the helps and advices of many people.

First and foremost, I would like to express my appreciation and respect to my advisor, Professor Kyoungdoug Min. During the graduate course, my knowledge and the attitude of a researcher grew with his advices. His advice and guidance in this project helped solve many problems and difficulties.

I would like to special thanks to colleagues who offered valuable assistance and memories of friendship. Youngbok Lee and Seungil Lee have been together most of the time, helping me with discussion, and being my good colleagues and friends. Dr. Seunghyun Lee was my good mentor and gave basic knowledge. Also, I'd like to thanks to all of my graduate schoolmates for unforgettably joyful lab life.

I would like to present my deepest respect and gratitude to my parents, Seoksang Lee and Gwisuk Kim, for their sacrifice and endless love. My brother and his wife, Minjoo Lee and Hyekyoung Sim, were my emotional anchor. And my precious nephews, Gunhoo Lee and Jian Lee, were my driving force to overcome any difficulties.

Abstract

Design of Combustion for Optimized Performance and Emissions in a Diesel Engine

Yongjoo Lee

Department of Mechanical Engineering
The Graduate School
Seoul National University

Recently, the researches for improving the performance of the internal combustion engines have been focused on the respect of thermal efficiency, emissions, noise and vibration. The thermal efficiency is related with decreasing carbon dioxide (CO_2) emission that has affected global warming. Also, nitrogen oxides (NOx) and soot emissions from diesel combustion are harmful for human. The harmfulness of exhaust gases has motivated governments of many countries to make vehicle emission regulations stringent. Recently, real-driving emissions (RDE) regulation was enforced, considering the discrepancy between the certified values in laboratory and the actual emission levels on the road. Noise pollution is also important in the perspective of human and public health problem. The combustion noise from the engine depends on the cylinder pressure excitation, which is affected by the engine parameters and combustion characteristics. Proper injection strategies or combustion shape can be optimized to meet the desired combustion noise level.

The engine development process takes a lot of effort and time to optimize each performance of thermal efficiency, emissions and noise. To achieve desired optimal performance, many trials and errors and experiments are required to optimize combustion and engine operating parameters. As an optimization tool, computational fluid dynamics (CFD) simulation needs substantial calculation cost. Thus, it is important to develop 0-D combustion optimization methodology that has low calculation cost. Previously studied 0-D combustion optimization methods have been optimized the injection strategy or engine parameters. The resulting combustion comes out of a narrow range and it is similar to the methodology of optimizing variables experimentally in terms of diversity of combustion. In this study, the combustion design methodology was developed that used the desired performance as input and derived combustion and combustion parameters as outputs in a diesel engine.

The thermal efficiency, noise and emissions were needed to be calculated by 0-D combustion simulation for the combustion optimization. As a one of emission models, the 0-D soot model was developed through cooperative research with Youngbok Lee. The engine test that evaluated the soot emission by EGR rate, intake and coolant temperature was conducted to develop the 0-D soot model and acquire initial conditions for combustion design. The soot formation model was based on the simplified spray model to calculate the equivalence ratio at lift-off length. The equivalence ratio at the lift-off length was used as a one of the main factor for the soot formation model. In the combustion design process, IMEP represented the thermal efficiency. For the combustion noise evaluation, the combustion noise index was used. The 0-D NOx model from previous research was applied to estimate NOx emission.

In the combustion design methodology, the initial parameters for constructing in-cylinder pressure were intake pressure, lambda and the mass

faction burned. The MFB was determined by using Wiebe function and polynomial function as new approach to combustion phase. The mass of in-cylinder air and EGR rate were calculated from intake pressure, temperature, lambda, that were determined as initial conditions, and the chemical reaction equation. Compression and expansion strokes were assumed as polytropic process. The gas compositions during the combustion were calculated for calculation of polytropic index and other thermodynamic parameters. The in-cylinder pressure was calculated by the heat release rate and polytropic process with the estimated polytropic index. In the optimization process, the optimization algorithms used in the combustion design method were a minimum of constrained nonlinear multivariable function (interior-point) and particle swarm optimization. MATLAB was used as the optimization tool. The boundary conditions and constraints were determined for efficient iteration in optimization process. The base form of objective function for optimization allowed to find specific combustion of desired performance that was used as input. The objective functions for various design concepts were used in maximizing target performance.

The results of combustion design were investigated by objective function and MFB function type at various operation point. The combustion design method was applied to WLTP by designing the steady points in WLTP operation region. The fuel consumption during WLTP decreased by 4.6% compared to experimental result The NOx and soot emissions could be reduced by 44.7% and 60.7%. In this study, the 0-D combustion simulation and optimization method that derived the combustion of desired performance were provided. This research can contribute to provide combustion shape with desired or optimized performance in combination with thermodynamic conditions, suggesting the development process different from existing research methods of engine and combustion strategies for target combustion.

Keywords: Combustion design method, Engine combustion optimization, 0-D combustion simulation, Spray model, Diesel engine

Student Number: 2015-20744

Contents

List of Figures

List of Tables

Nomenclature

Acronyms

BDC	bottom dead center
BMEP	brake mean effective pressure
BSFC	brake specific fuel consumption
CFD	computational fluid dynamics
CI	compression ignition
CKPS	crank position sensor
CNI	combustion noise index
CO	carbon monoxide
CO_2	carbon dioxide
dBA	A-weighted decibels
DOE	design of experiments
DPF	diesel particulate filter
ECB	EGR cooler bypass
ECN	engine combustion network
ECU	engine control unit
EGR	exhaust gas recirculation
EMS	engine management system
EOC	end of combustion
FFT	fast Fourier transform
FSN	filtered smoke number
GA	genetic algorithm
HC	hydrocarbons
HP	high pressure
HRR	heat release rate

IMEP	indicated mean effective pressure
LHV	lower heating value
LNT	lean NOx traps
LOL	lift-off length
LP	low pressure
MFB	mass fraction burned
MPRR	maximum pressure rise rate
NOx	nitrogen oxides
NVH	noise and vibration, harshness
PM	particulate matter
RDE	real-driving emissions
SCR	selective catalytic reduction
SI	spark ignition
SOC	start of combustion
SOI	start of injection
TDC	top dead center
TWC	three-way catalyst
WLTC	Worldwide Harmonized Light vehicle Test Cycle

Chapter 1. Introduction

1.1 Background

In these days, research to improve the performance of the internal combustion engines has been focused on thermal efficiency, emissions, noise and vibration. The thermal efficiency is an essential component of the engine performance and related with decreasing carbon dioxide (CO_2) emission that has affected global warming. Countries worldwide are making efforts to reduce it by tightening the CO_2 regulations. The spark ignition (SI) engines use a three-way catalyst (TWC) to reduce exhaust emissions to effectively reduce nitrogen oxides (NOx), carbon monoxide (CO) and hydrocarbons (HC). But SI engines have lower thermal efficiency than compression ignition (CI) engines. CI engines have higher thermal efficiency than SI engines due to their high compression ratio. Major issue of diesel engines is the emission of NOx and particulate matter (PM) due to their diffusion combustion characteristics. NOx formed in the high-temperature regions during the combustion process and PM are harmful for human and even threatens their lives [1-3], which have motivated governments of many countries to make vehicle emission regulations stringent [4, 5]. Recently, real-driving emissions (RDE) regulation was enforced, considering the discrepancy between the certified values in laboratory and the actual emission levels on the road [6-13]. Figure 1.1.1 shows the worldwide timeline of emission standards [14].

To satisfy strict emission standards, diesel vehicles need several aftertreatment systems. A diesel particulate filter (DPF) is an essential aftertreatment system, which effectively decreases PM and easily maintain performance by a regeneration stage. Lean NOx trap (LNT) and selective catalytic reduction (SCR) are the main systems for diesel engines to reduce NOx. LNT

under lean engine operation conditions traps NOx as nitrates and nitrites [15]. To maintain the NOx conversion efficiency of LNT, de-NOx regeneration, which releases bound NOx, is necessary [16-18]. Vehicle manufacturers use models to control the fuel injection strategy for de-NOx regeneration, and it is important to calibrate the timing of de-NOx regeneration in the engine management system [17, 19]. Ko et al. [20, 21] studied the characteristics of NOx emission and aftertreatment system of LNT-equipped diesel vehicles in laboratory tests and under real-driving condition. This study showed that NOx emission was affected by various factors, such as ambient temperature, regeneration of the LNT and the DPF, and traffic congestion. SCR with urea injection has been extensively used to reduce NOx emission because of its high NOx conversion efficiency; however, the chemical reaction of an SCR is affected by the gas temperature for activating the catalyst [22, 23]. Many efforts have been made to improve the SCR system by developing highly active catalysts at low temperature [24-26]. In addition, engine operation strategies to quickly reach and maintain catalyst activation temperature are closely related to the NOx conversion efficiency [27-29]. Although the use of aftertreatment systems to meet the emission regulations, development of advanced combustion strategy and engine control methods are needed to reduce raw emission because they increase production costs.

The regulation for the limits of noise from vehicle has been tightening. Although mandatory limits on noise emission from engines do not exist, the regulation indirectly forces to reduce the noise from engines [30]. Noise pollution is also important in the perspective of human and public health problem. The exposure to noise in long-term and regular period can cause various harm effects on human body such as annoyance, heart disease, hearing impairment and sleep disturbance [31-33]. Also, the noise in high magnitude induces permanent damage to human's ear [34, 35]. Since internal combustion engines generate power based on combustion and rotational motion, noise and vibration are generated, especially

for diesel engines. Manufacturers have made an effort to satisfy emission regulations while investing heavily in developing technologies that will improve fuel economy, noise and vibration for consumers' choice. Noise and vibration from diesel engines are closely related to the combustion characteristics within the cylinders. In the premixed combustion phase of compression ignition, the combustion steeply increases the in-cylinder pressure and sometimes produces a pressure wave. The noise originated from the excitation of structure-borne by pressure wave can be classified to the direct combustion noise. Figure 1.1.2 shows the classification of engine noise and excitation model [36]. The cylinder pressure excitation spectrum depends on various parameters of engine operation and combustion characteristics. Figure 1.1.3 shows excitation spectrum for combustion process [37]. Various engine variables and combustion characteristics cause changes in combustion shape, so proper injection strategies or combustion shape can be optimized to meet the desired combustion noise level.

The engine development process takes a lot of effort and time to optimize each performance of thermal efficiency, exhaust emissions, and noise. To achieve desired optimal performance and combustion shape, many experiments are required to optimize not only engine operating variables also engine hardware design. In the experimental process for optimization, design of experiments (DOE) method are used to vary the condition of combustion environments such as injection strategies, engine operating variables, exhaust gas recirculation (EGR) rate and so on to construct model that estimate each performance for deriving optimal combustion. Combustion simulations via computational fluid dynamics (CFD) are also being studied to explore combustion characteristics changes and conditions that are difficult to measure and acquire through the experiment process. Analysis using CFD simulation can provide thermal efficiency, heat loss and generation of emissions considering chemistry mechanisms through combustion process analyze at given hardware, injection strategies, boundary

conditions, etc. However, CFD simulation needs a lot of costs because it is based on 3D mesh grid calculation and considers fluid dynamics with various turbulence model and phenomenological emission models using detailed chemical mechanisms. Due to these characteristics, CFD analysis is important when the target components analysis is required under certain conditions, but are not cost-effective to optimize combustion and engine operating variables at specified load.

0-D simulation, which calculates and predicts combustion characteristics with simple formulas and factors, has the advantage of lower cost and faster computation speed compared to 3D CFD simulation, but are relatively inaccurate in detailed physical and chemical mechanisms. Even if it is relatively inaccurate than phenomenological models, using semi-empirical 0-D models that reflect the combustion characteristics well can significantly reduce the cost of the engine development process and simulate optimized combustion modes from various combustion shapes. Wiebe and other researchers developed non-dimensional analytical combustion model that is known as Wiebe function based on several chemical reaction equations [38]. Wiebe function that expresses mass burn rate can be used to optimize combustion with adequate 0-D model. The methodology that can optimize combustion with target performance is expected to contribute the cost reduction and development of advanced combustion shape in the engine development process.

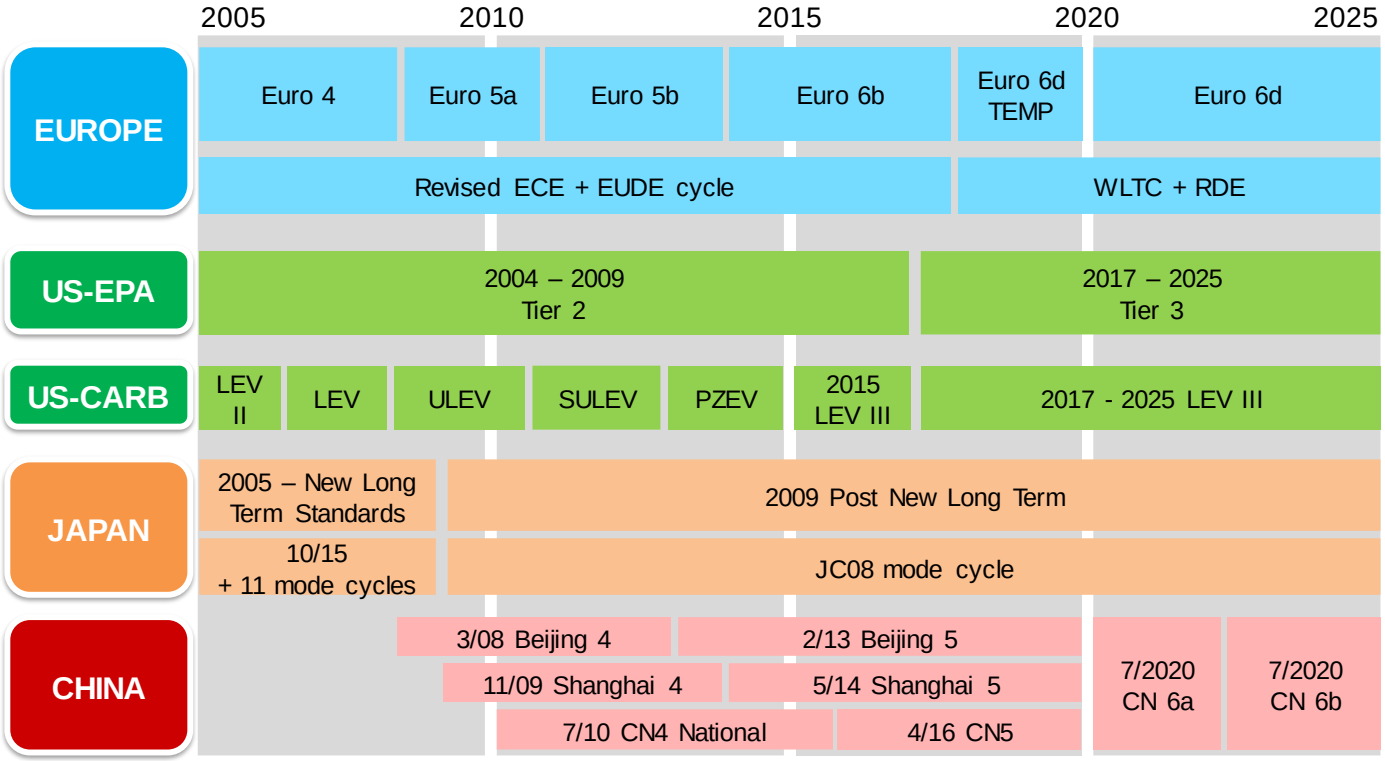

Figure 1.1.1 Global Emission standards timeline [14]

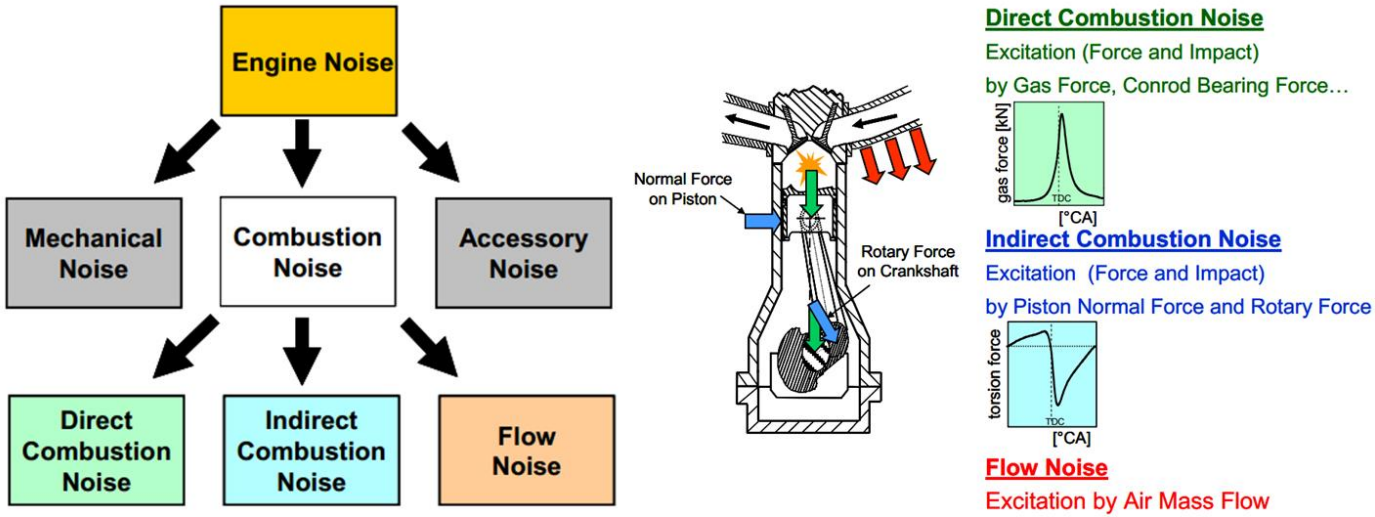

Figure 1.1.2 Engine noise contributions and excitation model [36]

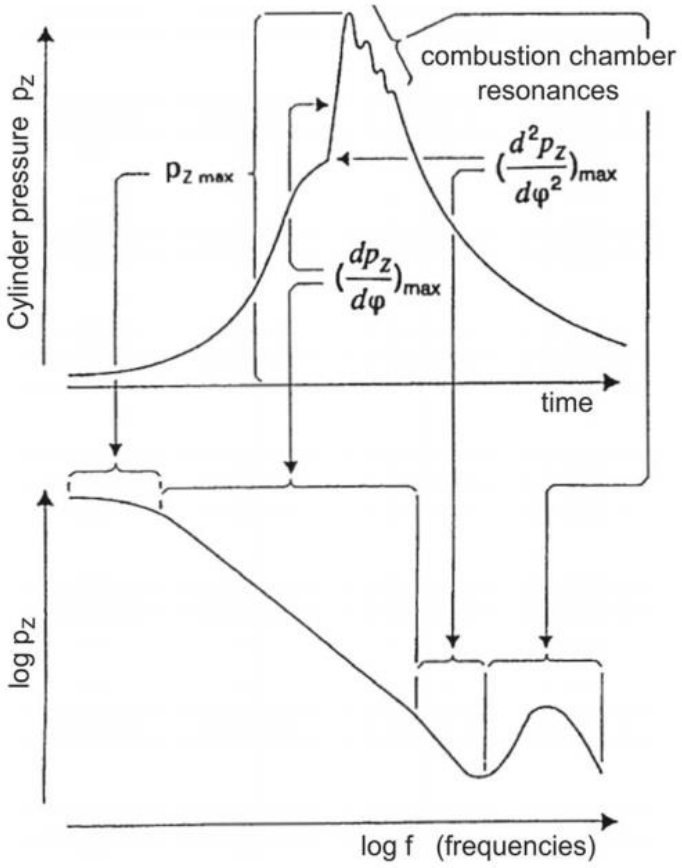

Figure 1.1.3 Cylinder pressure excitation spectrum [37]

1.2 Literature Review

1.2.1 Combustion noise model

To accurately measure the engine noise, the laboratory must be equipped with large-scale measuring equipment and facilities such as an anechoic room and microphones. Furthermore, the noise results from engine or vehicle dynamometer experiments include a large amount of ambient noise, such as the operating sound of the dynamometer, the high frequency noise of the fuel and cooling water pump, and the air flow noise of the air conditioning facility, in addition to the combustion noise. The exterior noise sources are hard to separate with combustion noise and some of them change with the engine operating range. To replace direct noise measurement, the cylinder pressure can be used to estimate the level of combustion noise in the engine experiment. The cylinder pressure is essential to the excitation characteristics of direct combustion noise. Among the several combustion characteristics, the maximum pressure rise rate (MPRR) has direct relationship with combustion noise. There have been many researches that use the MPRR as the representation of combustion noise level [39-43]. However, even if the MPRR is directly related to combustion noise, the accuracy may decrease depending on the shape of combustion pressure curve. The cylinder pressure is transformed from the time range into the frequency domain in order to evaluate the cylinder pressure acoustically. This process gives the excitation spectrum. Commonly, the frequency range is determined from the pressure increase degree or increase rate and it decides the A-weighted level of the combustion noise. Depending on the type of engine and combustion, a model can be established to estimate the noise level from various frequency range.

Beidl and Stucklschwaiger [44] developed the single number index that could be used in s a similar with A-weighted decibels (dBA) scale. The developed index, the Annoyance Index, contains four objective parameters that are loudness, periodicity, sharpness and impulsiveness. Among the four objective parameters, the loudness is correlated with the A-weighted sound pressure level. The authors developed and evaluated the index by combining not only sound pressure levels but also considerations for sound quality. While the assessment of individual sound quality is critical to the overall noise and vibration, harshness (NVH) performance of the vehicle, it is better to focus on direct combustion noise level that is calculated by in-cylinder pressure in the process of combustion design rather than the subjective sound quality index.

Payri et al. [45] introduced the in-cylinder pressure method and validated the method with combustion noise analysis. This study proposed to decompose the in-cylinder pressure to pseudo-motored, combustion and resonance excitation, and each component was analyzed with sound pressure level. The authors focused on the main source of noise in diesel engines and suggested guidelines for combustion noise improvement from the proposed analysis. The signal processing for calculating the pressure noise level starts from the power spectrum of the signal by the ensemble average of the square magnitude of the discrete frequency spectra. The equation (1.2.1) shows the power spectrum from the 400 pressure signal in 100 continuous cycles where $P_i^*(f)$ and $P_i^*(f)$ are the instantaneous frequency components and their complex conjugates of the frequency spectrum of the *i*th time signal. The power spectrum through the average of the harmonic amplitudes and overall pressure levels estimated from the power spectrum in the frequency range between f_1 and f_N are shown in the equations (1.2.2) and (1.2.3) where N is the number of harmonics between f_1 and f_N and p_0=20μPa. The structure of the equation (1.2.3) are most common form to use the Fast Fourier Transform (FFT) and the sum of the third octave band level of the in-cylinder

pressure. In this study, the results of the noise level from measurement were not presented and it was hard to validate noise estimation.

$$\mathrm{S_{pp}}(f) = \frac{1}{400}\sum_{i=1}^{400}[P_i^*(f)P_i(f)] \tag{1.2.1}$$

$$S_{overall} = \frac{1}{N}\sum_{f=f_1}^{f_N} S_{pp}(f) \tag{1.2.2}$$

$$L(\mathrm{dB}) = 10\log(\frac{\mathrm{S_{overall}}}{\mathrm{p_0^2}}) \tag{1.2.3}$$

Chiatti et al. [46] also studied about the engine noise emissions and analyzed to extract combustion related contribution. Similar to the equation (1.2.3), this study also calculated the noise index, combustion index, by the sum of the third octave band level of the in-cylinder pressure in the frequency range of 315 – 3150 Hz, which is expressed in the equation (1.2.4) where L_p is the third octave band level. The accuracy of the index was validated in the study and it showed the R-squared values from 0.897 to 0.924. However, the minimum speed of the validation area was 2000 rpm, which is high speed of the operating areas of Worldwide Harmonized Light vehicle Test Cycle (WLTC), and thus lacked applicability in a wider range.

$$\mathrm{CI} = 10\log(10^{\mathrm{L_p}\frac{315}{10}} + 10^{L_p\frac{400}{10}} + \cdots + 10^{L_p\frac{3150}{10}}) \tag{1.2.4}$$

1.2.2 NOx emission model

The NOx emission models are divided into phenomenological models that can be utilized for 3D CFD simulation and empirical models that can be used universally for engine control and diagnosis due to fast computational speed. Phenomenological models solve the equations and dynamics of turbulent flow motion and injection characteristics. During the combustion process, the chemical mechanisms are used to resolve combustion model and emission models. The complex characteristics of diesel combustion and emissions were described in many studies [47-49]. Several studies [50-55] gave basic concepts for NOx models that dividing the injection spray to fuel packages, ignition and combustion, and the Zeldovich mechanism which is the basis for NO formation kinetics. Empirical models are fitted by engine parameters and combustion characteristics to estimate NOx emission. Although the accuracy is insufficient compared to phenomenological model due to the lack of considering detailed mechanisms, the empirical model has advantage of low computational cost and, furthermore, the accuracy can be improved when utilizing physical based factors. The thermal mechanism that described NO formation was modeled and expressed in the equations (1.2.5) to (1.2.7). The thermal NO formation rate can be expressed under the equilibrium assumption. A large number of the NOx models have been studied based on Zeldovich mechanism [56-63].

$$N_2 + O \leftrightarrow NO + N \tag{1.2.5}$$

$$N + O_2 \leftrightarrow NO + O \tag{1.2.6}$$

$$N + OH \leftrightarrow NO + H \tag{1.2.7}$$

Andersson et al. [56] introduced a fast physically-based NOx model to predict the NOx emissions using single injections. This study considered injection characteristics, ignition delay and swirl. The model used two zone combustion model to calculate the adiabatic flame temperature and gas composition, and the table for the equilibrium temperature and concentration were used. In other paper [57], the results for transient conditions were presented and a 10.% mean relative error was shown. It showed god accuracy but this study did not consider the effect of pilot injection in conventional diesel combustion. Arregle et al.[58] developed the NOx model and sub-model for the adiabatic flame temperature. The adiabatic flame temperature was obtained as a fitted form from the combustion reaction in equilibrium conditions. Also, the heat release rate (HRR) from the experimental data was used to calculate the NOx formation mass. But other parameters such as swirl and spray characteristics were not considered. Scappin et al. [59] derived the 0-D NOx emission model for marine low speed diesel engines. A two zone combustion model and energy balance were applied using the extended Zeldovich mechanism. Asprion et al. [60] also presented the physics-based NOx model for numerical optimal control and model-based engine calibration. Querel et al. [61, 62] developed the mean-value NOx model by estimating the burned gas temperature and semi-physical NOx formation rate for diesel engine control. d'Ambrosio et al. [64] introduced the fast control-oriented semi-empirical model for the calculation of NOx emissions under steady-state and transient conditions. The model considered the maximum in-cylinder burned gas temperature by using three-zone real-time thermodynamic model developed by the authors [65].

The above studies developed semi-empirical 0-D NOx models with good accuracy by supplementing the physics-based principles. However, models did not consider swirl that has a significant effect on combustion speed and local equivalence ratio, or used a fixed value of polytropic index without considering in-cylinder gas conditions. Lee et al. [66, 67] introduced the semi-empirical model

with the consideration of swirl factor and two-zone combustion model for the adiabatic flame temperature. The 0-D model of polytropic index that can be used in pressure construction process by various intake temperature, pressure and in-cylinder gas composition was developed by Lee and Min 68. The estimated cylinder pressure variation at the end of the compression stroke is shown in Figure 1.2.1 [68].

1.2.3 Soot emission model

The soot emission is particularly difficult to predict by reflecting the exact chemical mechanisms because there are many chemical reactions involved in soot formation process and principle, as well as various paths of soot formation and oxidation. Due to the complex principle of soot formation, the studies [69-72] using 3D CFD simulation mainly used the phenomenological models that address and compute the soot emission with detailed chemical mechanisms. Tao et al. [72] developed soot model for a modern diesel engine over a wide range of engine conditions. The authors established the model by dividing the process of soot formation into the nine step: acetylene formation, precursor species formation, particle coagulation and so on. As mentioned in the NOx model, these phenomenological models consider detailed principles based on chemical reaction equations, which are highly accurate but have high computational costs. Empirical models, on the other hand, are capable of real-time computation due to low computational cost and high speed, and can be applied for engine control and diagnosis.

In order to have a physical basis for empirical soot model, it is important to reflect the characteristics of the spray. The in-cylinder temperature, pressure, gas

composition, and injection pressure change the spray characteristics such as penetration length and atomization in fuel injection sequence, and local equivalence ratio has a key effect on soot generation. The information related to the spray characteristics improve the physical basis of the model. There have been many researches [73-79] on numerical and experimental analysis for spray characteristics. Figure 1.2.2 [74] shows a schematic showing the conceptual model of diesel combustion. The author conceptually explained the NOx and soot formation region, and soot oxidation region. Naber and Sibers [73] analyzed the effects of gas density and vaporization on penetration length of diesel sprays. The authors investigated the characteristic penetration time and length scales by using previous research [80]. In this paper, the equation (1.2.8) that shows the penetration correlation was introduced where $\tilde{t}$ and $\tilde{S}$ are the non-dimensional time and penetration distance. Also, the dependence of penetration length on orifice diameter, time, injection pressure and ambient gas density and pressure were shown in the equation (1.2.9) where C_v and C_a are the orifice velocity contraction coefficient and the area contraction coefficient, a is constant with a value of 0.66, θ is cone angle of the spray, P_f and P_a are pressure of fuel and ambient gas, ρ_a is density of ambient gas, d is the diameter of orifice exit. The equation (1.2.9) gave the fundamental basis for the correlation between fuel injection parameters and penetration length.

$$\tilde{t} = \frac{\tilde{S}}{2} + \frac{\tilde{S}}{4}\sqrt{1 + 16\tilde{S}^2} + \frac{1}{16}\ln(4\tilde{S} + \sqrt{1 + 16\tilde{S}^2}) \tag{1.2.8}$$

$$S = \sqrt{\frac{C_v \cdot \sqrt{2C_a}}{a \cdot tan(\theta/2)}} \cdot \sqrt{\frac{\sqrt{(P_f - P_a)}}{\rho_a} \cdot d \cdot t} \tag{1.2.9}$$

Siebers [75, 81] investigated the liquid-phase fuel penetration length and used the scaling law to provide a fundamental baseline on liquid fuel penetration length and vaporization in diesel sprays. Author analyzed the trend of the liquid length in the experimental with respect to injection parameter. The relationship for the axial variation of the fuel ($\dot{m}_f$) and ambient gas ($\dot{m}_a$) mass flow is shown in the equation (1.2.10) from the spray mass and momentum balance equations where $\tilde{x}$ is the axial distance in the spray normalized by the spray penetration length scale (x^+) [73]. From the research [75], the scaling law for liquid length was developed and shown in the equation (1.2.11), where *a* and *b* are the constant 0.66 and 0.25, ρ_f is density of fuel, and B is the ratio of the fuel and ambient gas mass flow rates at the end of liquid length.

$$\frac{\dot{m}_f(x)}{\dot{m}_a(x)} = \frac{2}{\sqrt{1 + 16 \cdot \tilde{x}^2} - 1} \tag{1.2.10}$$

$$Liquid\ \ length = \frac{b}{a} \cdot \sqrt{\frac{\rho_f}{\rho_a}} \cdot \frac{\sqrt{C_a} \cdot d}{tan(\theta/2)} \sqrt{\left(\frac{2}{B} + 1\right)^2 - 1} \tag{1.2.11}$$

The flame lift-off length of diesel fuel jets, the distance from the injector tip to stabilized reaction zone, is one of important injection characteristics. The lift-off length is determined from the condition of air-fuel mixture, so it can represent the degree of air-fuel mixing. Several studies have investigated the lift-off length through experiments and simulations [76-78, 82-86]. Siebers et al. [77, 84] showed the correlation between the lift-off length and various parameters in the equation (1.2.12) where C is scale constant, U is injection velocity, T_a is the temperature of ambient gas and Z_{st} is stoichiometric mixture fraction. Although it was suggested that flame propagation played the dominant role in the flame lift-off,

the equation (1.2.12) did not use the laminar flame speed for lift-off length estimation because there was not experimental data at lower temperature conditions. By using the Arrhenius equation and experimental results, the fitted equation for residence time for the lift-off length scaling was suggested by Pickett et al. [78]. Siebers [87] had also suggested the equations (1.2.13) based on a scaling law for lift-off length[83] where, D_{T} is thermal diffusivity and S_L is laminar flame speed. Peters [83] developed a scaling law for lift-off length based on the flame stabilization concept. Pickett and Siebers [85] shown that the equivalence ratio at the lift-off length was related to soot formation. Figure 1.2.3 [85] shows the experimental result at the constant volume chamber and it shows a good relationship between the soot density and the equivalence ratio at the lift-off length . It is confirmed that he lift-off length is a significant factor in soot formation.

$$\text{Lift}-\text{off length(H)} = \mathrm{C}\cdot T_a^{-3.74}\rho_a^{-0.85}d^{0.34}\cdot U\cdot Z_{st}^{-1} \tag{1.2.12}$$

$$\text{Lift}-\text{off length} = 0.2\cdot\text{Liquid length} + \mathrm{C}\cdot\frac{U_0\cdot Z_{st}\cdot D_T}{S_L^2(Z_{st})\cdot tan(\theta/2)} \tag{1.2.13}$$

Hiroyasu et al. developed a soot model [52, 88] based on the Arrhenius form and calculated by 1-D simulation. The authors used a multi-zone model which considered the spray behavior. The model was consisted with soot formation and oxidation model expressed in the equations (1.2.14) and (1.2.15), where m_s, $m_{s,f}$ and $m_{s,o}$ are the mass of the total soot, the formed soot and oxidized soot, A_f and A_o are the constants, m_f is the mass of the injected fuel, p is the in-cylinder pressure, p_{O2} is the partial pressure of oxygen, and E_{sf} and E_{so} are the activation energy terms of soot formation and oxidation) each had activation energy term for soot formation and oxidation [88]. As the soot oxidation model,

Nagle and Strickland-Constable [89, 90] investigated the oxidation rate of carbon in temperature range of a 1000 – 2400℃. The authors divided oxygen reaction zones to two sites A and B by correlation between chemical reaction equations and it is expressed in equation (1.2.15) where the x is the fraction of the A type site surface, p_{o_2} is oxygen partial pressure, and k_A, k_B, k_T, k_Z are the rate constants from the experimental results [89, 90]. The soot oxidation model has been used to various research about soot model [91-93].

$$\frac{dm_{s,f}}{dt} = A_f \cdot m_{fg} \cdot p^{0.5} \cdot \exp(-\frac{E_{sf}}{RT})$$

(1.2.14)

$$\frac{dm_{s,o}}{dt} = A_o \cdot m_s \cdot \frac{p_{O2}}{p} \cdot p^{1.8} \cdot exp(\frac{-E_{so}}{RT})$$

(1.2.15)

$$rate\ \ of\ \ reaction = \left(\frac{k_A p_{o_2}}{1 + k_Z p_{o_2}}\right) x + k_B p_{o_2}(1 - x)$$

(1.2.16)

Cebi et al. [94] developed the 0-D model for particulate matters in diesel engine by using combustion durations, characteristics time, valve timings and so on. The authors validated the model as an efficient tool for real-time particulate matters calculation. The advantage of the developed model was simple and fast to calculate in real-time, and it was easy to implement in vehicle [95]. However, even if the combustion characteristics, combustion duration and characteristics time, are reflected, the accuracy of the model may be reduced in the wider engine operation area because it is difficult to reflect the physics basis of soot formation. Finesso et al. [96] used the more various parameters related with combustion

characteristics such as chemical heat release at the end of the main injection and the equivalence ratio of the spray at start of the main combustion. The authors proposed two types of the soot models that were used differently depending on the quantity of injected fuel. The parameters used in the model were identified by correlation with soot formation and oxidation. This semi-empirical model [96] reflected the physics and chemical principle for soot formation well, but the equivalence ratio at the start of the combustion (SOC) had weak point in soot formation mechanism. Since the lift-off length is the distance from the injector tip to the surface of the flame, it can be thought that the penetration length at the start of the combustion is the lift-off length. However, the lift-off length as a concept that occurs under the quasi-steady combustion conditions, so the penetration length at the start of the combustion and the lift-off length are exactly different parameters. It would be better to use the equivalence ratio at the lift-off length for more rigorous physical basis.

1.2.4 Combustion optimization

In optimization studies associated with engine combustion, the subjects to optimization mainly have hardware aspects such as piston shape, compression ratio and combustion chambers, and parameter aspects such as engine control parameter and combustion characteristics factors. The hardware optimization is performed to find optimal geometry for thermal efficiency gains, thermal loss reductions, or emission reduction by advanced combustion [97-99]. On the other hand, in terms of engine parameters, optimization is performed to control combustion by optimizing injection parameters, inlet pressure, EGR for optimal thermal efficiency and emission results.

Many studies of the engine optimization have carried out optimization through experimental investigation [100-104]. The experiments by changing each parameter inputs or DOE, which designs according to the plan with in the input area are used for modeling [100-102]. The model of target performance is established by control variables with acquired data and it is utilized for optimization. There were various optimization methods and algorithms for optimizing parameters or engine hardware. Millo et al. [103]used genetic algorithm for the engine calibration. Two cases for the calibration with a pre-existing and without data set. The pre-existing case was optimized with one target constraint and the rest target optimizing, and the data absent case used with single- and multi- objective optimization. Liu et al. [104] applied the artificial intelligence method with 3D simulation for the optimization of the performance and emissions characteristics of duel fuel engine.

The optimization with CFD simulations has been investigated [104-108] on boundary conditions and hardware to optimize performance as a result of calculations on input conditions. Although CFD simulation is expensive, optimization using CFD simulation has high accuracy because it calculates using detailed mechanisms in turbulent flow or chemical reactions for combustion and emissions. In addition, CFD simulation can also be useful for optimizing hardware, such as piston shape and compression ratio, because it can reflect changes in flow and combustion by geometry. Ge etl al. [105, 106] investigated on the optimization of the piston bowl geometry, spray targeting, and swirl ratio at three different load area. A non-dominated sorting genetic algorithm II was used. The new spray model was integrated and a characteristic-time combustion model was used for time savings. The model was validated with experiments results. In terms of the objective function, genetic algorithm (GA) used two types of objective function; single-objective and multi-objective function. Single-objective function has been used in several studies [109-112] by combining thermal efficiency, emissions and other

objectives. The single objective optimization minimizes a one objective function and it is important to determine the objective function and correlation between objectives. The equation (1.2.17) is the objective function in [111] with the expression about each performance objectives where the last term in denominator is brake-specific fuel consumption (BSFC). The multi-objective optimization searches the Pareto front that consists of several optimal points, so it is useful to find the optimal points while keeping diversity of the performances. Figure 1.2.4 shows the Pareto solutions from the study [105].The studies [105, 106, 113] about engine optimization using the multi-objective function have been existed to find optimal performance or parameters.

$$f(x) = \frac{1000}{\left(\frac{NOx}{NOx_0}\right)^2 + \left(\frac{PM}{PM_0}\right)^2 + \left(\frac{CO}{CO_0}\right)^2 + \left(\frac{HC}{HC_0}\right)^2 + \left(\frac{BSFC}{BSFC_0}\right)} \quad (1.2.17)$$

The optimization using 0-D models has low computational cost, so the calculation speed for combustion or emission result is fast. It is adequate for real-time engine control and global optimization in wide operating area. The 0-D models in optimization studies [114-117] for combustion and emission usually have been used with Wiebe function that expressed the mass fraction burned. The heat release rate is calculated from the mass fraction burned. The in-cylinder can be calculated with the initial conditions. Longanathan et al. [118] used the double Wiebe function model with the two-zone concept to get the heat release rate and the in-cylinder pressure. The authors developed several thermodynamic models such as heat transfer model and ignition delay model to predict accurate in-cylinder pressure. The fitted coefficients of Wiebe functions and the comparison with experimental results were presented. The stochastic combustion model was suggested by Liu et al. [119] to simulate the combustion processes with multi-stage

fuel injection. A 0-D spray model for propagation and spray-to-spray interaction was applied. Kamaltdinov et al. [114] investigated the method for determining parameters of double-Wiebe function for simulation of combustion process. The optimization studies based on 0-D sub-models have advantages of the flexibility of the combustion simulation and computational cost in optimization sequence. Smallbone et al. [107] developed virtual mapping method for optimized performance and emissions. Although the model developed as a tool for CFD simulation, optimization was performed with the use of 0-D models in the process. Shibata et al. [120] presented the optimized HRR shape and connecting rod crank radius ratio for low engine noise and high thermal efficiency. Simulation results on the parameter of Wiebe functions and the effect 50% of the mass fraction burned were presented. The authors in other study [116] introduced the optimization method of multiple heat releases by a genetic-based algorithm method. The three Wiebe functions were used to optimize the heat release shape for noise reduction with maintaining high thermal efficiency. Also, the authors investigated the optimum number of fuel injection and heat release rate shown in Figure 1.2.5. Franken and Mauss [121] introduced a methodology for predictive combustion simulation with 0-D models and optimized engine operating parameters such as injection parameters, air fuel ratio, speed and so on using multi objective simulated annealing optimization.

The above studies used the 0-D models that well-established spray and thermodynamic properties to optimized the desired performance. However, for prediction of NOx and soot emission, 3D simulation is often applied or dependent on experimental values. Because the boundary conditions for calculating exhaust emissions are limited through experiments or CFD simulations, the combustion also comes out of a narrow range. It is similar to the methodology of variable optimization by experiment in terms of diversity of combustion. If the target of the input is reversed over a wide range of combustion satisfying the desired

performance, rather than engine parameters or combustion factors, the optimization of the performance can be achieved for a wide range of combustion.

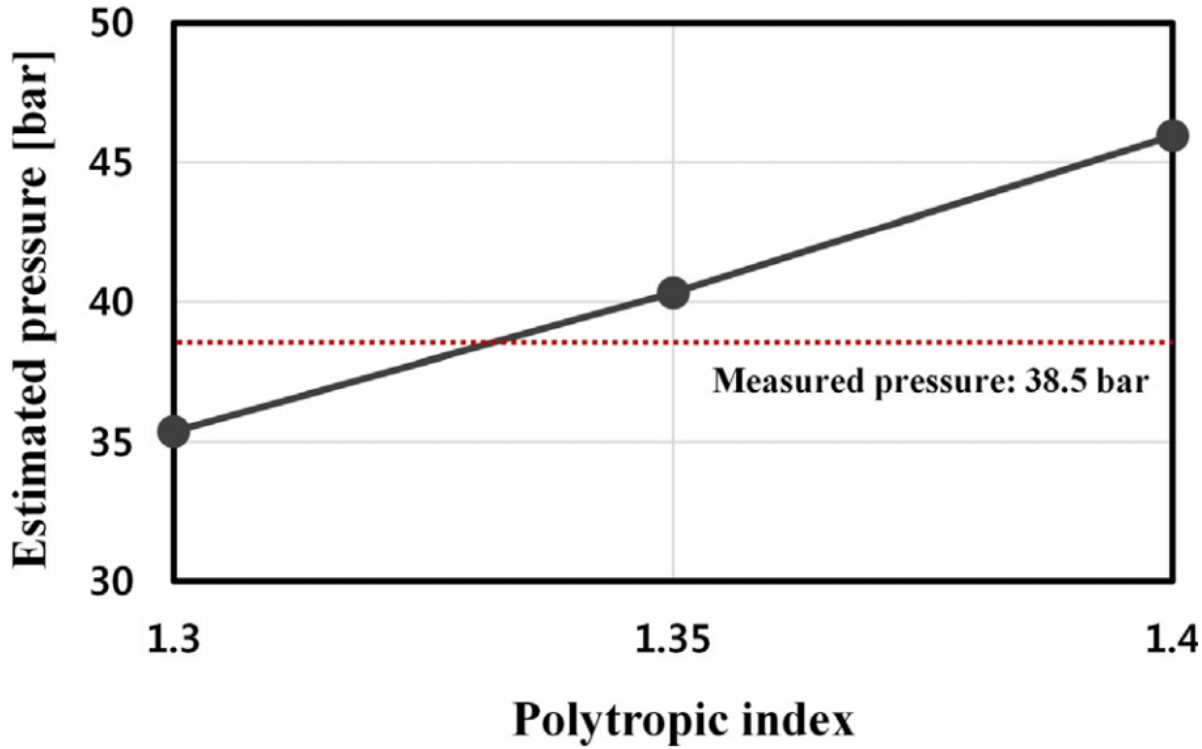

Figure 1.2.1 The estimated pressure range at the end of the compression stroke by polytropic index [68]

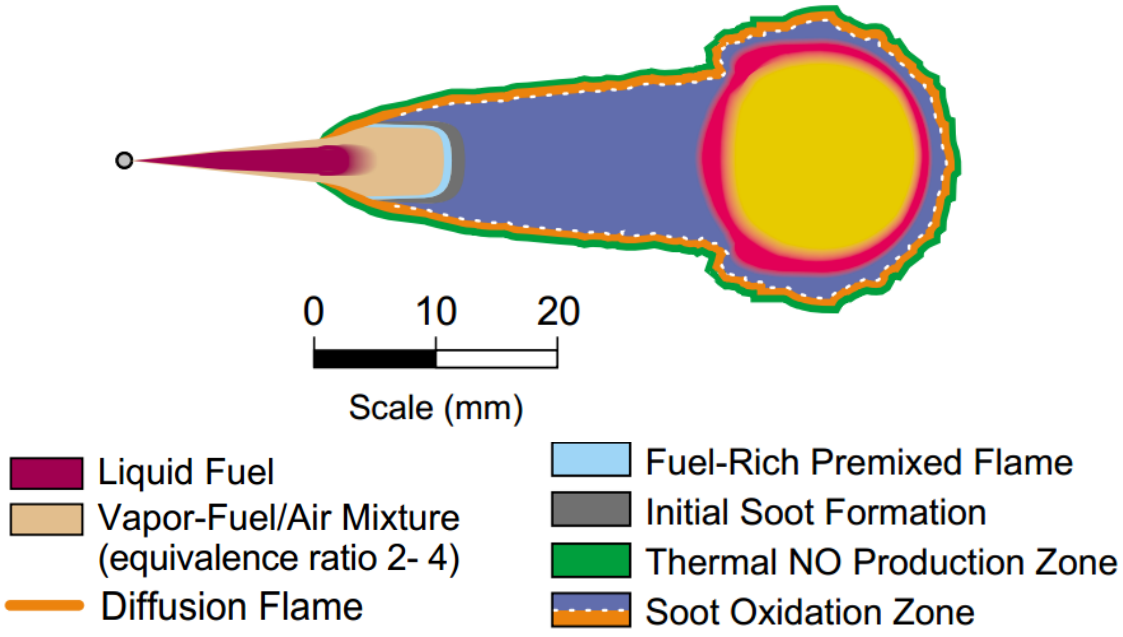

Figure 1.2.2 The conceptual model of direct injection diesel combustion [74]

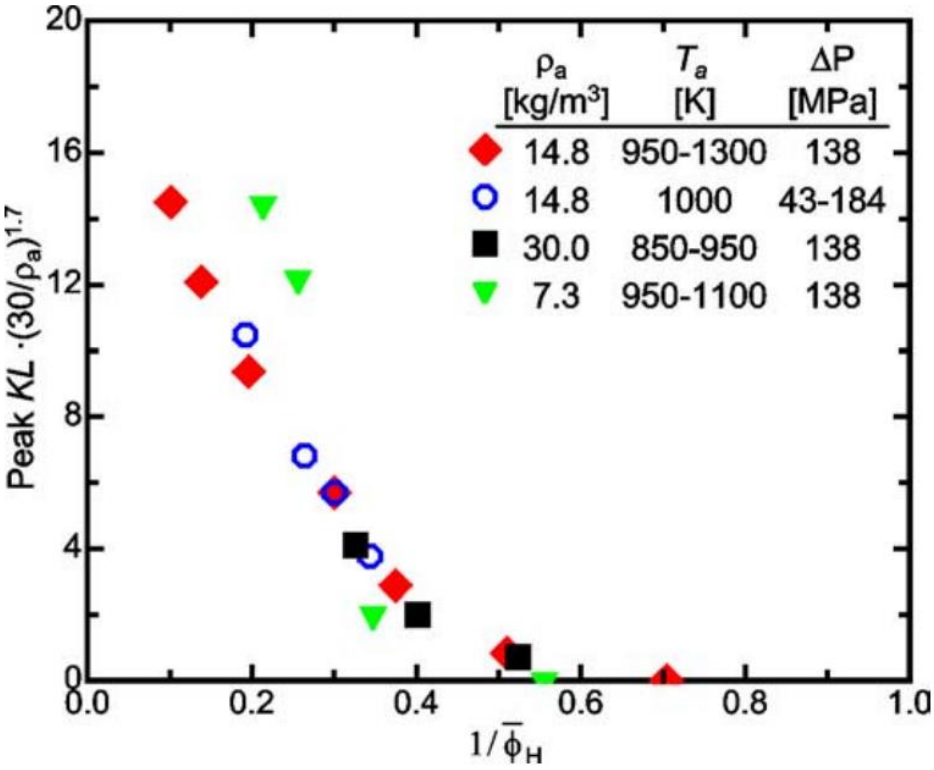

Figure 1.2.3 Peak KL values from the axial profiles of KL measured normalized by ambient gas density to the 1.7 power versus the inverse of the estimated cross-sectional average equivalence ratio at the lift off length [85]

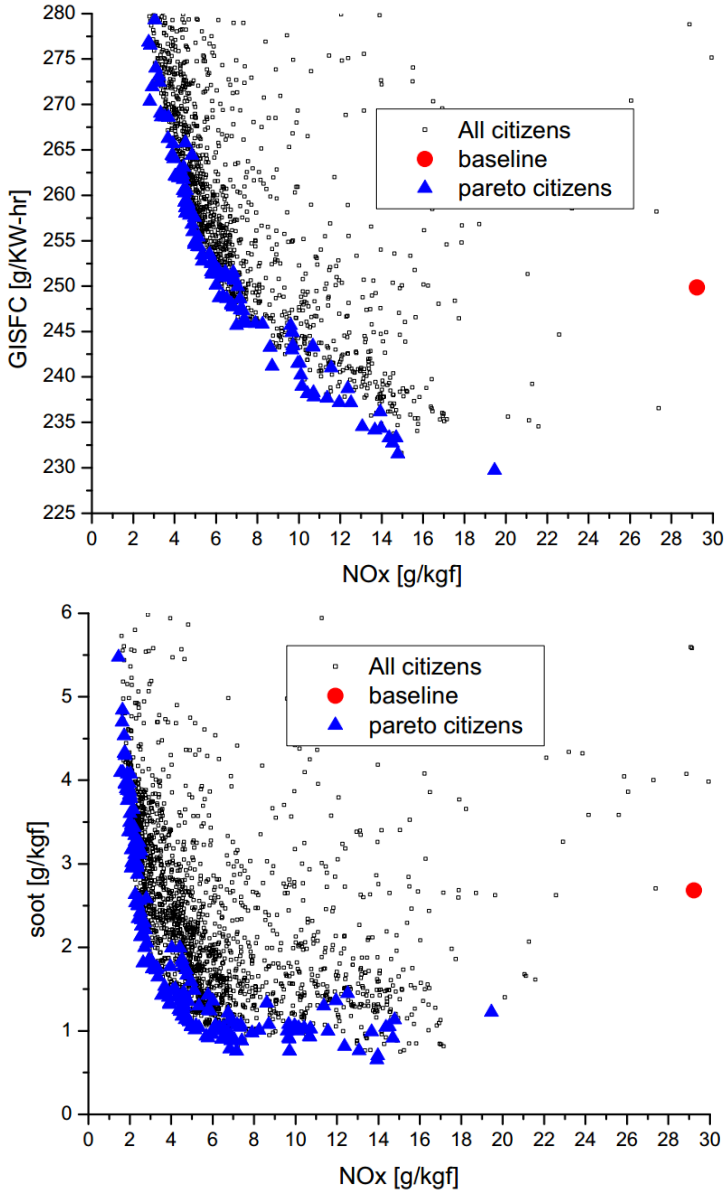

Figure 1.2.4 The Pareto solutions from optimization, all citizens and baseline

105

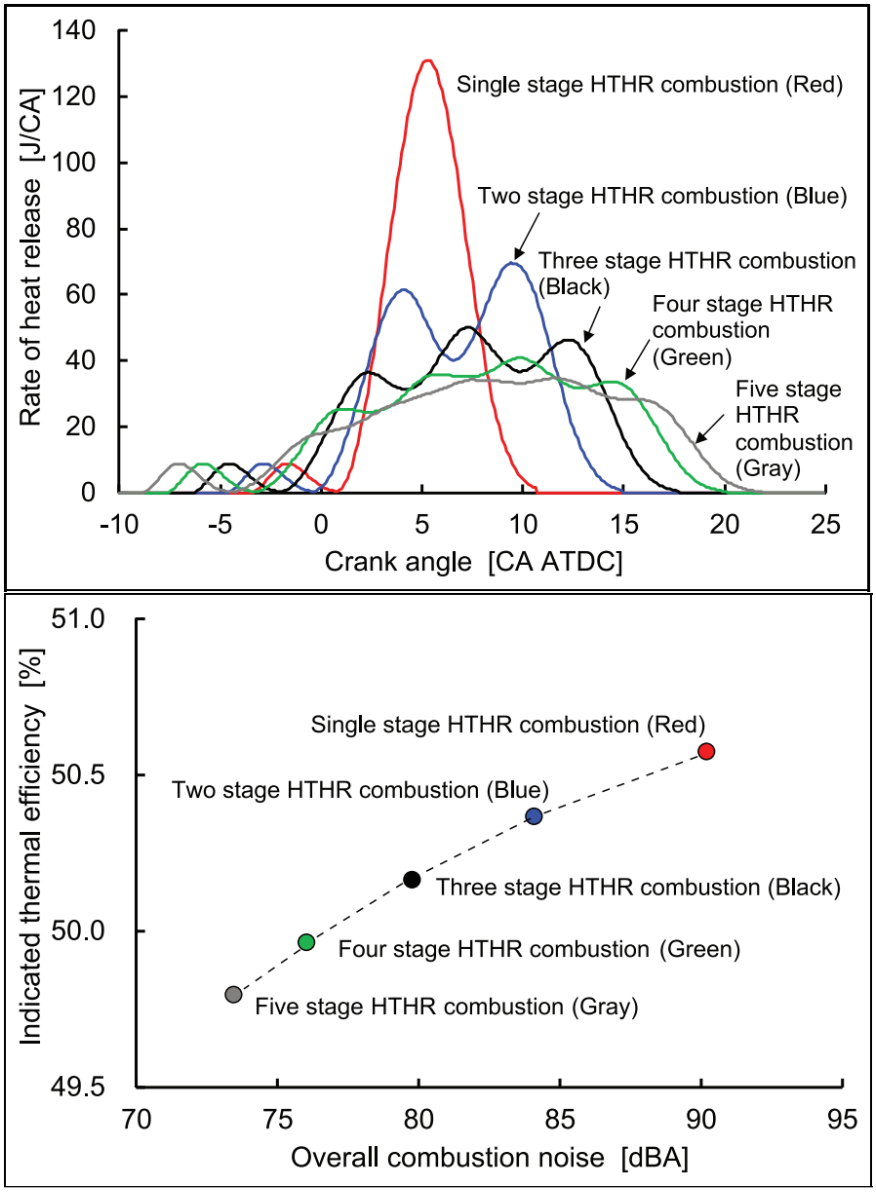

Figure 1.2.5 Optimum heat releases by the number of injection (top) and overall combustion noise versus indicated thermal efficiency (bottom) [116]

1.3 Research Objectives and Contributions

In this study, the combustion design method was developed that optimized combustion with desired performance. The 0-D models used in the research included the combustion noise index (CNI) [122] for combustion noise estimation, the NOx estimation model developed by Lee et al. [66, 67, 123]. The soot model was developed by using engine parameters and combustion characteristics through cooperative research with Youngbok Lee [124] in this research. The detailed key research objectives are as follow:

1. Development of the spray model and real-time 0-D soot model
   - The spray model for the equivalence ratio at lift-off length model
   - Numerical calculation of the lift-off length and validation with the experimental data
   - Establishing the soot model with the equivalence ratio at lift-off length and other combustion parameters (Youngbok Lee) [124]
2. Development of the combustion design method
   - Determining the mass fraction burned and thermodynamic in-cylinder conditions with the initial conditions
   - Constructing the combustion pressure with the polytropic index developed by Lee and Min [68].
   - Investigation of the objective function for optimization
   - Optimization algorithms by the determining method of the mass fraction burned
3. Analysis of the combustion design results in various optimization objectives
   - Introduction of the combustion design process for the target performance and the optimized performance.

- Investigation of the optimization results by the objective functions
- Analyzing the results of the combustion design method and optimization at the steady state points.

4. Application the combustion design method to transient case
   - The process for applying the combustion design method to wide engine operating area
   - The application results of the combustion design method on WLTP mode.

The combustion design method, which has not been previously studied, can propose combustion with optimized performance in the engine development process. Furthermore, it is possible to present a form of combustion pressure and heat release rate in the initial engine development phase or in the development of a new combustion concept. These processes can be simulated by using existing Wiebe function for optimization of well-known mass fraction burned, or by substituting the new form of the mass fraction burned function.

1.4 Structure of the Thesis

This study consists of seven main chapters and begins with an introduction to the study. In chapter 2, experimental apparatus and results are presented. The experimental data were used to validate 0-D models for emission results and initial conditions of optimization. The semi-physical 0-D soot models used in the combustion design method are introduced in chapter 3. The soot estimation model was developed with the spray model for the equivalence ratio at the lift-off length. The equivalence ratio at the lift-off length is the key factor of the soot formation model and the soot oxidation model is established with the Nagle and Strickland-

Constable model [89, 90] for oxidation rate. In chapter 6, other 0-D models for thermal efficiency, noise and NOx emission are introduced. In chapter 5, the processes of combustion design method are explained. This method can change the objective function according to the intent of the designer and the combustion shape and performances can be optimized by utilizing conventional Wiebe function or a new function to set the mass fraction burned. In the optimization using Wiebe function, the constrained nonlinear multivariable function was used as optimization algorithms and particle swarm optimization was used in the various mass fraction burned form. In chapter 6, the results of optimization are presented and the method is applied to transient condition. The processes for the application and the results are explained. This study is summarized and the conclusion is stated in chapter 7.

Chapter 2. Experimental Apparatus

2.1 Experimental Setup

2.1.1 Test engine

The test engine was a 2.2-liter 4-cylinder direct injection diesel engine with a compression ratio of 16. The detailed test engine specifications are shown in Table 2.1.1. The test engine used solenoid type injector and the maximum rail pressure of this injector was up to 2200 bar. The specifications of fuel injection system of the test engine are shown in Table 2.1.2. This engine equipped with a DPF, LNT, and SCR and it used a dosing control unit as well as engine control unit to control the urea injection and monitor NOx emission upstream and downstream of the SCR. In this research, the dosing control was deactivated in the experimental procedure because it could cause unexpected control of air mass flow for the fast heating of the catalyst.

2.1.2 Test cell and data acquisition systems

The engine torque and speed were controlled by AVL PUMA AC-dynamometer system control. The dynamometer can operate in transient conditions by controlling in speed/alpha or speed/torque mode. The temperature of coolant was kept at 85-90℃ and the temperature of downstream of intercooler was kept about 40℃ except intake air temperature swing cases. In the coolant temperature swing cases, the temperature of coolant was controlled by coolant

controller. The cylinder pressure was measured by a Kistler 6056A piezoelectric type pressure sensor and the specifications are shown in Table 2.1.3. After removing the glow plug in the engine, the pressure sensor was mounted via the glow plug adaptor to measure the pressure of 4 cylinders. The measured in-cylinder pressure was calculated to heat release rate with crank position sensor (CKPS) signal at the combustion analyzer and it was used to monitor the combustion phase and control the injection strategy. Also, the injection signal was logged together with the in-cylinder pressure data for the verification of injection control from the engine control unit (ECU). The specifications of the combustion analyzer are shown in Table 2.1.4. The communication with the engine management system (EMS) and engine control were performed by ETAS ES592 that provided ETK communication. The dynamometer data such as torque, speed, fuel rate, pressure and temperature transducer at each measurement points, and emission measurement data from MEXA-7100DEGR were gathered in dynamometer controller. The schematic experimental setup is shown in Figure 2.1.1. The mass of fuel flow rate was measured by OVAL coriolis type flow meter.

2.1.3 Emission measurement systems

The exhaust emission from the test engine was measured by several equipment. In the steady state test procedure, CO, CO2, O2, NOx, THC were measured by HORIBA MEXA-7100DEGR and the specifications are shown in Table 2.1.5. The sample points of MEXA-7100DEGR were positioned at the upstream of the LNT and the concentration of CO2 at the intake manifold was also measured to calculate EGR rate. A smoke meter (AVL 415S) measured the soot concentration at upstream of the DPF. The specifications of the smoke meter are shown in Table 2.1.6. The smoke meter used the principle of filter paper

blackening and it needed a sample volume for measuring the concentration of the soot. Therefore, the smoke meter was not proper to measure the transient soot concentration. In the transient test case, the soot concentration was measured by a Cambustion DMS500 and the specifications are shown in Table 2.1.7. The DMS500 used corona charger and electrometer detectors as measurement principle. The DMS500 could classify the particles number by size and provide size distribution of particulate matters. Because there was a difference between the measurement principle in the smoke meter and DMS500, the measurement result values of the two equipment differed in unit and exact objective of measurement. The equation (2.1.1) is the conversion equations from the filtered smoke number (FSN) to the smoke concentration [125]. To compare the results between the smoke meter and DMS500, the experimental results of 18 cases at wide range of soot emission level were compared in Figure 2.1.2. The scale was about 1.65 times different, but the relationship was good, so it was corrected when verifying the transient result of the soot model.

$$smoke\ \ concentration\ \ [mg/m^3] = \frac{1}{0.405} 4.95 \cdot FSN \cdot \exp(0.38 \cdot FSN) \tag{2.1.1}$$

2.1.4 Engine operating conditions

2.1.4.1 Steady-state conditions

For evaluating the performances of the base engine condition, 63 cases at the wide operating range were tested. The cases of the intercooler out temperature swing (22 cases), the coolant temperature swing (28 cases) and EGR swing (56 cases) were also conducted to obtain indicated mean effective pressure (IMEP), noise, NOx and soot emissions. In the process of developing the 0-D soot model, it was conducted that swing experiments on various intake and coolant temperature, and EGR conditions to establish a robust model despite changes in various conditions. The experimental points for each condition are shown in Figure 2.1.3. In the swing case of intercooler out temperature, the temperature was tested from 35℃ as base condition to 133℃ and it was controlled by the bypass valve of the intercooler. The coolant water temperature was changed at four steps up to 40℃ at intervals of 15℃ from the base condition of 90℃ and the performances were evaluated. The test engine used the both of low pressure (LP) EGR and high pressure (HP) EGR systems. To verify and distinguish the effect of LP and HP EGR, the cases of EGR swing were tested by the type of EGR and it was added that bypass conditions to HP EGR test conditions to experiment under conditions with high cooler out temperatures. The maximum temperature of intake air in the cases of HP EGR cooler bypass (ECB) increased up to 151℃. In addition, EGR swing at low coolant temperature experiments was conducted at 1750rpm brake mean effective pressure (BMEP) 6bar condition.

2.1.4.2 Transient conditions

The transient experiment was conducted by using Worldwide Harmonized Light vehicle Test Cycle (WLTP). This cycle is used in regulatory emission test

and considered as standardized transient experimental cycles. The profile of WLTP is shown in Figure 2.1.4. The dynamometer controlled speed and the EMS controlled torque by receiving the input as accelerator pedal signal from the dynamometer. The acquisition of experimental data during a WLTP was basically the same as steady state experiments. The measurement of soot concentration was different and it was measured by DMS500.

Table 2.1.1 Test engine specifications

Type	4-cylinder(in-line) CI engine
Bore	83.0mm
Stroke	99.4 mm
Displaced volume	2151 cc
Compression ratio	16
Maximum power and torque	154.4 kW / 45.0 kg·m
EGR system	Low pressure (LP) + high pressure (HP) EGR
Aftertreatment system	DPF + LNT + SCR

Table 2.1.2 Test engine fuel injection system specifications

Manufacturer	Bosch
Type	Common rail injection (Solenoid)
Nozzle diameter	0.127 mm
No. of nozzle holes	8
Spray angle	153 °
Rail pressure	2200 bar
Fuel injection system	Common rail injection (Solenoid)
Maximum power and torque	154.4 kW / 45.0 kg·m

Table 2.1.3 Specifications of the in-cylinder pressure sensor

Manufacturer	Kistler
Model	6056A
Pressure sensor type	Relative pressure
Measuring range (bar)	0 ~ 250
Overload (bar)	300
Linearity (% FSO)	< ±0.4
Sensitivity (pC/bar)	-18.3
Natural frequency (kHz)	160
Operating temperature (°C)	-20 ~ 350

Table 2.1.4 Specifications of the combustion analyzer

Item	Specification
Manufacturer	Kistler
Model	Kibox to go 2893
Sampling rate for analog input	1.25 MHz
Uncertainty	Approximately 1 ms(<<1 cycle)
Resolution of measurement data	312.5 kHz / 0.1 CA

Table 2.1.5 Measuring principles of MEXA 7100-DEGR by the emissions

Emissions	Measurement principle
NOx	Chemiluminecent Detector
THC	Flame Ionization Detector
O_2, CO_2, CO	Non Dispersive Infrared Rays

Table 2.1.6 Specifications of the smoke meter

Item	Specification
Manufacturer	AVL
Model	AVL 415S
Measurement principle	Filter paper blackening
Measurement range	0 ~ 10 FSN / 0 ~ 32,000 mg/m³
Resolution	0.001 FSN / 0.01 mg/m³
Repeatability (as standard deviation)	$\sigma \leq \pm$(0.005 FSN + 3 % of measured value)
Reproducibility (as standard deviation)	$\sigma \leq \pm$(0.005 FSN + 6 % of measured value)

Table 2.1.7 Specifications of DMS500

Item	Specification
Particle size range	5nm – 1μm
Measurement principle	Corona charger and electrometer detectors
Size Classification	Electrical mobility
Number of electrometers	22
Time response	$T_{10\text{-}90\%}$: 200ms
Max concentration	1×10^{11} N/cc

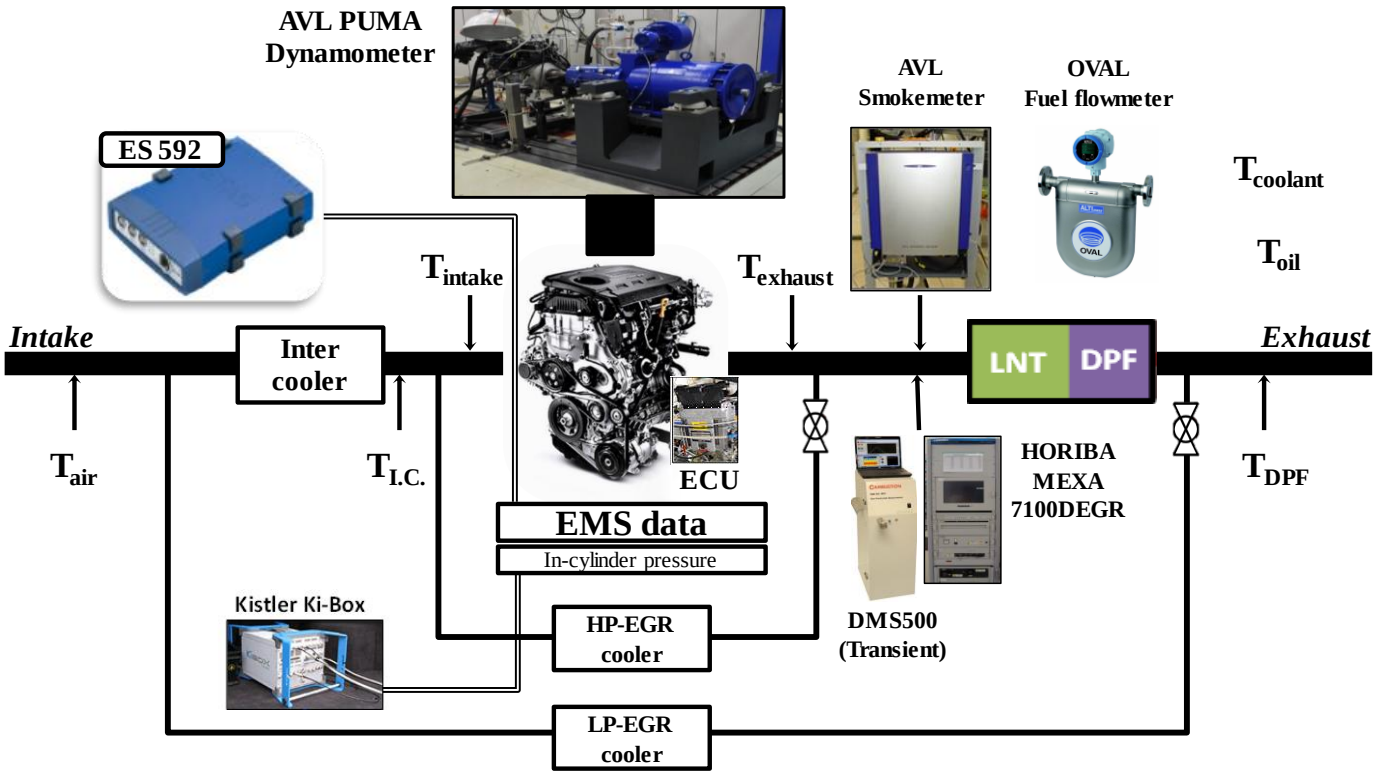

Figure 2.1.1 Schematic experimental set up

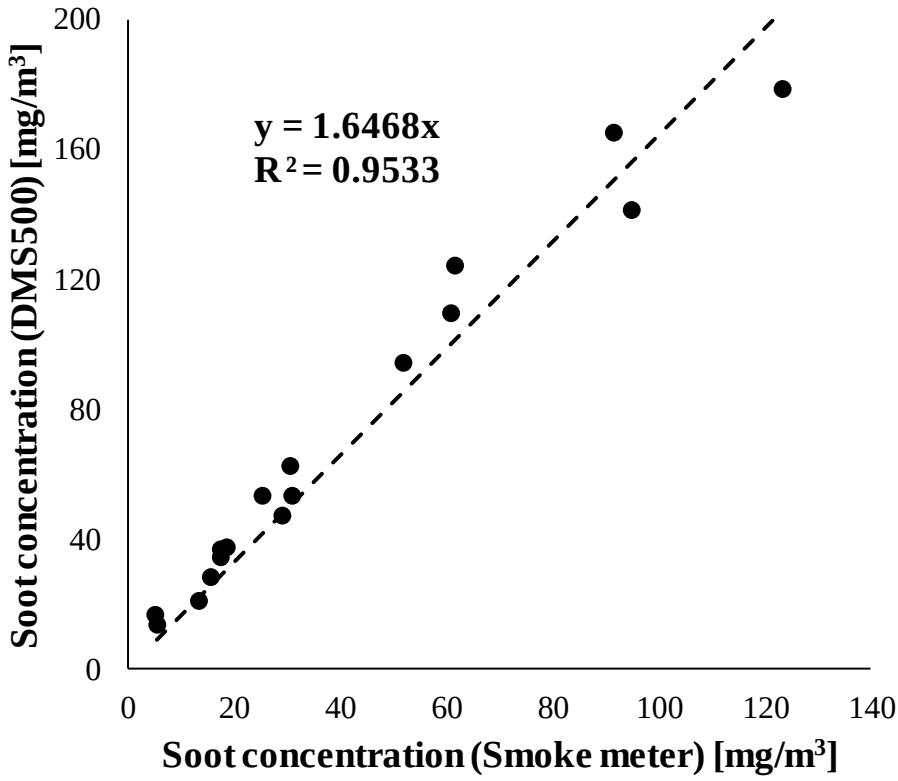

Figure 2.1.2 The soot concentration correlation between the result form the smoke meter and DMS500

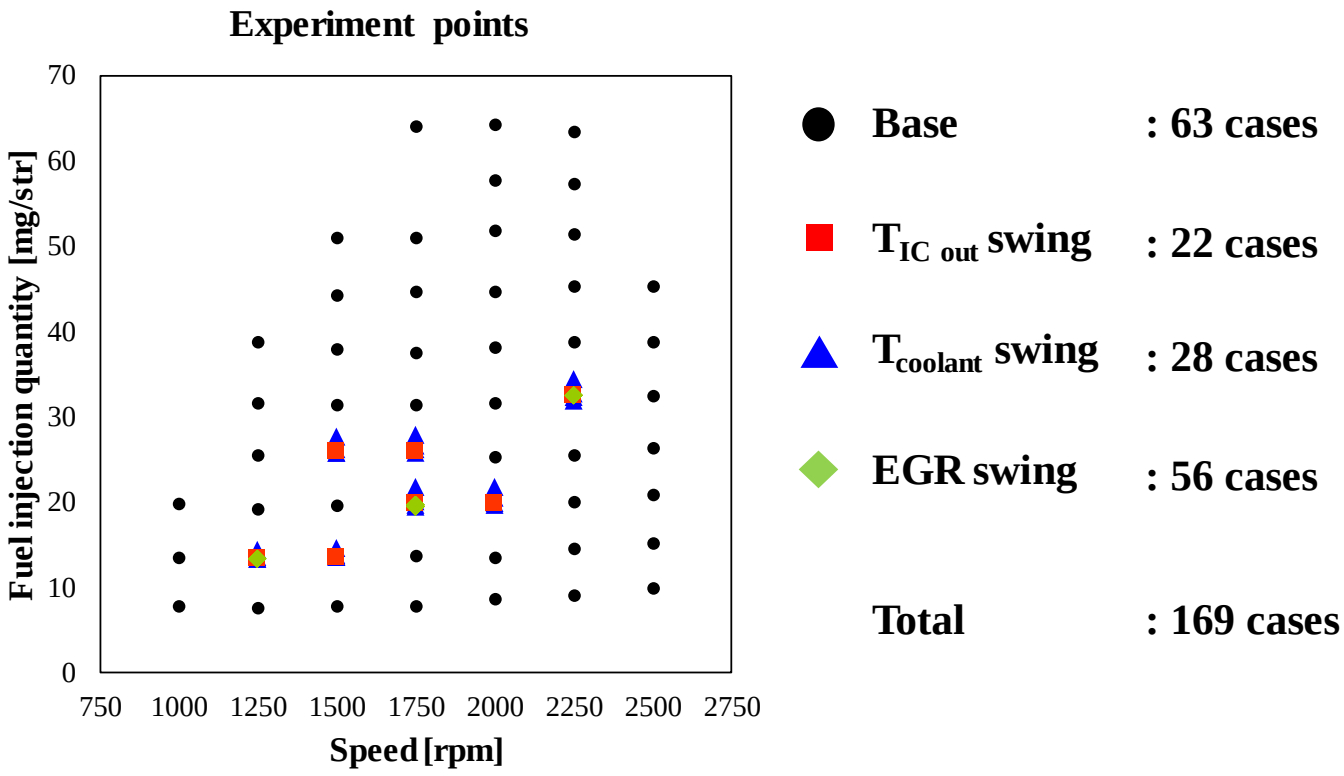

Figure 2.1.3 Steady state experimental points

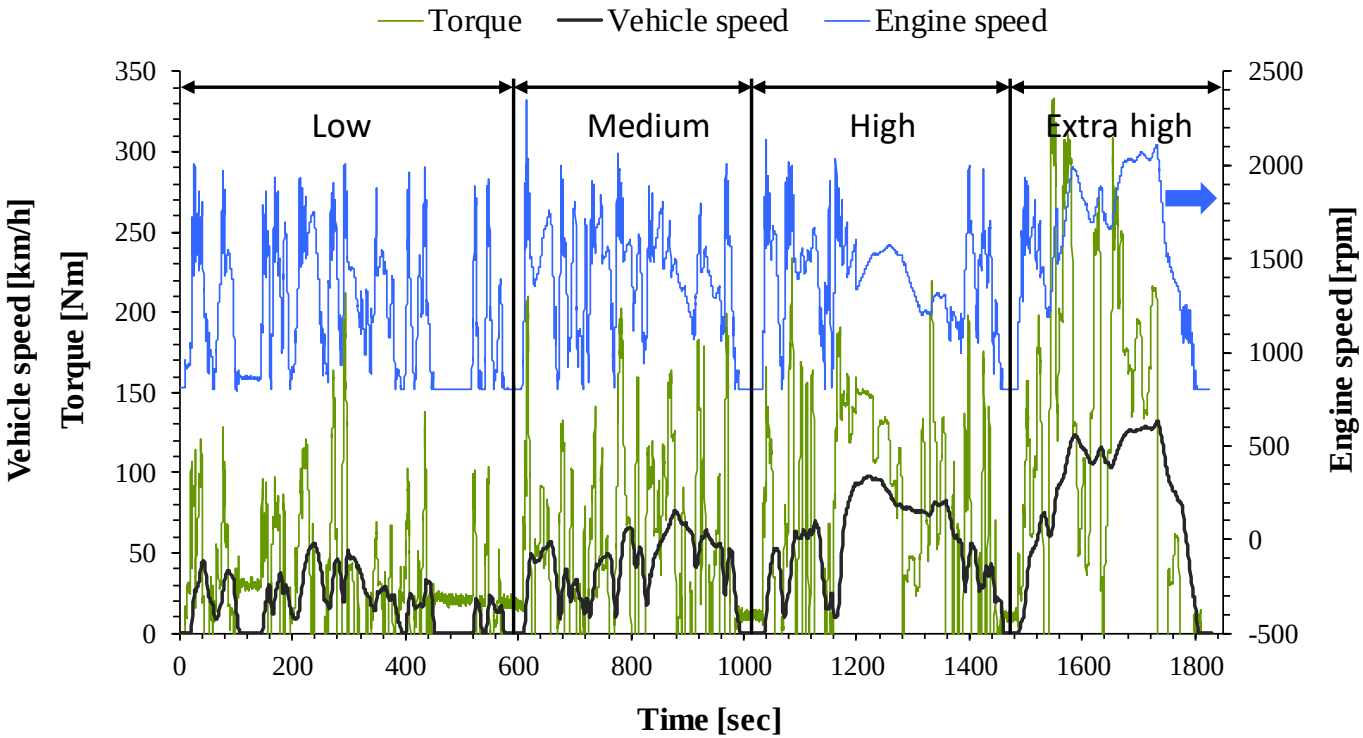

Figure 2.1.4 Speed and torque profile of WLTP

Chapter 3. Semi-physical 0-D Soot Model

Semi-physical soot model with collaborative work with Youngbok Lee [124] was developed. This paper focused on developing the spray model for equivalence ratio at the lift-off length and Lee [124] focused on constructing the soot formation and oxidation model with other parameters.

3.1 Simplified Spray Model

3.1.1 Spray model description

The soot formation in the diesel combustion is closely related to the behavior of the spray. The dynamics of the spray explain the distribution and behavior after the fuel injection, and the flame structure during the combustion process. The previous researches showed that soot formation begins after autoignition and pathway through the premixed combustion phase [74]. The soot is continuously formed in the mixing-controlled phase of the combustion. In the mixing-controlled phase, the flame structure is a major factor to the soot formation. The mixing-controlled diesel combustion for quiescent diesel engine conditions occurs in the diffusion flame mode [74, 76, 77, 85]. The fuel rich area near the center of the spray with the high soot concentration is located past the lift-off length as shown in Figure 1.2.2. The lifted flame allows the fuel and air to mix in front of the lift-off length and form premixed mixture. The equivalence ratio at the lift-off length can be considered as representative index for the degree of oxygen entrained in the fuel jet or mixing of the fuel and air [85].The equivalence ratio at the lift-off length was used as a main factor of the soot formation model. The equation (1.2.13)

in chapter 1 developed by Siebers was used for the calculation of lift-off length [87] and the equation was re-marked to remind.

$$\text{Lift} - \text{off length(H)} = 0.2 \cdot \text{Liquid length} + \text{C} \cdot \frac{U_0 \cdot Z_{st} \cdot D_T}{S_L^2(Z_{st}) \cdot tan(\theta/2)} \quad (1.2.13)$$

Based on the equation (1.2.13), the simplified spray model was developed to calculate the equivalence ratio at the lift-off length using the engine operating parameters and combustion factors. The equation (1.2.13) consists of the 0.2 times the liquid length and the scaling expressions of the lift-off length developed by Peters [83]. The liquid length was numerically calculated by the maximum penetration distance of liquid length that was derived using jet theory applied to a simplified model of a diesel spray. The laminar flame speed (S_L) was calculated at the stoichiometric conditions. Based on the equation developed by Kim [126], the laminar flame speed was corrected by considering the dilution effect of diluents. The U_0 is the initial axial spray velocity. The simplified spray model presented in this study aims to calculate the lift-of length using each factor at the start of the injection (SOI) to obtain the equivalence ratio at the lift-off length for applying to the soot formation model. This model was validated with the experimental data from engine combustion network (ECN) that was an international collaboration among experimental and computational researchers in engine combustion. The conditions for the validation data in engine combustion network database were n-heptane as a fuel, ambient gas temperature in range of 800-1300K, and the oxygen concentration of the ambient gas in range of 8-21%. The experiment to obtained the data in engine combustion network was conducted in the combustion vessel and the principle of hydroxide (OH) chemiluminescence was used to measure the lift-off length [76].

3.1.2 Liquid length calculation

In a diesel spray, the liquid fuel penetrates to a point that the fuel evaporation rate in the spray and the fuel injection rate are equal [81]. The liquid fuel stops penetrating and begins fluctuating after the equal point. The scaling law for liquid length developed by Siebers [75] provided a fundamental basis on liquid fuel penetration length in a diesel spray. The derivation of the scaling law for liquid length used the schematic idealized spray model shown in Figure 3.1.1 to expand physical relationship during the spray penetration. The idealized spray model needed to assume the several physical characteristics as follows [75]:

i. quasi-steady flow with a uniform growth rate

ii. uniform velocity, fuel concentration and temperature profiles

iii. no velocity slip between the injected fuel and the entrained ambient gas

In the Figure 3.1.1, the dashed line defined as the control surface and the variables P, T, and ρ presented the pressure, temperature and density of the fuel (f) and ambient gas (a). The α was the spray spreading angle. The axis x was the distance from the injector tip and L was the liquid length. So, the thermodynamic assumptions were needed at the control surface that including liquid length as follows [75]:

i. the vapor phase fuel is at a saturated condition.

ii. the vapor phase fuel is in thermodynamic equilibrium with the entrained ambient gas and the liquid phase fuel.

iii. idealized phase equilibrium assumptions apply

iv. gas absorption in the liquid phase is neglected.

v. the recovery of kinetic energy in the fuel vaporization region of the spray is neglected.

The mass flow rate ratio (B) of the fuel ($\dot{m}_f$) and the ambient gas ($\dot{m}_a$) at the liquid length ($x = L$) was derived from the mass and energy balances equations, and the real gas equation. The organized equation form of the mass flow rate ratio is shown in the equation (3.1.1) where the variables Z, M and h mean the gas compressibility, gas molecular weights and the specific enthalpy at the state of fuel (f), ambient gas (a) and the saturation state (s) [75].

$$B = \frac{\dot{m}_f(L)}{\dot{m}_a(L)} = \frac{Z_a(T_s, P_a - P_s) \cdot P_s \cdot M_f}{Z_f(T_s, P_s) \cdot [P_a - P_s] \cdot M_a} = \frac{h_a(T_a, P_a) - h_a(T_s, P_a - P_s)}{h_f(T_s) - h_f(T_f, P_a)} \tag{3.1.1}$$

In the combustion process and experimental data, the unknown variable among the parameters in the equation (3.1.1) is T_s. The author of the previous research [75] suggested to solve iteratively with the fuel and ambient gas properties and conditions. In this study, Cantera, the tools for solving chemical kinetics, was used to obtain B by calculating the saturation temperature at the equation (3.1.1). The Cantera calculated the thermodynamic properties at the specific temperature and pressure for fuel and various gas composition, so the saturation temperature that satisfying the equation (3.1.1) was able to be obtained. The obtained B was used to develop the scaling law for liquid length.

The equations (3.1.2) and (3.1.3) show the spray penetration length scale (x^+) and the normalized distance ($\tilde{x}$) where ρ_f and ρ_a are the densities of the fuel and air, d is the orifice diameter, α is the spray angle. With the equations (3.1.2)

– (3.1.3) and the mass and momentum balances equations, the relationship for the axial fuel and air mixture distribution can be derived and the equation (3.1.4) show the dimensionless form of the mass flow rates ratio in the spray [75].

$$x^{+} = \sqrt{\frac{\rho_f}{\rho_a}} \cdot \frac{d}{\tan(\alpha/2)} \tag{3.1.2}$$

$$\tilde{x} = \frac{x}{x^{+}} \tag{3.1.3}$$

$$\frac{\dot{m}_f(x)}{\dot{m}_a(x)} = \frac{2}{\sqrt{1 + 16 \cdot \tilde{x}^2} - 1} \tag{3.1.4}$$

By using the above equations, the substitution of the B in the equation (3.1.4) and solving it for the dimensionless liquid length ($\tilde{L}$) derives the equation (3.1.5) that is the scaling expression of the liquid length. The dimensional form of the equation (3.1.5) is the equation (1.2.11).

$$\tilde{L} = b \cdot \sqrt{\left(\frac{2}{B} + 1\right)^2 - 1} \tag{3.1.5}$$

3.1.3 Laminar flame speed model

The laminar flame speed is a concept originally used a lot in spark-ignition engine to predict and analyze the combustion process. However, the laminar flame speed in the calculation of the lift-off length was used to induce the scaling formulas of the lift-off length at the stabilization point of turbulence combustion. Thus, unlike describing the flame propagation in the combustion process, the lift-off length was used close to the physical and chemical properties when quasi-steady state was achieved in the conditions at fuel injection timing. In this study, the basic form of the equation for the laminar flame speed followed the equation (3.1.6) and (3.1.7) proposed by Kim [126], where a, b, ζ, ξ, ϕ_m, α and β are fitting coefficients. The coefficients used in this study were listed in Table 3.1.1, Table 3.1.2 and Table 3.1.3. The reference temperature and pressure for the evaluation of the dependency were T_0=600 K and P_0=5 bar.

$$S_L = a\,exp[1-\exp\{b(\phi-\phi_m)\}-\exp\{-\zeta(\phi-\phi_m)\} + \xi(\phi-\phi_m)^2]\left(\frac{T}{T_0}\right)^{\alpha(\phi)}\left(\frac{P}{P_0}\right)^{\beta(\phi)}(1-2.1Y_{dil}) \tag{3.1.6}$$

$$\alpha(\phi)=\sum_{i=0}^{5}\alpha_i\phi^i \quad and \quad \beta(\phi)=\sum_{i=0}^{5}\beta_i\phi^i \tag{3.1.7}$$

The last term $(1-2.1Y_{dil})$ in the equation (3.1.6) presented the diluent effect developed by Metghalchi and Keck [127]. In the SI engine combustion process, the burned gas and the internal or external exhaust recirculation gas caused the decrease in the laminar flame speed. Figure 3.1.2 shows experimental result of the burned gas mole fraction effect on laminar flame speed. However, for diesel combustion, it is difficult to apply the above concept of diluent effect. CI engines had a lower proportion of residual gas because of their high compression ratio and high intake pressure due to turbo charging. In addition, unlike SI engines that burn

under stoichiometric condition, the composition of the gas including burned gas varies at the same rate because CI engines burn under lean condition. Therefore, when calculating the lift-off length, the laminar flame speed needs to be considered for the effect of diluents, unlike the equation (3.1.6). When the lift-off length was calculated with considering the effect of diluents, the estimated lift-off length calculated by the equation (1.2.13) in the case of the same gas composition showed good relationships as shown in Figure 3.1.3 compared to the experimental data from engine combustion network. However, in cases with the same ambient temperature and pressure and different oxygen concentration as shown in Figure 3.1.4, the estimated values showed linear errors with the experimental data depending on the oxygen concentration.

The major gases that affected on the laminar flame speed by dilution were O_2, CO_2, N_2 and H_2O. As previous studies [128-130] have shown, the laminar flame speed increased with oxygen concentration and the rest of the gases (CO_2, N_2 and H_2O) decreased the laminar flame speed as shown in Figure 3.1.5. Because oxygen acted as an oxidizer, an increase in oxygen concentration leads to an increase in the laminar flame speed. Other gases reduced the laminar flame speed by a combination of thermal effect, which decreases the adiabatic temperature due to increased heat capacity, and chemical effect that reduced the concentration and production rate of free radicals [128, 130]. Using the gas composition ratio, the heat capacity ratio of oxygen in the entire gas can be calculated to simultaneously consider the change of laminar flame speed with the oxygen concentration and the thermal effect of other gases. The ratio of oxygen's heat capacity to the total heat capacity was defined as H_{O_2} and the equation for the calculating H is shown in the equation (3.1.8) where C_p is specific heat capacity and X means the volume fraction of the gas. The H_{O_2} ratio of the mixture at the condition at injection timing ($H_{O_2,mixture}$) to air ($H_{O_2,air}$) was used as a factor to compensate the effect of diluents for the laminar flame speed. However, the volume fraction (X_{O_2}),

which shows the good correlation with the H_{O_2} ratio as shown in Figure 3.1.6, was used to compensation rather than calculating the heat capacity of specific temperature and pressure conditions. In this study, the equation (3.1.9), which was modified from the equation (3.1.6) by considering the effects of diluents as described above, was used to calculate the laminar flame speed. The value of 0.74 in the equation (3.1.9) is the constant value fitted by the experimental data from engine combustion network.

$$H_{O_2} = \frac{X_{O_2} C_{p,\,O_2}}{X_{O_2} C_{p,\,O_2} + X_{N_2} C_{p,\,N_2} + X_{H_2O} C_{p,\,H_2O} + X_{CO_2} C_{p,\,CO_2}} \tag{3.1.8}$$

$$S_L = a e x p[1 - \exp\{b(\phi - \phi_m)\} - \exp\{-\zeta(\phi - \phi_m)\} + \xi(\phi - \phi_m)^2] \left(\frac{T}{T_0}\right)^{\alpha(\phi)} \left(\frac{P}{P_0}\right)^{\beta(\phi)} \left(\frac{X_{O_2,\,mixture}}{X_{O_2,\,ambient}}\right)^{0.74} \tag{3.1.9}$$

3.1.4 The equivalence ratio at the lift-off length

The thermal diffusivity was calculated by using the Cantera with the gas composition, temperature and pressure at the fuel injection timing. The injection velocity (U_0) was given by Bernoulli equation and calculated by the equation (3.1.10) where C_v is the velocity coefficient of the injector, P_f and P_a are the fuel and air pressure, ρ_f is the fuel density. The rail pressure was used as the fuel pressure and it was based on the experimental value at the base engine condition.

$$U_0 = C_v \sqrt{\frac{2(P_f - P_a)}{\rho_f}}$$

(3.1.10)

By using the above parameters, the lift-off length could be obtained through the equation (1.2.13). Figure 3.1.7 shows the validation result of the lift-off length from the simplified spray model with the measured lift-off length from the experimental data of engine combustion network. Table 3.1.4 and 3.15 show experimental conditions from engine combustion network for constant volume chamber experiment and experimental data at injection timing. The estimated lift-off length by the developed spray model showed good relationship with the measurement data. The equivalence ratio at $\tilde{x}$, which is the distance from the injector scaled by characteristic length scale x^+, was calculated from the equation (3.1.4) that shows the mass flow rate ratio between fuel and air and the equation. By substituting the lift-off length (H) for the distance term of the induced formula, the equivalence ratio at the lift-off length can be obtained, which is expressed in the equation (3.1.11) where α_{st} is air and fuel ratio at the stoichiometric condition. The lift-off length depended on the air entrance into fuel jet at the upstream of the lift-off length and the equivalence ratio at the lift-off length was used as a one of the main factors in the soot formation model.

$$\phi_{\mathrm{H}} = \frac{2\alpha_{st}}{\sqrt{1 + 16\tilde{x}_H^2} - 1}$$

(3.1.11)

Table 3.1.1 Model constants in the laminar flame speed fitting equations

	a	b	ζ	ξ	ϕ_m
n-heptane	2.5	1.9	1.85	9	1.1

Table 3.1.2 Coefficients for fitting temperature dependency

$\alpha(\phi)$	α_0	α_1	α_2	α_3	α_4	α_5
High temperature regime (600-900 K)						
n-heptane	6.253	-3.876	-8.627	13.795	-6.094	0.818
Low temperature regime (400-600 K)						
n-heptane	2.368	14.331	-45.612	50.307	-23.321	3.901

Table 3.1.3 Coefficients for fitting pressure dependency

$\beta(\phi)$	β_0	β_1	β_2	β_3	β_4	β_5
n-heptane	-0.954	-1.319	8.365	-11.400	6.147	-1.161

Table 3.1.4 Experimental conditions of data from engine combustion network for lift-off length

	Lift-off length [mm]	Oxygen concentration [%]	Ambient temperature [K]	Ambient pressure [bar]	Injection pressure [bar]
Min	7.7	8	750	31.6	1380
Max	67.0	21	1300	54.8	1550

Table 3.1.5 Experimental conditions at injection timing of experimental data for soot model

	Oxygen concentration [%]	Ambient temperature [K]	Ambient pressure [bar]	Injection pressure [bar]
Min	12	825	42.4	382
Max	20	1159	109.3	1497

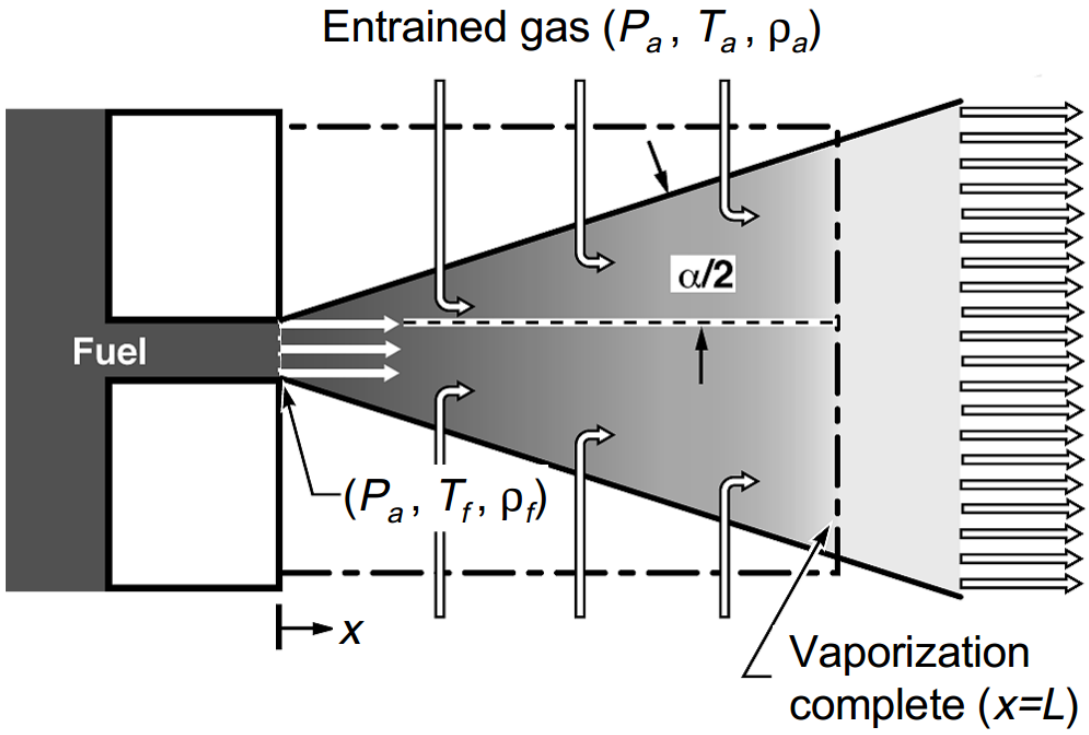

Figure 3.1.1 The schematic of the spray idealized model [75]

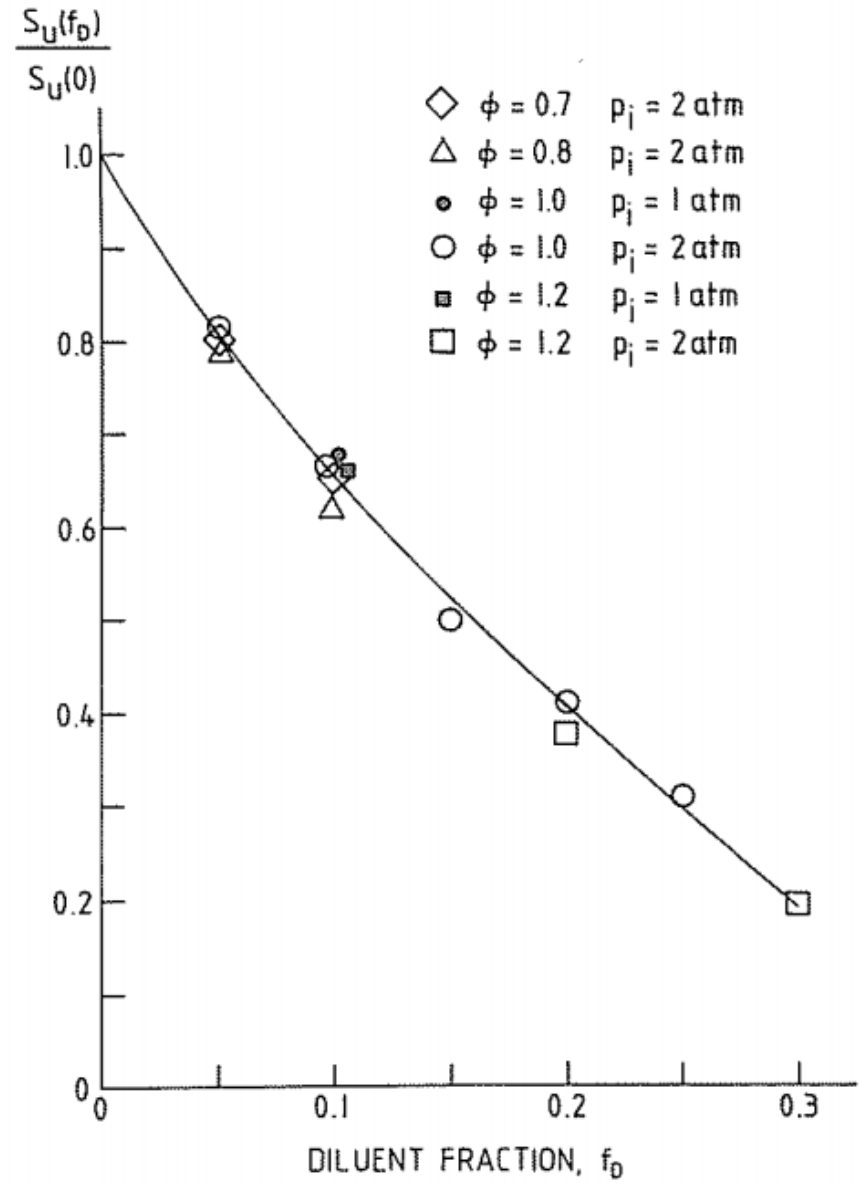

Figure 3.1.2 Effect of diluent (burned gas) mole fraction on laminar burning velocity [131]

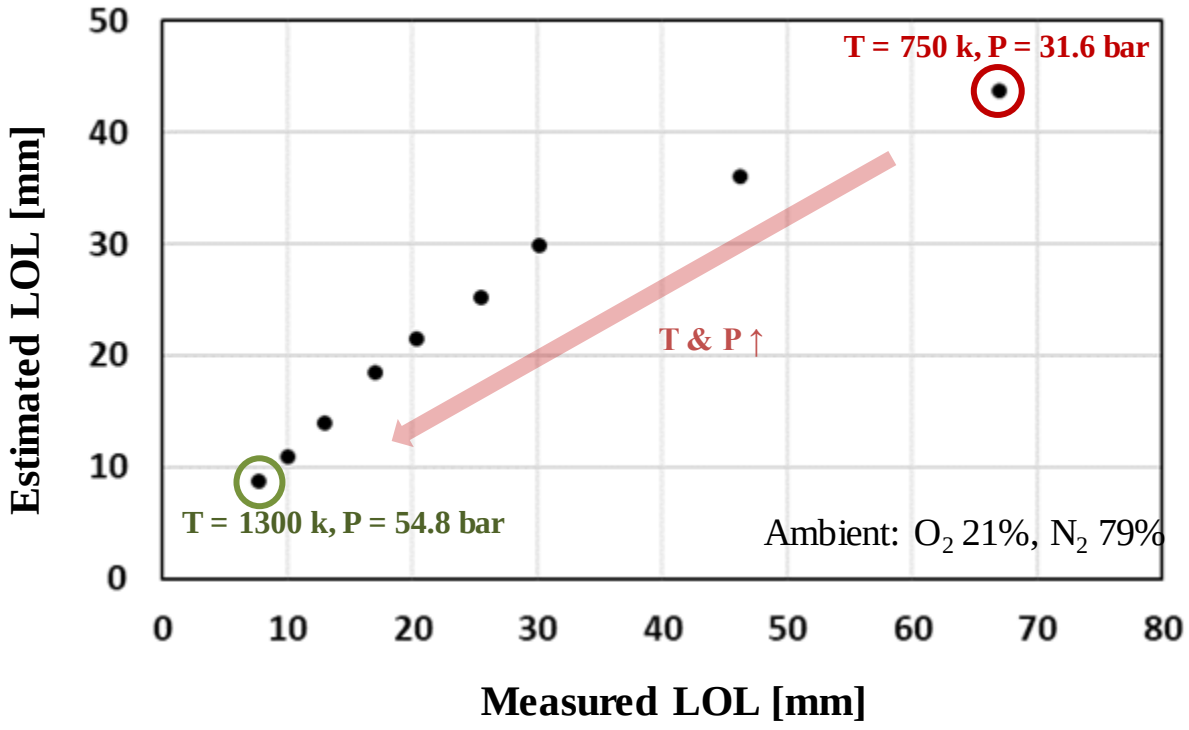

Figure 3.1.3 The estimated lift-off length without considering the dilution versus experimental data from engine combustion network at the constant gas composition

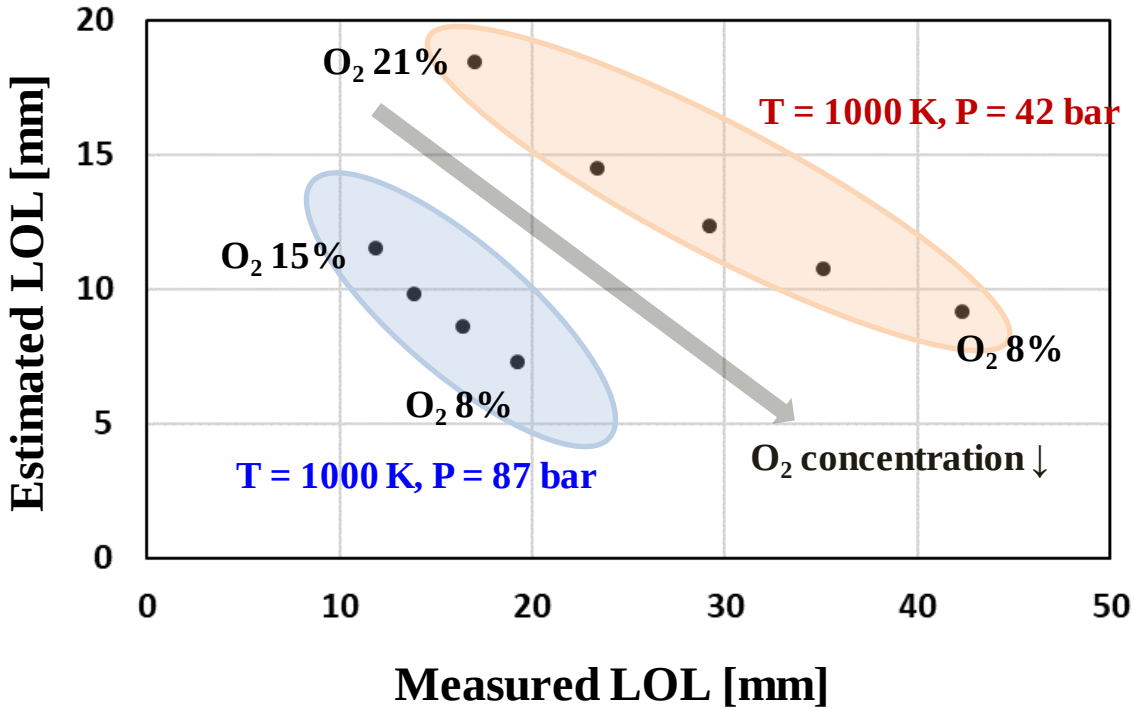

Figure 3.1.4 The estimated lift-off length calculated without considering the dilution effect at various

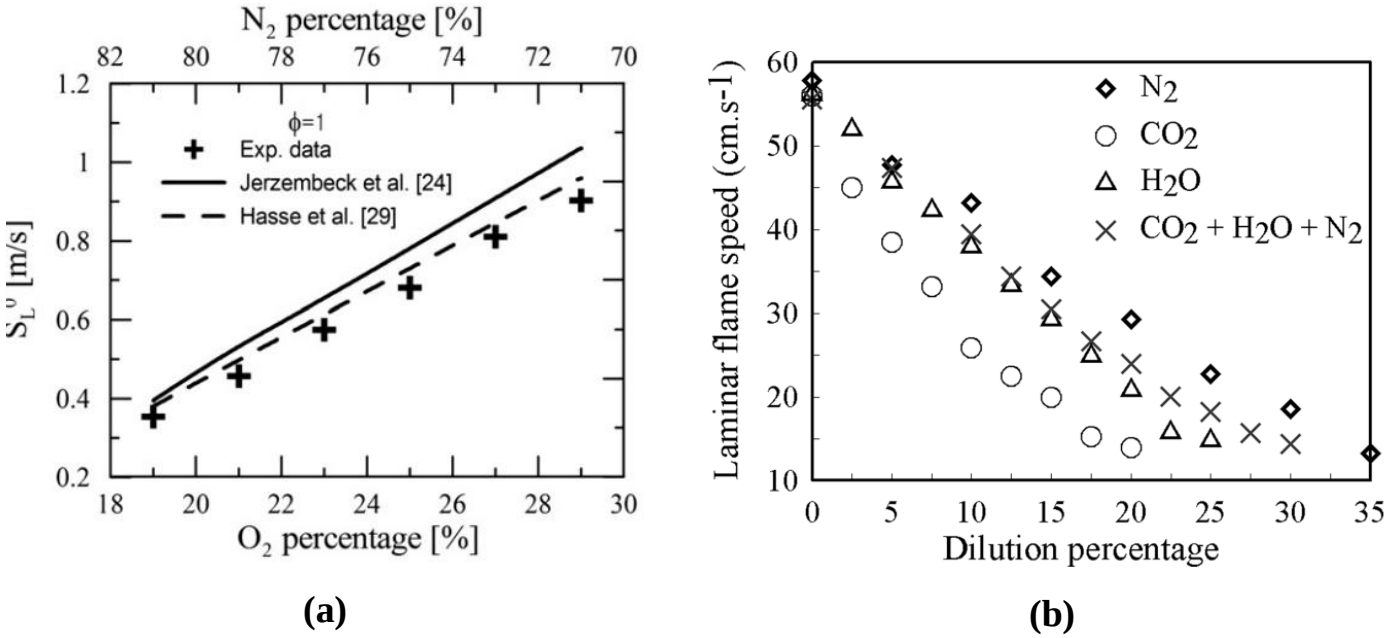

Figure 3.1.5 The effects of diluents on the laminar flame speed as a function of (a) O_2 [129] (b) N_2, CO_2, H_2O [128]

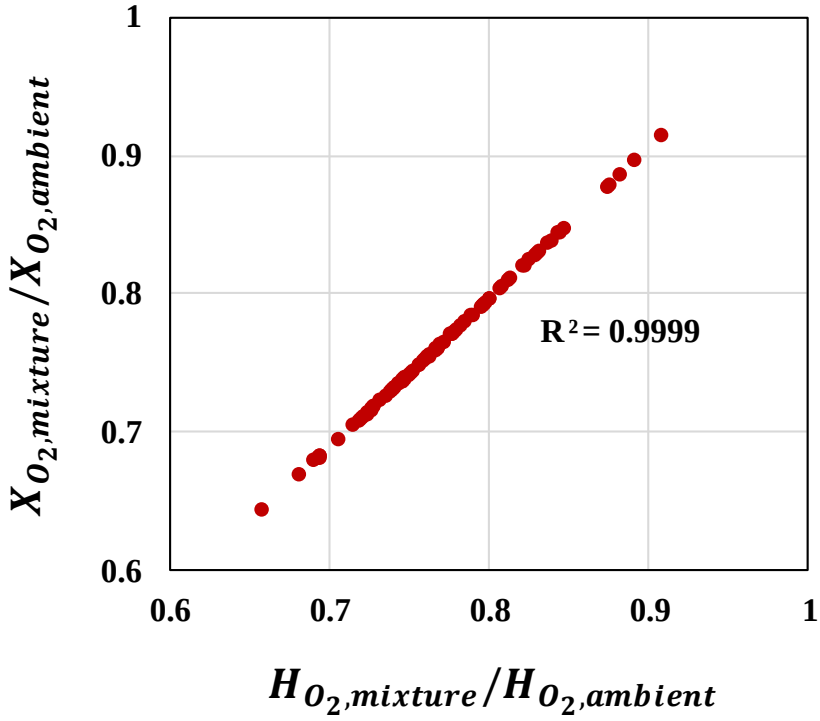

Figure 3.1.6 The correlation between the heat capacity ratio and the volume fraction ratio of the oxygen in 85 cases of experimental data in the test engine

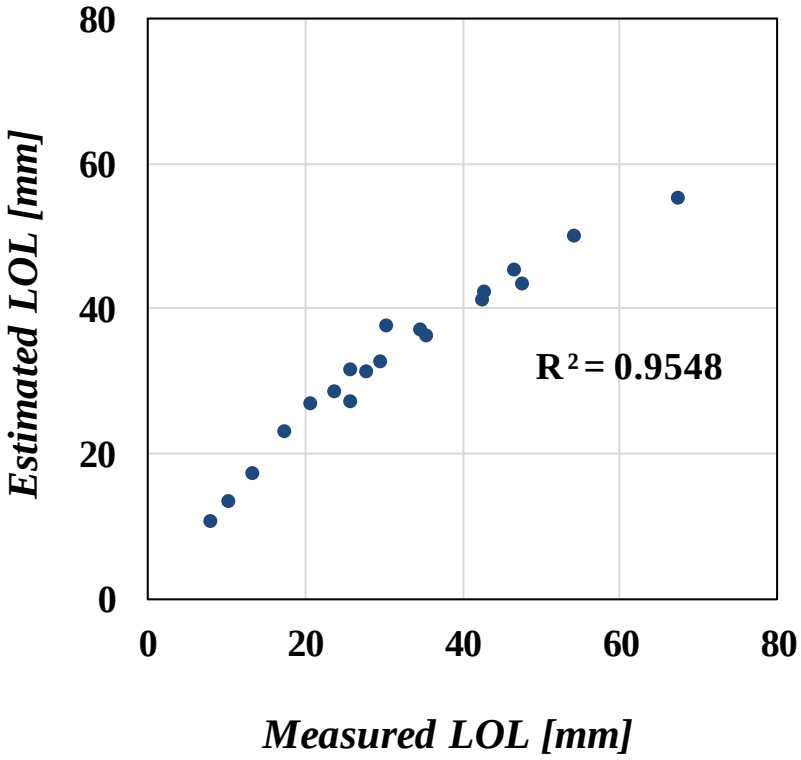

Figure 3.1.7 The validation result of the estimated lift-off length (LOL) developed in this study with experimental data from engine combustion network

3.2 Semi-physical 0-D Soot Model

The 0-D soot model was constructed by the local equivalence ratio and other parameters. Lee [124] investigated the model construction and other parameters. The soot model consisted with the soot formation model that calculated the formed soot mass from the precursor and soot oxidation model that calculated the oxidized soot mass by oxidizer such as oxygen and acetylene. The soot mass was calculated by the difference of the two models as shown in the equation (3.2.1). Each model was calculated by the EMS parameters and several combustion factors calculated from the in-cylinder pressure. Therefore, the model allowed real-time calculation and applied to transient condition.

$$m_{soot} = m_{soot,formation} - m_{soot,oxidation} \tag{3.2.1}$$

3.2.1 Soot formation model

The major features of the soot formation model are considered several factors such as the amount of precursor underlying the soot formation, the degree of mixing of air and fuel, and duration of soot formation. The most effective factor for representing the amount of precursor was the fuel injection quantity (m_{fuel}). The soot particle formation was triggered by the inception of precursor polycyclic aromatic (PAH) and growth by collision with other particles and surface growth with chemical reaction [132]. As the objective for the initial trigger of soot formation, the injected fuel was proper factor for the soot formation model. Diesel engines have been used multi-injection strategy that consisted with pilot, main and post

injections. Usually, the pilot injection was used to reduce combustion noise and control the emissions. Since the long ignition delay of the pilot injection, combustion from the pilot injection was considered as premixed combustion. The low soot formation of premixed combustion and the low fuel mass compared to the main injection were enough to consider the effect of pilot injection quantity as relatively negligible factor compared to the main injection. Therefore, the soot model used the fuel mass term with excluding the pilot injection quantity.

The representative factor for the mixing degree was the equivalence ratio at the lift-off length (Φ_H). As described in chapter 3.1, the lift-off length was the distance from the injector to combustion flame, and the upstream of the lift-off length was the place where air entrained into the fuel jet. The equivalence ratio at the lift-off length could be used to representative index for the equivalence ratio inside the spray where the soot was formed. The duration for the soot formation was used the mass fraction burned (MFB) 5 to 90 (MFB_{05-90}). Since the soot could be formed through the entire combustion period, the total combustion duration should be considered as the soot formation period, but the combustion duration used in the model was set from 5 to 90 considering the uncertainty of the pressure measurements that required to calculate the heat release rate. The soot formation model takes the form of the equation (3.2.2).

$$m_{soot,formation} = A \times m_{fuel}^{x_1} \times \Phi_H^{x_2} \times (MFB_{05-90})^{x_3} \tag{3.2.2}$$

3.2.2 Soot oxidation model

The development concept of the soot oxidation model was that the mass of the formed soot was oxidized with oxidation rate. The formed soot was oxidized by the oxidizers such as oxygen, acetylene and OH at the high temperature condition. The reaction rate of the oxidation was calculated by conjugating the equation from Nagle and Strickland-Constable [89, 90]. The equation (3.2.3) shows the oxidation reaction rate and the equations (3.2.4)-(3.2.8) show the coefficients and parameters for the equation (3.2.3) where k_A, k_B, , k_z and k_T are the reaction coefficients related with activation energy in Arrhenius equation, x is the coefficient of the surface fraction by the reactive type, T is the reaction temperature, and p_{o_2} is the partial pressure of the oxygen.

$$\dot{r} = \left(\frac{k_A p_{o_2}}{1 + k_Z p_{o_2}}\right) x + k_B p_{o_2}(1 - x) \tag{3.2.3}$$

$$x = \left(1 + \frac{k_T}{p_{o_2}}\right)^{-1} \tag{3.2.4}$$

$$k_A = 20 \cdot exp(\frac{-15100}{T}) \tag{3.2.5}$$

$$k_B = 4.46 \times 10^{-3} \cdot exp(\frac{-7650}{T}) \tag{3.2.6}$$

$$k_T = 1.5 \times 10^{5} \cdot exp(\frac{-48800}{T}) \tag{3.2.7}$$

$$k_Z = 21.3 \cdot exp(\frac{2060}{T}) \tag{3.2.8}$$

The partial pressure of the oxygen and temperature in calculating the reaction rate process were considered as the representative pressure and temperature for oxidation condition. Finesso et al. proposed the late combustion phase as a factor that was correlated with soot oxidation and the authors used the burned temperature at MFB95 [96]. In this study, the end of combustion was determined as MFB90, so the representative pressure and temperature for the oxidation reaction rate were used as the pressure and temperature at MFB90.

In the developed soot model, heat transfer from the cylinder wall was considered to cope with environmental conditions with varying the coolant temperature. The relationship between heat flux from the wall and temperatures was suggested by Angelberger et al [133] in the form of the equation (3.2.9). The wall temperature in the equation (3.2.9) was calculated by the temperature of coolant and oil as shown in the equation (3.2.10) that was often used in CFD simulation. If the temperature of the cylinder wall dropped due to reduced coolant temperature, oxidation, which mainly occurs in the flame surface, would be more affected than generation near the center of the spray. Therefore, the heat flux was applied to the soot oxidation model so that it could be compensated according to the coolant and oil temperature.

$$Wall\ \ heat\ \ flux\ \ \propto\ \ T \cdot ln\left(\frac{T}{T_{wall}}\right) \tag{3.2.9}$$

$$T_{wall} = \frac{T_{coolant} + T_{oil}}{2} + 67\ \ k \tag{3.2.10}$$

The developed soot oxidation model is organized like the equation (3.2.11). The net soot emission can be calculated by the difference of the soot formation and oxidation models. The semi-empirical soot model from the soot formation and

oxidation models was fitted in the exponential form with the experimental data from the test engine and had the form of the equation (3.2.12) with the fitted coefficients.

$$m_{soot,oxidaiton} = m_{soot,formation} \times A' \times \dot{r}^{x_4} \times \left[T_{mfb90}\, ln\left(\frac{T_{mfb90}}{T_{wall}}\right)\right]^{x_5} \quad (3.2.11)$$

$$\begin{aligned} m_{soot,net} &= m_{soot,fomation} - m_{soot,oxidaiton} \\ &= A \times m_{fuel}^{0.18} \times \Phi_{LOL}^{1.82} \times (MFB_{05-90})^{4.42} \\ &\times \left(1 - A' \times \dot{r}^{0.5} \times \left[T_{mfb90}\, ln\left(\frac{T_{mfb90}}{T_{wall}}\right)\right]^{-1.24}\right) \end{aligned} \quad (3.2.12)$$

3.2.3 The model validation

3.2.3.1 Steady state condition

The developed soot estimation model was validated in the steady conditions shown in Figure 2.1.3 and the results are shown in Figure 3.2.1. The soot results from the base conditions and the coolant temperature swing cases showed 0.741 and 0.62 of r-squared value and relatively lower than other parameter swing conditions. In the coolant temperature swing cases, the cases of the coolant temperature 40℃ showed low accuracy and the r-squared value except the coolant temperature 40℃ cases was 0.845. The EGR swing cases also showed lower accuracy in the EGR swing at 40℃ of the coolant temperature. For the reason of low accuracy in the coolant temperature of 40℃ cases, it was assumed that the effect of the heat transfer on the soot formation and oxidation under low coolant

temperatures were more complex than the heat transfer effect considered in the developed model. The developed model showed good estimation accuracy in the intercooler out temperature swing cases with r-squared value of 0.99. In the total cases, the developed soot model showed 0.90 of the r-squared value.

3.2.3.2 Transient condition (WLTP)

In transient condition, the EGR rate was hard to measure in real-time. The EGR rate was calculated by the CO_2 concentration ratio of exhaust and intake. The test engine used EGR system both LP and HP EGR. Two EGR system had different air path and delay from exhaust to mixing point. The CO_2 concentration from the measurement system (MEXA-7100DEGR) was hard to compensate for the delay and transient behavior. The EMS system incorporated the EGR model that could be predicted even in transient conditions. Figure 3.2.2 showed the comparison of EGR rates from the measurement system and EMS. The EGR rate from EMS showed lower delay and good correlation compared with that from the measurement equipment. In the process of transient condition, the EGR rate from EMS was used for calculating model parameters. Figure 3.2.3 and Table 3.2.1 show the estimated soot results in the transient condition. It was confirmed that the developed model could respond to peak soot level and transient behavior. The error in phase 4 showed 12.1% compared to experimental data. The reason for the higher error than other phase was assumed that the model accuracy at the high load area was insufficient to consider different combustion phase and characteristics because the model had the unified form in entire operating area.

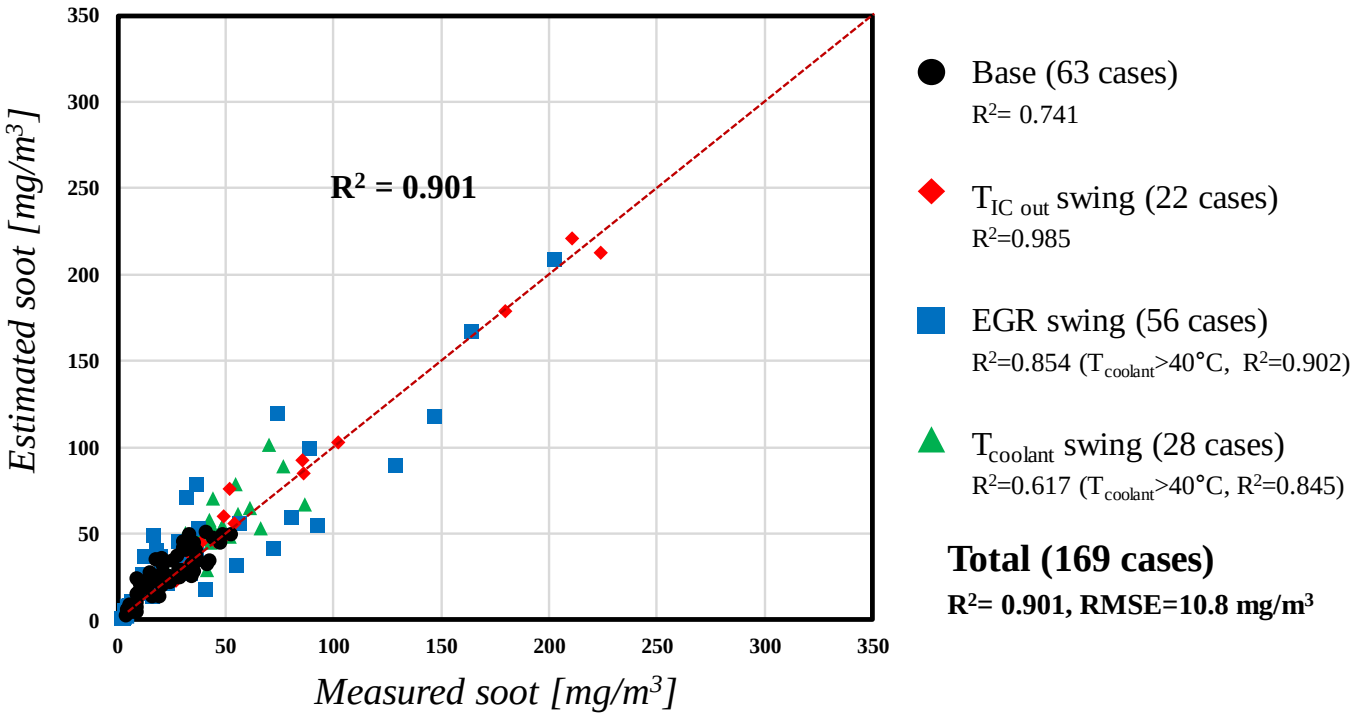

Figure 3.2.1 The validation results of the developed soot model in the steady state conditions

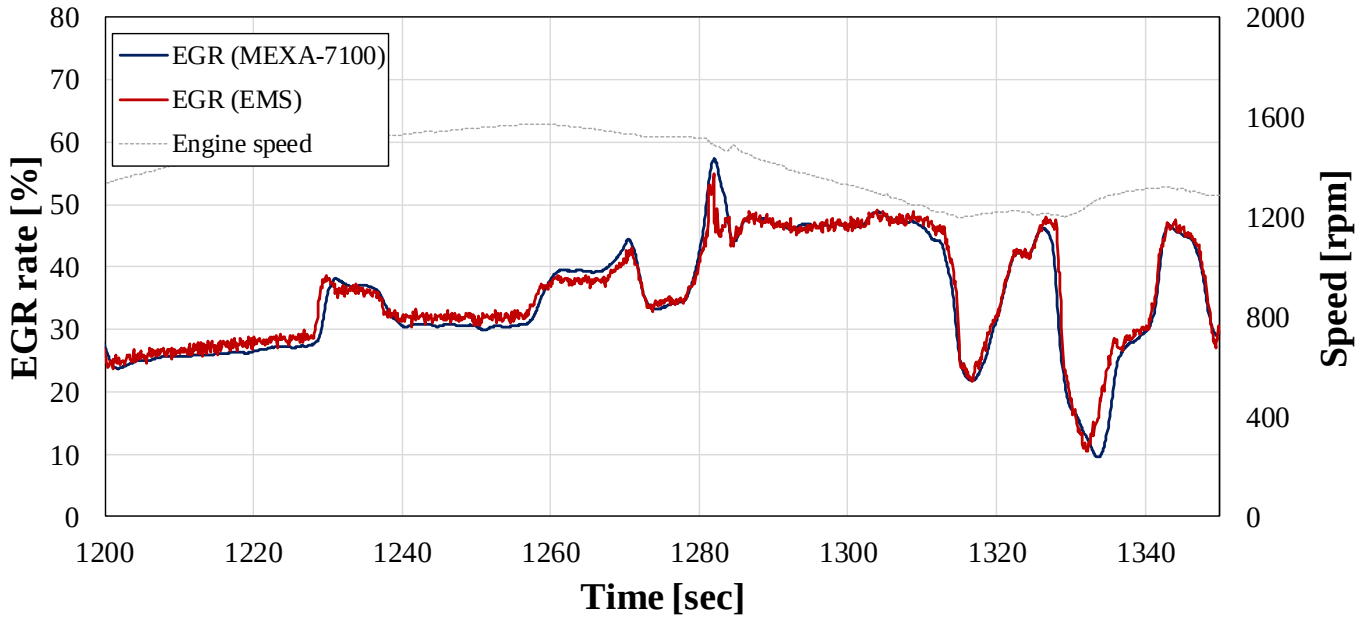

Figure 3.2.2 EGR rates calculated by the results from MEXA-7100 and EMS data

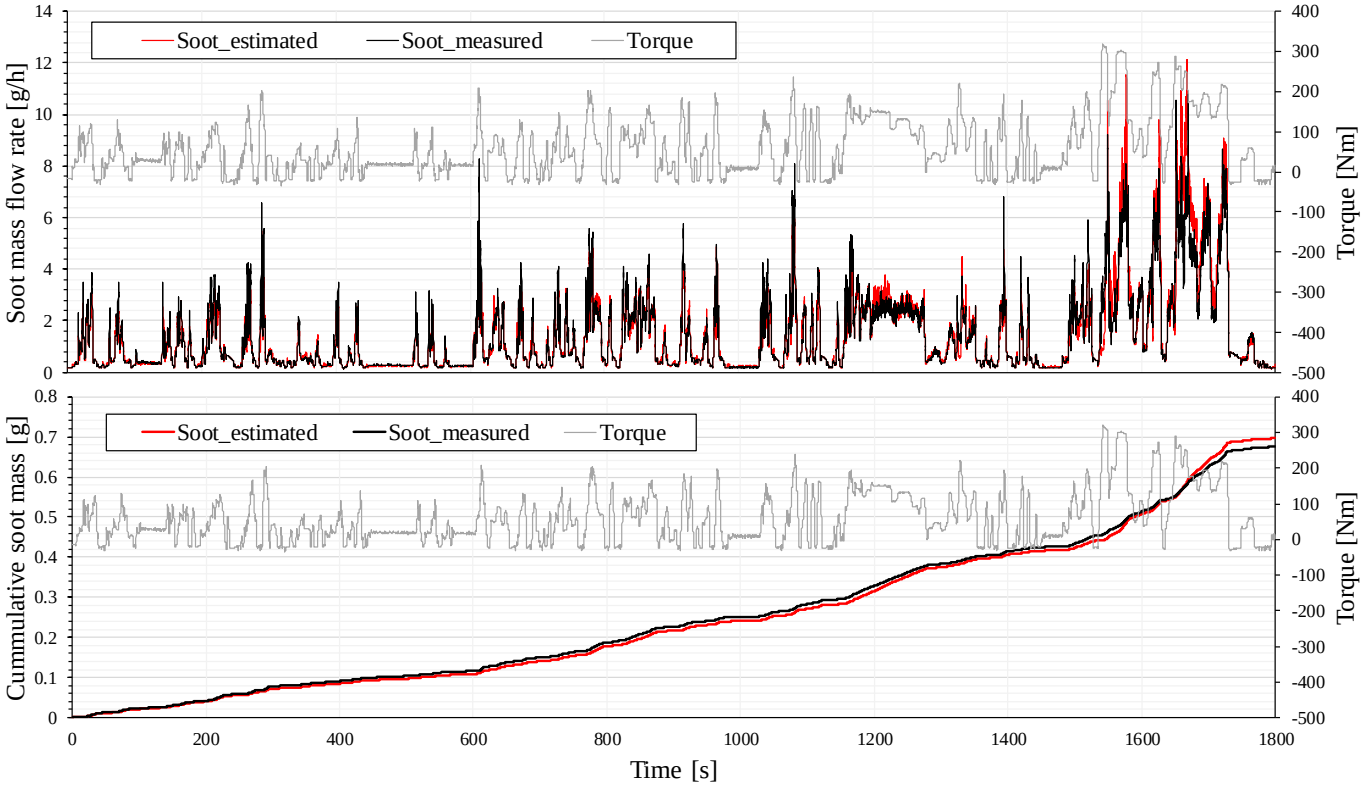

Figure 3.2.3 The transient mode result of the soot model

Table 3.2.1 The soot emission results from the experimental data and the developed model

	Phase1	**Phase2**	**Phase3**	**Phase4**	**Total**
Measured [g]	0.116	0.134	0.176	0.250	0.676
Model [g]	0.109	0.132	0.176	0.280	0.697
Error [%]	**-6.5**	**-1.6**	**0.3**	**12.1**	**3.1**

Chapter 4. Other Models for Thermal Efficiency, Noise and NOx Emission

4.1 Thermal Efficiency

Thermal efficiency from the experimental results has been analyzed with BSFC. Since the combustion optimization methodology to be introduced later was a 0-D simulation, the fuel rate measured by the experiment was not presented and was set to the initial value. To apply the combustion design methodology, the IMEP was used as a factor that could represent thermal efficiency based on the same amount of fuel injection. The IMEP was different from BMEP because it could not consider loss due to friction and etc., but IMEP could be considered representative of thermal efficiency when optimization was achieved under the same operating conditions. The IMEP was obtained through the equation (4.1.1).

$$IMEP = \oint PdV \tag{4.1.1}$$

4.2 Noise – Combustion Noise Index (CNI)

In the previous researches, the maximum pressure rise rate has been used as the index for the combustion noise [39-43]. However, the maximum pressure rise showed insufficient correlation with engine noise changes due to engine parameters or combustion phase [122, 134]. In this study, the combustion noise was estimated by combustion noise index (CNI) developed by Jung et al. [122, 134]. The

CNI was calculated by the pressure interpreted as frequency domain via FFT and the sum of the 1-3.15 kHz range of the third octave band level as shown in the equation (4.2.1) and Figure 4.2.1. Figure 4.2.2 shows how max pressure rise rate and combustion noise index relate to the measured noise data respectively at 1500 rpm, BMEP 6 bar [122]. The experimental data were test result of the sensitivity of injection parameters such as injection pressure, pilot injection quantity and timing, and main injection timing. The correlation of CNI with the measured noise were better than that of max pressure rise rate.

$$\begin{aligned}\text{CNI (dB)} = {} & 10\log\left(10^{1kHz\frac{level}{10}}\right) + 10\log\left(10^{1.25kHz\frac{level}{10}}\right) \\ & + 10\log\left(10^{1.6kHz\frac{level}{10}}\right) + 10\log\left(10^{2kHz\frac{level}{10}}\right) \\ & + 10\log\left(10^{2.5kHz\frac{level}{10}}\right) + 10\log\left(10^{3.15kHz\frac{level}{10}}\right) + \end{aligned} \tag{4.2.1}$$

The combustion design method used the optimization process for the pressure satisfying the target performance. The pressure produced during each iteration process was calculated as the CNI to predict the noise performance.

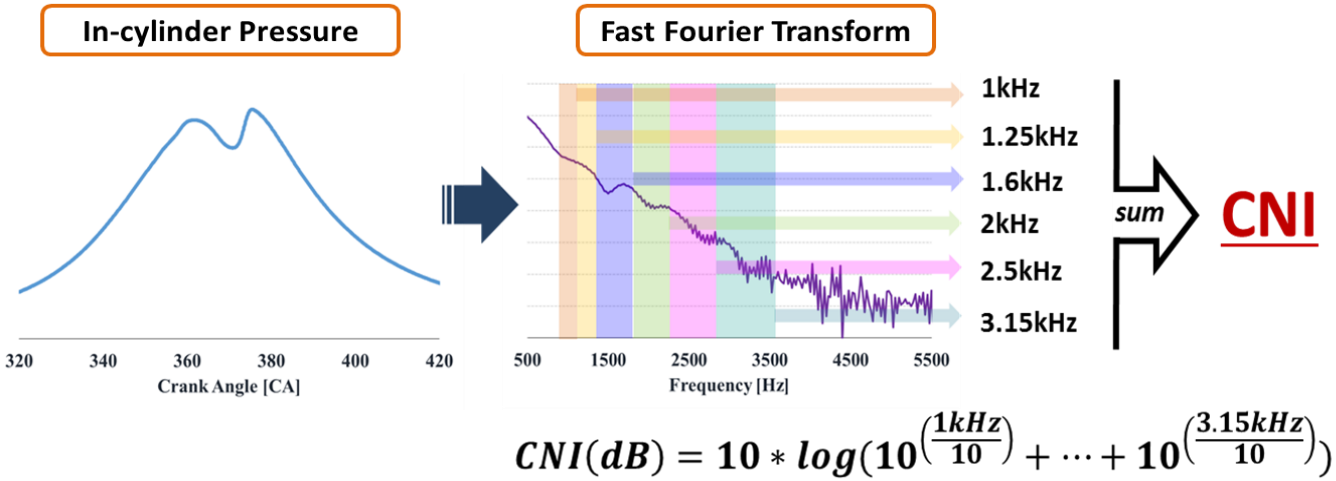

Figure 4.2.1 The schematic process of calculating the combustion noise index (CNI)

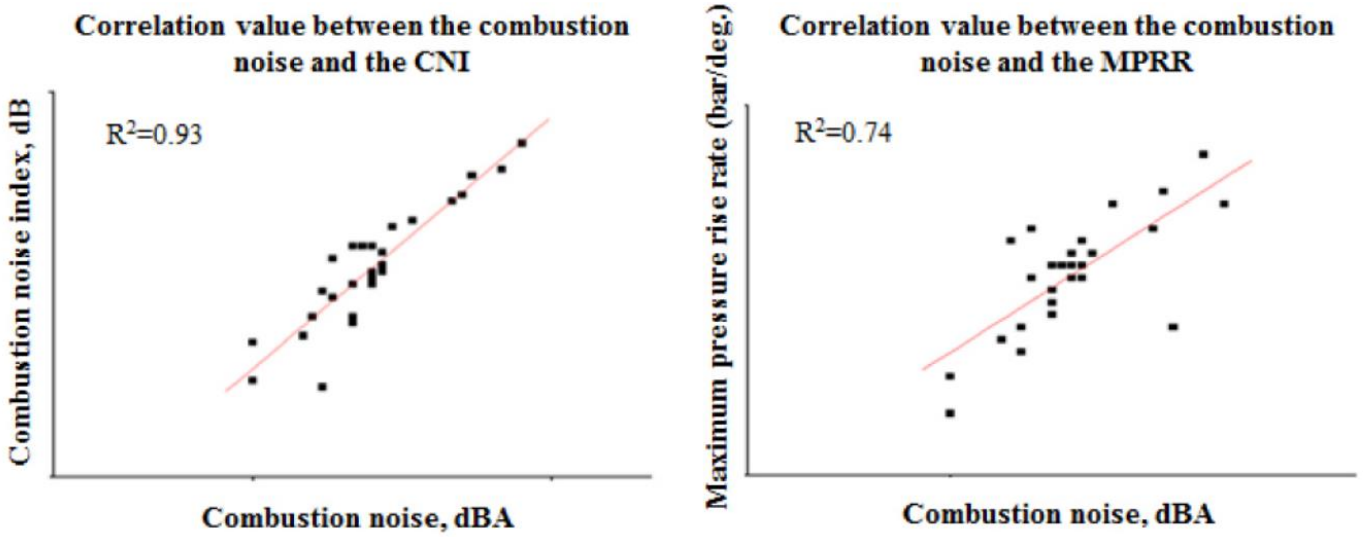

Figure 4.2.2 The measured combustion noise compared with CNI (left) and maximum pressure rise rate (right) [122]

4.3 The NOx Estimation Model

The 0-D NOx estimation model developed by Lee et al. [66, 67] was used for estimating the NOx emissions. Although the model by Lee did not include NO_2 in estimation process because the model originally a model for predicting NO, in this study, NOx was predicted and used only as a NO occurrence, ignoring the occurrence of NO2 that produced only a small amount under low load. The model was based on the extended Zeldovich mechanism expressed in the equation (4.3.1).

$$NO \ \ [ppm] = \int \left(\frac{dNO}{dt}\right)_{max} dt = \int \frac{C_1}{{T_{max}}^{1/2}} exp\left(\frac{-69090}{T_{max}}\right)[O_2]^{1/2}[N_2] \ \ dt \tag{4.3.1}$$

The gas composition in calculating the concentrations of O_2 and N_2 was calculated with the consideration of pilot burned zone. The fuel of main injection was injected into the area where the pilot is burned, so it should be assumed that the temperature was high and the oxygen concentration was lower than other in-cylinder gas conditions. The mixing of the pilot burned zone and unburned zone was assumed to be proportional to the swirl ratio and dwell time of pilot injection and main injection.

The main concept for estimating the model was that the NO formation was proportional to the maximum NO formation rate [135]. Due to the characteristics of the 0-D model which predicts physical values with one representative factor, the temperature used in the NOx model was determined to be the maximum burned gas temperature. In addition to the NO formation rate, the volume and duration for the NO formation should be considered. It was assumed that the fuel injection quantity was proportional to the product of NO formation volume and duration.

The equation (4.3.1) was converted to the equation (4.3.2) with the above assumption.

$$NO\ \ [ppm] = \frac{C_2}{{T_{max}}^{\frac{1}{2}}} exp\left(\frac{-69090}{T_{max}}\right)[O_2]^{\frac{1}{2}}[N_2] \times fuel\ \ quantity/rpm \tag{4.3.2}$$

The equation (4.3.2) calculated the NO concentration in the burned zone, so it was needed to convert the concentration in the burned zone to the concentration in total area. The concentration correction factor was used for the spatial concentration correction that was expressed in the terms of the global equivalence ratio and the ratio of the maximum temperature and the unburned gas temperature [67]. During the combustion process, NO was produced through a chemical reaction, but there was also a decomposition reaction. The activation energy constant -69090 in the equations (4.3.1) and (4.3.2) were modified to -33050 by considering decomposition reaction through the fitting of experimental results. The estimated NOx, in this study, was calculated by the equation (4.3.3).

$$NO\ \ [ppm] = \frac{C_3}{{T_{\max}}^{\frac{1}{2}}} \exp\left(\frac{-33050}{T_{\max}}\right)[\mathrm{O_2}]^{\frac{1}{2}}[\mathrm{N_2}] \times \frac{\text{Fuel quantity}}{\text{rpm}} \times \mathrm{PHI}(\emptyset) \times \frac{T_{\max}}{T_{\text{unburned}}} \tag{4.3.3}$$

The NOx emission from the test engine was used to verify the NOx estimation model. Figure 4.3.1 shows the results of the NOx model and measured NOx emissions in base cases.

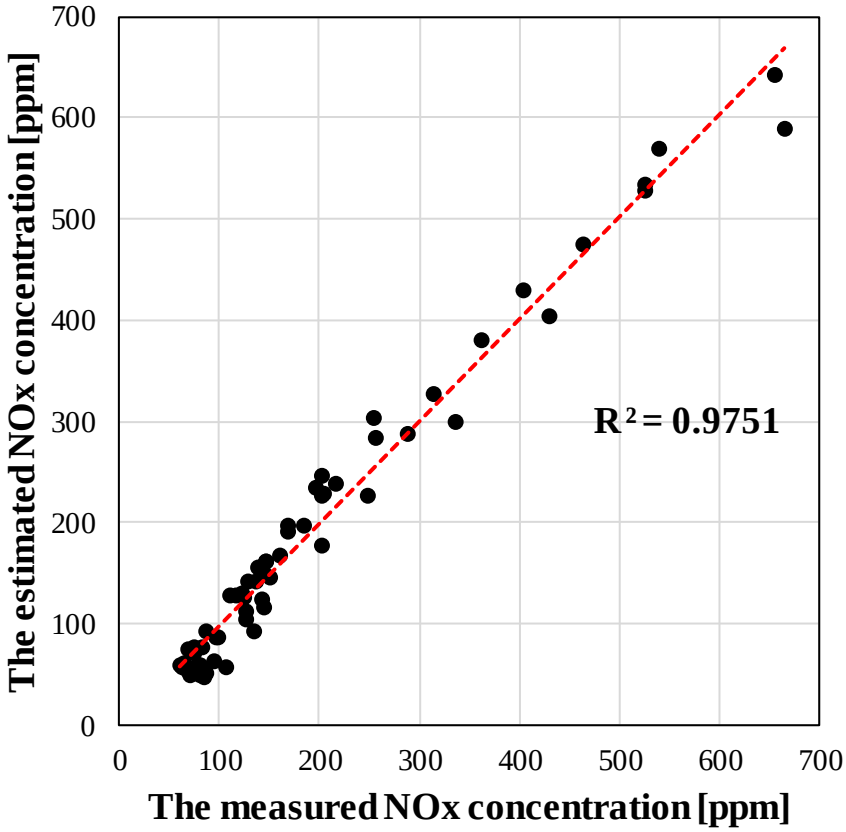

Figure 4.3.1 The comparison of the NOx results between the measured values and estimated values

Chapter 5. Combustion Design Methodology

5.1 Concept of Combustion Design Method

In the engine development process, the engine parameters were calibrated to have high thermal efficiency and exhaust performance to satisfy regulatory limit after the base hardware specification had been determined. The calibration process first determined the swing range of the target engine parameters and then generated variables swing experimental points with DOE plan. After conducting performance evaluation experiments in the range of variations of many parameters, the models for various performances were generated to find the optimal points. The optimal points were needed to evaluation process to verify the actual performance because the calibration process by DOE and most of the generated models were not based on the physical principle. The performance evaluation needed various equipment by the target performance. The fuel rate was needed to be measured accurately with a fuel flowmeter and the emissions should be measured by highly reliable measuring equipment. Especially for noise measurement, an anechoic room was needed to separate ambient noise from the equipment such as dynamometer, pumps, air conditional system and so on. These processes were repeated until satisfactory performance was achieved.

The combustion design method developed in this study can suggest the new process for the engine development. The traditional development process produced optimal performance as output after many attempts with various engine operation strategies and parameters as input. A new engine development strategy utilizing the combustion design method begin with the concept of reversing the inputs and outputs of the traditional development process. Figure 5.1.1 shows the concept for the new engine development process. The combustion design method

uses the performance of thermal efficiency, emissions and noise as the input for desired combustion. In the early stages of the combustion design, the combustion phase established by Wiebe functions or other forms goes through the design process so that the combustion phase satisfies the performance given by input.

Figure 5.1.2 shows the schematic process of the combustion design method. The combustion design process was conducted under specific fixed engine speed and fuel injection quantity. Input parameters were IMEP representing thermal efficiency, noise index, NOx and soot emissions. The parameters for building in-cylinder conditions were intake pressure, lambda and the mass fraction burned. EGR rate was determined by intake pressure and lambda. The intake air temperature, which could be changed by the cooling of the intercooler and the use of HP EGR, was fixed at room temperature (35℃). The mass burn fraction contained combustion parameters such as start of the combustion and combustion duration. The heat release rate could be derived from the mass burn fraction.

Next, the gas composition was calculated by combustion sequence. The gas composition ratio of the intake was used for polytropic index calculations. In addition, the gas composition at the start of combustion was used for calculating the maximum temperature and burned gas temperature. The in-cylinder pressure from the start of the compression stroke to the start of combustion was constructed by intake pressure and polytropic index. From the start of the combustion, the combustion pressure was shaped by solving the differential equation of the heat release rate.

The fuel injection timing was derived by calculation using the ignition delay model, not from the optimization variables. The ignition delay model allowed to calculate reversely the injection timing from the thermodynamic conditions and parameters at the start of the combustion. The developed combustion design method did not suppose a fuel injection profile. Assuming a fuel injection, the

combustion phase from the optimization was not different with that from a conventional engine, and the result will be similar with the combustion derived from the experiments.

The optimization was conducted in the direction of minimizing the objective function that was calculated from the performance of designed combustion and target values. A minimum of constrained nonlinear multivariable function (interior point) and particle swarm optimization (PSO) were used as optimization algorithms. The optimization using Wiebe function as the mass burn fraction function used the minimum of constrained nonlinear multivariable function and the optimization using other functions used PSO due to characteristics of each algorithm. Finally, the combustion phase with the closet performance to the target performance value was derived.

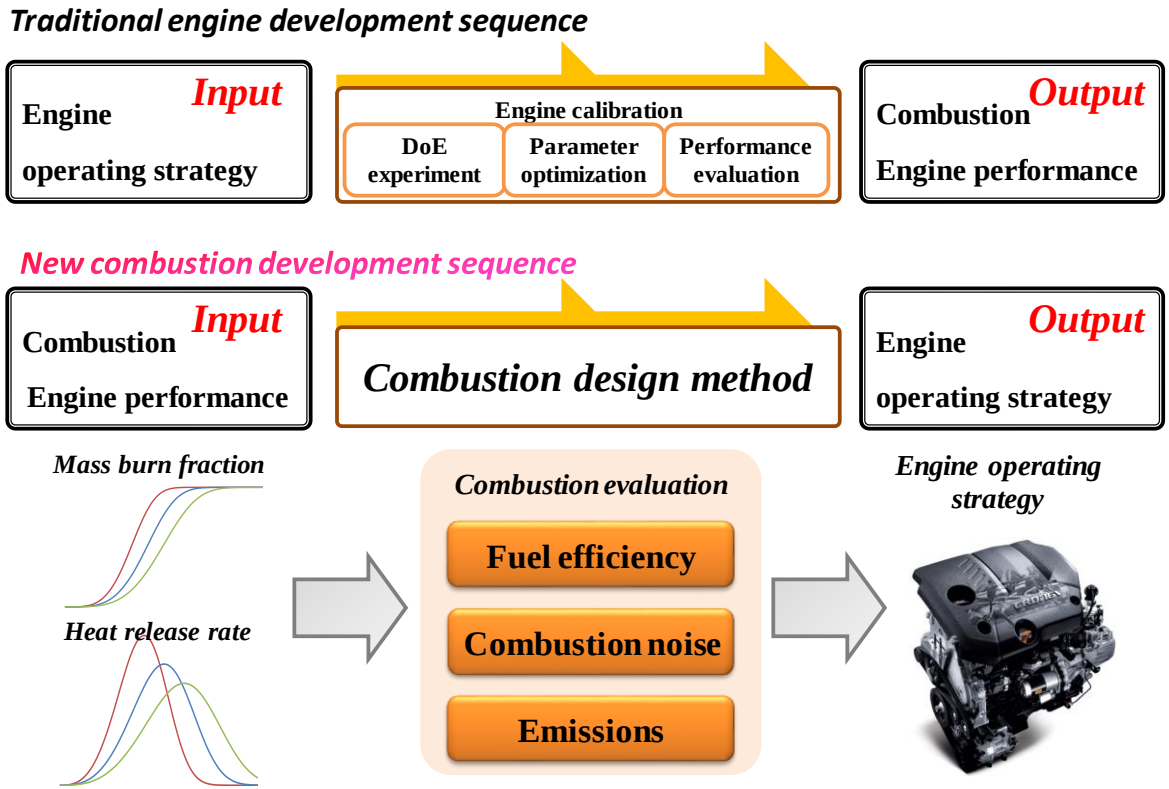

Figure 5.1.1 The concept for newly developed engine development process

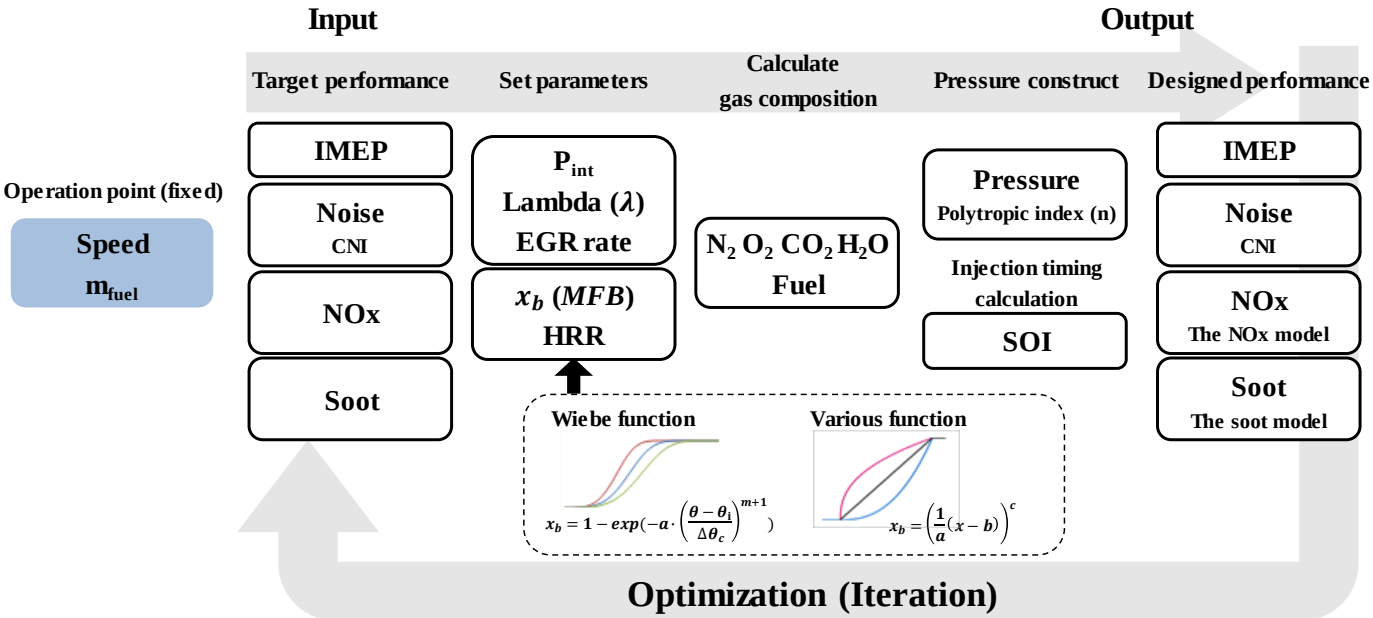

Figure 5.1.2 Schematic process of the combustion design method

5.2 Process of Constructing Combustion Pressure

5.2.1 Mass fraction burned and heat release rate

The first step in the combustion design was to set up the mass fraction burned. The MFB allowed analysis of the combustion speed and duration, and the HRR was calculated from the MFB with the cumulative heat release. In this study, the previously widely known Wiebe function and other functions as a new approach for a method of establishing MFB. Since Wiebe function could simulate general engine combustion, it could present realistic combustion phases. On the other hand, other functions were able to suggest the possibility of exploring new combustion concept, although the physical feasibility was hard to clarify.

5.2.1.1 Using Wiebe function

Wiebe function expressed the mass fraction burn developed by Wiebe and other researchers based on several chemical equations [38]. The equation (5.2.1) shows the basic form of Wiebe function where x_b is mass fraction burned, a is efficiency parameter, m is shape factor, θ is crank angle, θ_0 is start of combustion and $\Delta\theta$ is combustion duration.

$$x_b = 1 - exp(-a \cdot \left(\frac{\theta - \theta_0}{\Delta\theta}\right)^{m+1}) \tag{5.2.1}$$

Generally, the diesel combustion can be divided into three phases; the premixed combustion, the diffusion combustion and the late combustion phases. Several researches used two or three Wiebe functions to simulate diesel combustion [38, 114-117]. The pilot combustion can be expressed more simply than

main combustion because the pilot injection quantity is less than main injection and the ignition delay is longer, so most of the pilot injection is burned as premixed combustion. In this study, three Wiebe functions were used, one for the pilot combustion and two for the main combustion. Table 5.2.1 shows the parameters list in the determining the coefficients of three Wiebe functions.

The function of mass fraction burned starts from 0 and converges to 1. The heat release rate was derived from the mass fraction burned with total heat (Q_{total}) as shown in the equation (5.2.2).

$$\frac{dQ}{d\theta} = a \cdot (m+1) \cdot (\frac{Q_{total}}{\Delta\theta}) \cdot \left(\frac{\theta - \theta_0}{\Delta\theta}\right)^m \cdot \left(\exp\left[-a \cdot \left(\frac{\theta - \theta_0}{\Delta\theta}\right)^{m+1}\right]\right) \tag{5.2.2}$$

The net heat release can be obtained from the total heat release, the mass of fuel, the fuel lower heating value (LHV), and heat loss. The total heat release is reduced by heat transfer, crevice effects, and heat of vaporization and the summation becomes the net heat release. In this study, the net heat release was calculated from the difference of the total heat release and the heat loss. The model for the heat loss was obtained simply with operation parameters; engine speed and the fuel injection quantity. The equation (5.2.3) shows the heat loss equation and Figure 5.2.2 shows a comparison between the calculated total heat release and the net heat release results from the test engine experiment. The coefficients in the equation (5.2.3) were fitted by experimental data.

$$Q_{loss} = 119.16 \times Speed^{-0.57} \times m_f^{1.31} \tag{5.2.3}$$

Experimental data were represented as Wiebe function to utilize them to validate the 0-D combustion models and use as the initial values in optimization

process. Figure 5.2.3 is the fitted mass faction burned and HRR by Wiebe function at 1500rpm, BMEP 4bar. Although the peak of HRR from the Wiebe function was slightly lower than the experimental value, the overall shape was well matched with the experimental data. The lower peak was due to the use of only two Wiebe functions to simulate the main combustion. However, when the main combustion was simulated with three Wiebe functions, there were too many optimization variables compared to the gain, so the number of Wiebe function for the main combustion was maintained at two functions.

5.2.1.2 Using other functions

Much of the combustion design results were evaluated using Wiebe function, but new mass fraction burned forms were also used to suggest the combustion. There were several conditions for functions that expressed the mass fraction burned in the combustion design method.

i. The function starts from 0 and ends at 1.

ii. The function has the form of a monotonically increasing function.

iii. The start of combustion and combustion duration can be expressed with the coefficients in the function.

The condition i explains the basic characteristics for the function of mass fraction burned. The derivation of HRR was similar with Wiebe function and total heat release was also calculated and used in the same way. The condition ii refers to the basic physical law that mass fraction burned, which means the rate of combustion of fuel, cannot be reduced. The condition iii explains that the factors of the start of combustion and combustion duration needed to establish combustion model and utilize performance models. The equation (5.2.4) shows the mass fraction burned of polynomial form and Figure 5.2.4 shows the shape of

functions. In the equation (5.2.4), the coefficient $\Delta\theta$ means combustion duration, θ_0 is the start of combustion and $\theta_0 + \Delta\theta$ is the end of combustion. The shape of the function varies by the coefficient a. Basically, it has a polynomial form, so when *a* is 1, it has a simple straight line form, but if *a* is less than 1, the function has a convex form upward and a convex form downward if it is greater than 1. Table 5.2.2 shows the parameters from polynomial functions to determine the MFB.

$$x_b = \left(\frac{1}{\Delta\theta}(x - \theta_0)\right)^a \tag{5.2.4}$$

Combustion from these various functions was hard to clarify the possibility of reality and it was suggested the performances and development direction of new combustion shape.

Table 5.2.1 The parameters for determining the MFB by Wiebe function

	Parameters				
Pilot combustion	a_p	m_p	$\theta_{0,p}$	$\Delta\theta_p$	$Q_{total,p}$
1st main combustion	a_{m1}	m_{m1}	$\theta_{0,m1}$	$\Delta\theta_{m1}$	$Q_{total,m1}$
2nd main combustion	a_{m2}	m_{m2}	$\theta_{0,m2}$	$\Delta\theta_{m2}$	$Q_{total,m2}$

Table 5.2.2 The parameters for determining the MFB by polynomial function

	Parameters			
Pilot combustion	a_p	$\theta_{0,\mathrm{p}}$	$\Delta\theta_p$	$Q_{total,p}$
Main combustion	a_m	$\theta_{0,\mathrm{m}}$	$\Delta\theta_m$	$Q_{total,m}$

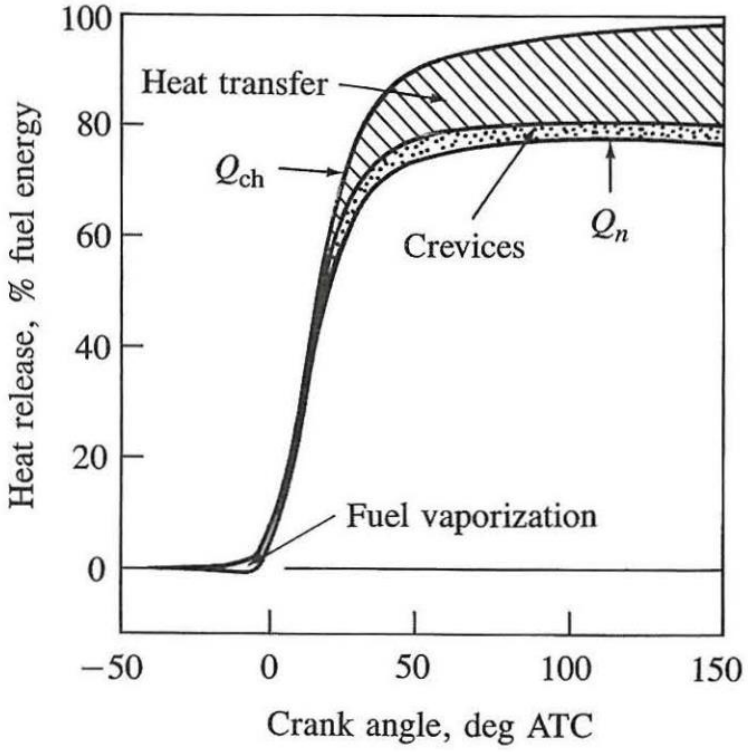

Figure 5.2.1 Heat release and losses during combustion [49]

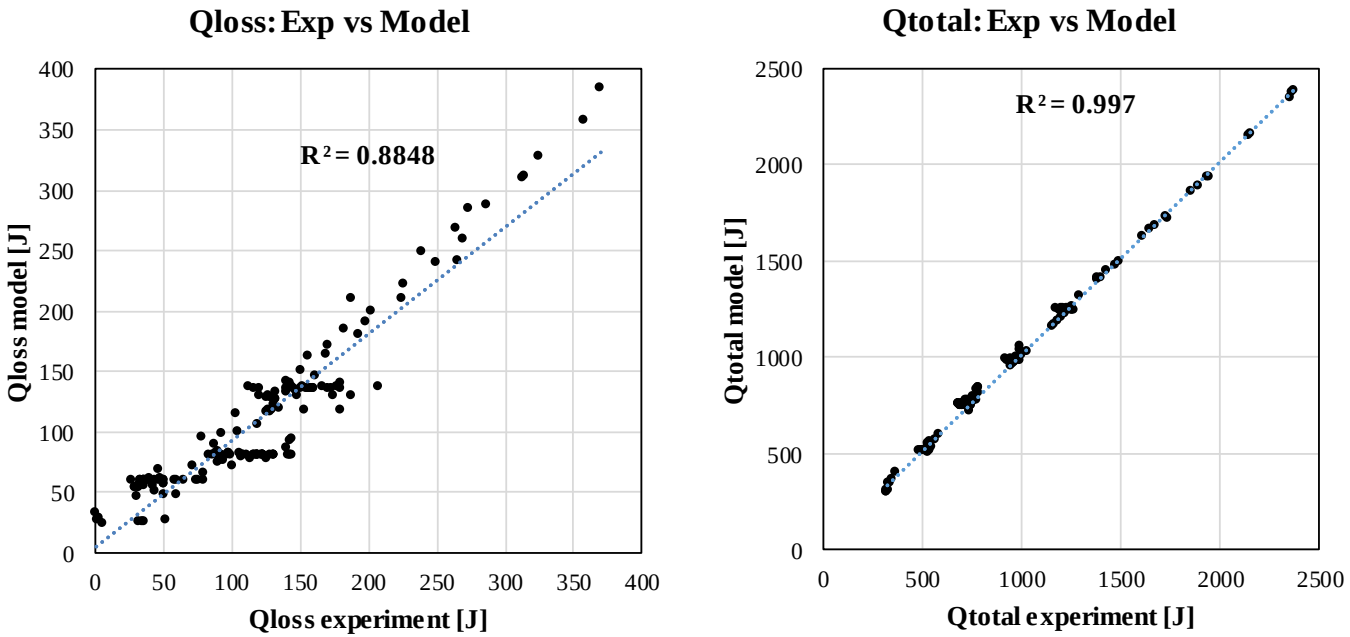

Figure 5.2.2 The results of the heat loss and total heat in 169 cases of test engine.

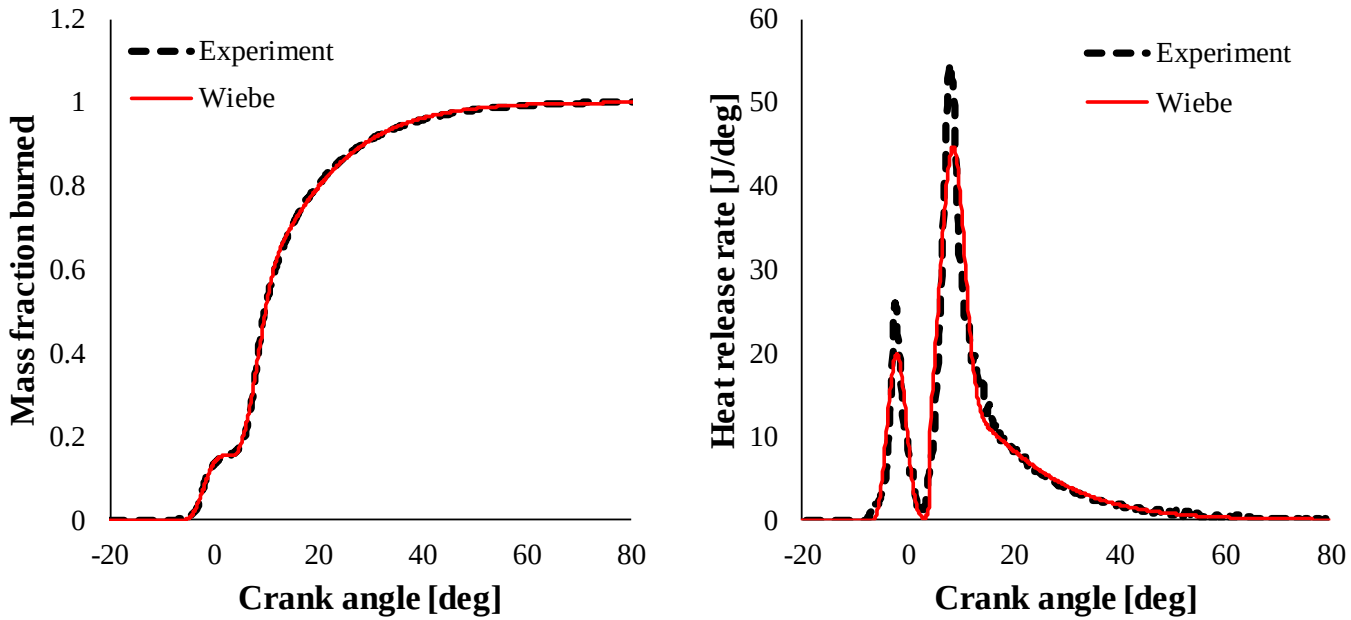

Figure 5.2.3 The mass fraction burned and heat release rate from the experiment and Wiebe function at 1500 rpm, BMEP 4bar

$$x_b = \left(\frac{1}{\Delta\theta}(x - \theta_0)\right)^a$$

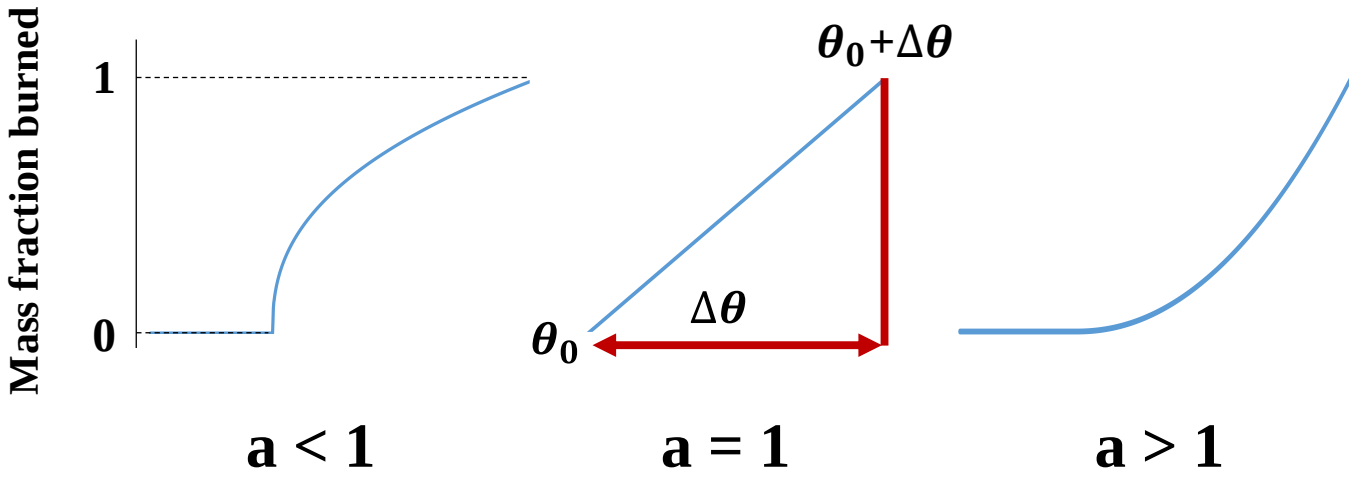

Figure 5.2.4 The function of mass fraction burned using the polynomial form

5.2.2 Calculation of in-cylinder air flow and EGR rate

The process of obtaining the correct in-cylinder air mass in the 0-D combustion model is important because it is fundamental to obtaining thermodynamic parameters and ensuring reliability and accuracy when calculating the performance models. Previous researches [136, 137] used the delta-p method to estimate in-cylinder air mass. The delta-p method used the pressure at two points in the compression process. By using the pressure and volume at the two points, the trapped mass could be derived with the ideal gas law. In this study, it was impossible to apply the delta-p method because the pressure was unknown in the initial step. From the ideal gas equation with the intake pressure and temperature, the cylinder trapped mass was obtained.

The intake system such as the air filter, intake manifold, intake valve has a resistance that prevents the air from entering the cylinder. The volumetric efficiency (η_v) is the parameter of the effectiveness of an engine's induction process. The volumetric efficiency is influenced by a variety of factors as well as speed and load. The design of the intake system, along with engine operating variables such as intake air temperature and pressure, ratio of intake and exhaust pressure, compression ratio, and characteristics of intake and exhaust valves, is also an influential parameter. In addition, dynamic effects, such as friction losses, ram effect, and reverse flow of in-cylinder air are also compounded in the volumetric efficiency. The volumetric efficiency was used as map-based data acquired by engine manufacturers in advance, rather than individually identifying and quantifying multiple complex effects. Figure 5.2.5 shows a map of the normalized volumetric efficiency for the test engine. Combining the ideal gas equation and volumetric efficiency, the equation for the estimating trapped mass with initial condition has a form as shown in the equation (5.2.5). Figure 5.2.6

shows the result of the trapped mass from the equation (5.2.5) and from the EMS that calculated as the sum of the fresh air mass and EGR.

$$PV = \frac{m}{\eta_v M} RT \tag{5.2.5}$$

where P is the intake pressure, V is the volume at bottom dead center (BDC), T is the intake temperature, m is the in-cylinder mass and M is the molar mass of air.

Prior to calculating the EGR rate from the above parameters, in this study, EGR system was assumed to use only LP EGR. The HP EGR has disadvantages of the higher temperature at mixing with fresh air, loss of the enthalpy in exhaust gas that leads to loss of thermal efficiency. Modern engines used more LP EGR than HP EGR in the fraction of EGR systems due to the above reasons, and HP EGR is mainly used for specific purposes at cold start sequence and warm-up of aftertreatment system. The EGR rate can be estimated from the calculated in-cylinder air mass and lambda using the equation of combustion expressed in the equations (5.2.6) – (5.2.10).

$$C_x H_y + \lambda\gamma(O_2 + \psi N_2) + EGR(aO_2 + bN_2 + cCO_2 + dH_2O) \rightarrow aO_2 + bN_2 + cCO_2 + dH_2O \tag{5.2.6}$$

$$a = \gamma(\lambda - 1)/(1 - EGR) \tag{5.2.7}$$

$$b = \gamma\lambda\psi/(1 - EGR) \tag{5.2.8}$$

$$c = x/(1 - EGR) \tag{5.2.9}$$

$$d = y/(2(1 - EGR))$$

(5.2.10)

where x and y are the composition ratio of the fuel, λ is lambda determined in initial step, γ is equal with $x + y/4$, ψ is the constant of 3.773 and a, b, c, d are the mole number expressed by λ, γ, x, y and EGR [138].

The left terms in the equation (5.2.6) are the composition of in-cylinder mixture. Among them, the terms of $\lambda\gamma(O_2 + \psi N_2) + EGR(aO_2 + bN_2 + cCO_2 + dH_2O)$, excluding fuel, represent the composition of gas mixed with fresh air and EGR. The ratio of the total mole number of the equation (5.2.6) from the mass and the molar weight of fuel can be obtained, and the mole number of the gas can be calculated from the chemical equation as molar weight and the equation of mole number from the trapped air mass. It is expressed in the equation (5.2.11). The EGR rate was expressed as the equation (5.2.12) using lambda, the in-cylinder mass and coefficients by combination with the equations (5.2.7) – (5.2.11).

$$\lambda\gamma\left(M_{O_2} + \psi M_{N_2}\right) + EGR\left(aM_{O_2} + bM_{N_2} + cM_{CO_2} + dM_{H_2O}\right) = \frac{m_{cyl}}{1000} \times \frac{1}{M_{fuel}}$$

(5.2.11)

where M_X means the molar weight of X and m_{cyl} is the in-cylinder air mass.

$$EGR\ rate = \frac{\frac{m_{cyl}}{1000} \times \frac{1}{M_{fuel}} - \lambda\gamma\left(M_{O_2} + \psi M_{N_2}\right)}{\left(\gamma(\lambda - 1)M_{O_2} + \gamma\lambda\psi M_{N_2} + xM_{CO_2} + \frac{y}{2}\ M_{H_2O}\right) + \frac{m_{cyl}}{1000} \times \frac{1}{M_{fuel}} - \lambda\gamma\left(M_{O_2} + \psi M_{N_2}\right)}$$

(5.2.12)

The EGR calculated from the equation (5.2.12) showed offset compared with the measured EGR rate from experimental data, which was an error due to the residual gas. Diesel engines had a lower proportion and small deviation of residual gas according to the operating area because of their high compression ratio and turbo-charged intake pressure. In this study, the residual gas fraction was considered as a constant of 6% regardless of operating area and conditions. Figure 5.2.7 shows the comparison of the calculated EGR rate considering residual fraction and the measured EGR rate from the experiment.

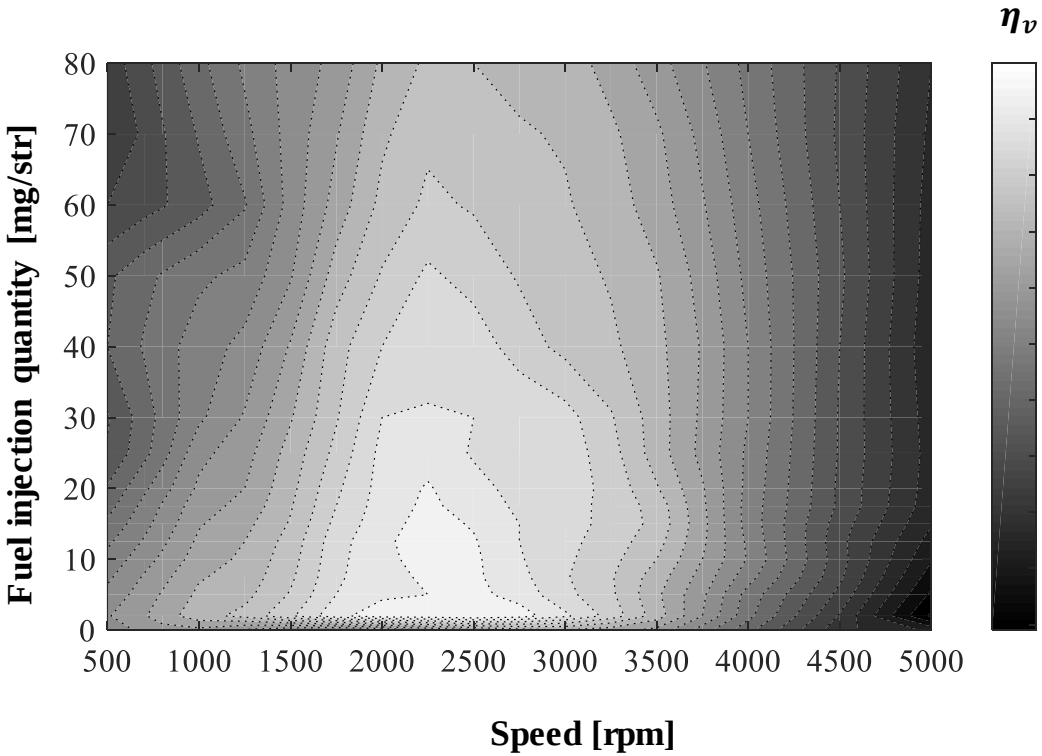

Figure 5.2.5 The volumetric efficiency map of the test engine

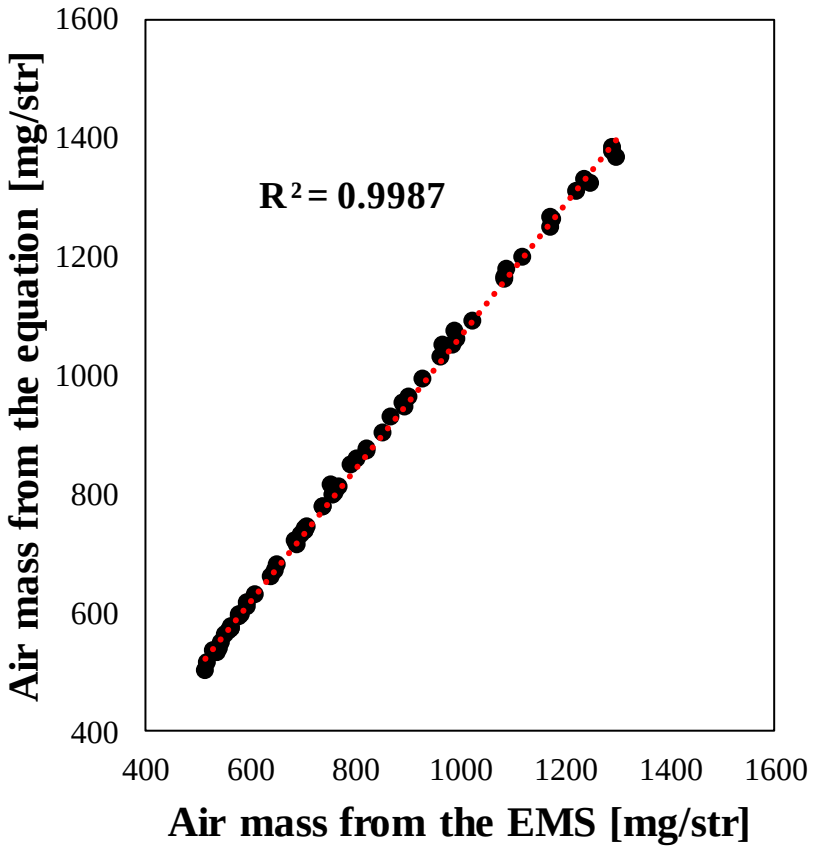

Figure 5.2.6 The trapped air mass from the EMS and equation (5.2.5)

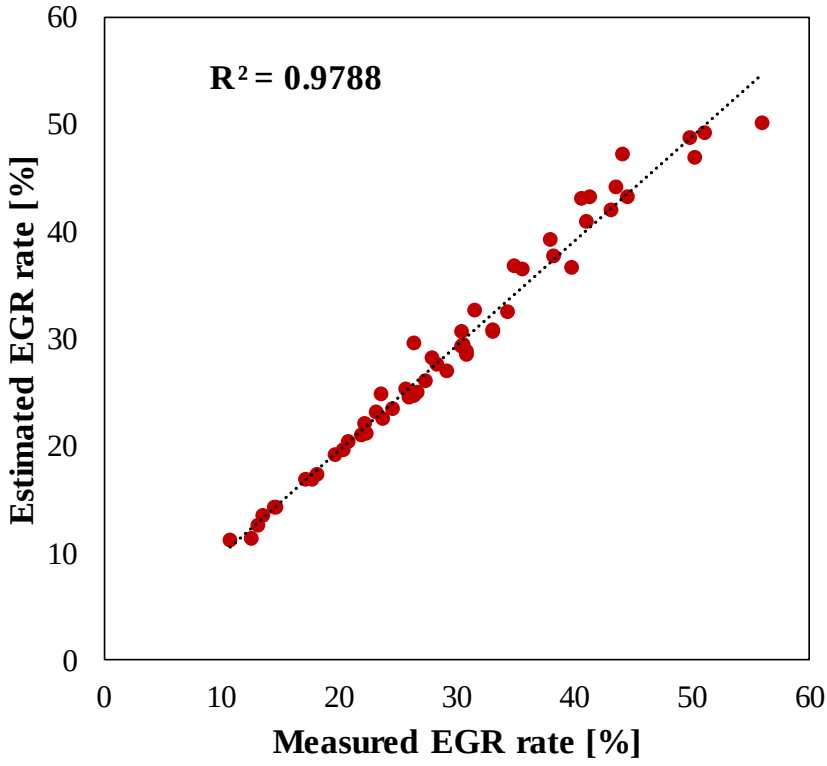

Figure 5.2.7 The EGR rate calculation results compared with the experimental data

5.2.3 Gas composition during the combustion process

The gas composition during the combustion process was an essential condition for the thermodynamic properties such as temperature and heat capacity. The properties were used in calculation of adiabatic temperature, polytropic index and other parameters. When obtaining the adiabatic temperature, the gas composition calculated the fuel concentration assumed to be a stoichiometric condition for oxygen concentration. Basically, the average temperature in the cylinder during the combustion was calculated from the ideal gas equation. At the start of combustion, the unburned gas temperature was calculated by the equation (5.2.13) where m_{SOC} is the mass at the start of combustion including the fuel mass.

$$T_{SOC} = \frac{P_{SOC} V_{SOC}}{m_{SOC} R} \tag{5.2.13}$$

The adiabatic temperature (T_{ad}) was calculated using Cantera under the gas composition and thermodynamic conditions such as the unburned gas temperature at SOC. The 0-D NOx model used the maximum burned gas temperature as one of the index for NOx formation rate. It was assumed that the maximum burned gas temperature occurred where the pressure was maximized. Then, the maximum burned gas temperature was calculated by using the adiabatic temperature at SOC as shown in the equation (5.2.14) where k is the polytropic index. .

$$T_{max,burned} = T_{ad,SOC} \times \left(\frac{P_{max}}{P_{SOC}}\right)^{\frac{k-1}{k}} \tag{5.2.14}$$

5.2.4 Polytropic index and constructing cylinder pressure

To construct the pressure precisely during the compression stroke, the polytropic index was important factor by the in-cylinder conditions. The estimation method for the polytropic index developed by Lee and Min [68] considered the heat loss during the compression stroke and the correlation of compression ratio and polytropic index. The polytropic index in this study was calculated by the equation (5.2.15) [68] where n_{isen} is the polytropic index in isentropic process, Q_{loss} is heat loss and S is the degree of decrease in n with the increase of heat loss. The parameter S was calculated by the inverse proportional to compression ratio during the compression stroke as shown in (5.2.16) where c is the constant. The isentropic index (n_{isen}) was obtained by the fitted equation of temperature (T), heat specific ratio (γ) and compression ratio. The fitted form is shown in the equation (5.2.17). The heat loss term was calculated by the equation (5.2.17) by considering the heat convection coefficient (h) and engine speed. In the sequence of calculating the polytropic index, the gas composition calculated by EGR rate and lambda, and initial pressure were used.

$$n = n_{isen} + \frac{Q_{loss}}{T} \times S \tag{5.2.15}$$

$$S = -\frac{\mathrm{c}}{R_{c.comp.}} \tag{5.2.16}$$

$$n_{isen} = A_1 \times T^{-A_2} \times \gamma^{A_3} \times R_{c.comp.}^{-B_4} \tag{5.2.17}$$

$$Q_{loss} = \frac{C_0 \times h \times (T - T_0)}{Speed \times m} - C_1$$

(5.2.18)

The in-cylinder pressure construct process started from the intake pressure. The intake pressure was compressed from the IVC point to the SOC point determined by the MFB with the calculated polytropic index. After the SOC, the combustion phase started with the previously established MFB. The heat release rate was available to obtain in the preceding phase from the determined MFB, which had the meaning of cumulative heat release. A principle of calculating heat release rate from combustion pressure was the apparent net heat release rate equation that is shown in the equation (5.2.19). Solving the equation (5.2.19) can derive pressure from heat release rate. Therefore, the combustion pressure during the combustion duration from SOC to end of combustion (EOC) was constructed by a solution of the differential equation with the pressure at the end of compression stroke as the initial value.

$$\frac{\mathrm{dQ}}{dt} = \frac{\gamma}{\gamma - 1} P \frac{dV}{dt} + \frac{1}{\gamma - 1} V \frac{dP}{dt}$$

(5.2.19)

After the combustion, in expansion stroke, the in-cylinder pressure was calculated by the polytropic process in the same way as the compression stroke. The in-cylinder pressure was constructed through the above sequences and used to calculate the models for each performance. Figure 5.2.9 shows schematic whole processes of pressure construction.

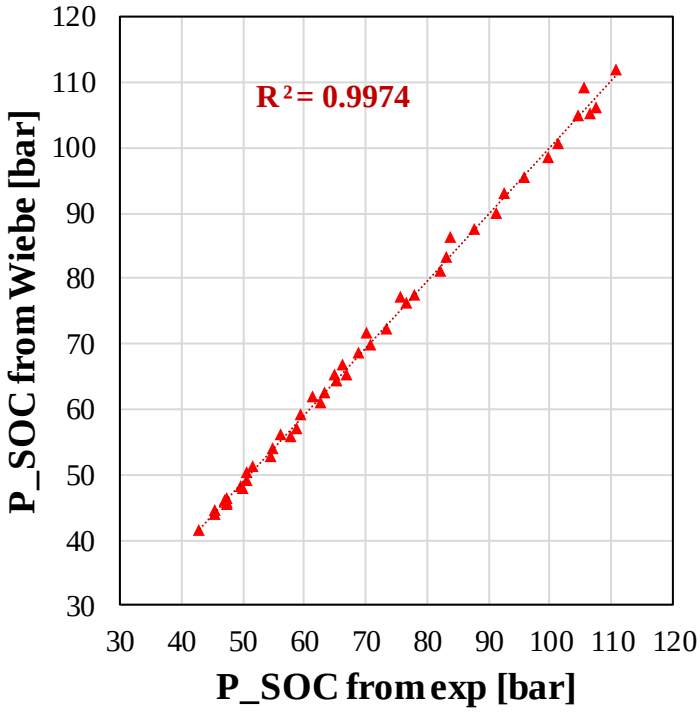

Figure 5.2.8 The pressure at SOC from Wiebe function calculated by modeled n.

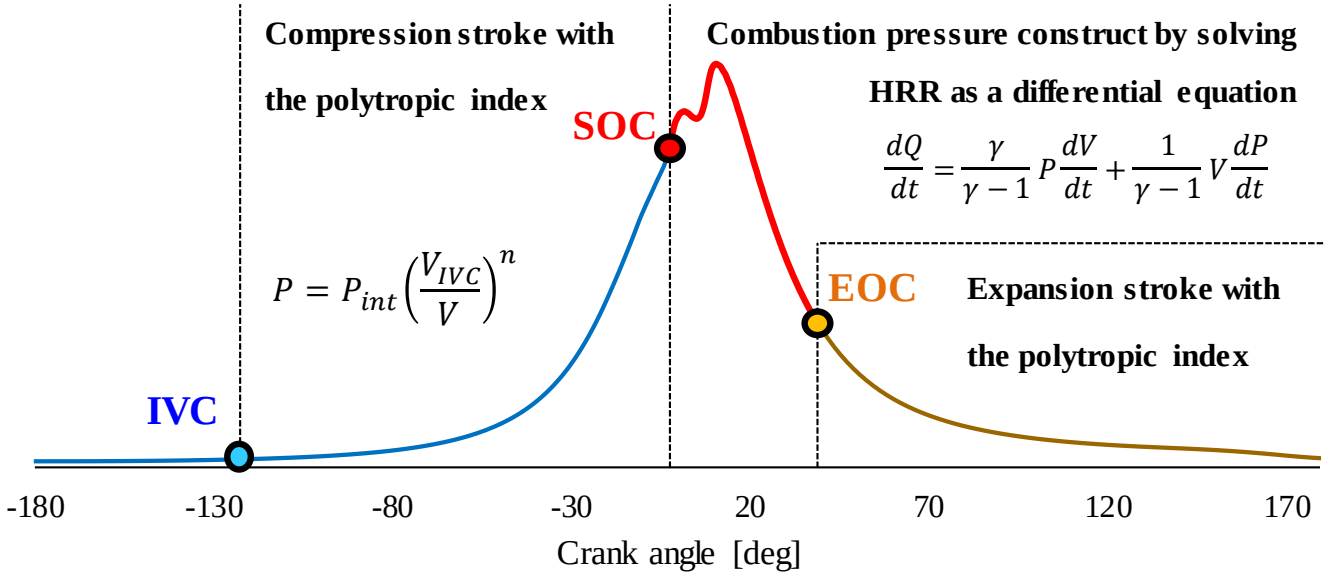

Figure 5.2.9 Schematic process of in-cylinder pressure construct

5.2.5 Calculation of the fuel injection timing

Through the preceding processes, the combustion pressure was finally built. Thermal efficiency, noise and exhaust emissions could be calculated with to input variables, parameters derived by the gas composition and thermodynamic conditions, and estimated in-cylinder pressure during combustion. However, since the combustion model presented in this study did not consider the injection parameters, so the timings of the pilot and main injection that required for NOx and soot models should be provided. If the injection required for the exhaust model was replaced by the start of combustion, the main injection had ignition delay of less than 5 degrees, so there was a small difference in timing, but the difference in the temperature and pressure at the start of combustion caused a non-negligible error in the NOx and soot model results.

In this study, the injection timing was derived from the thermodynamic conditions at the start of combustion. Generally, the ignition delay models estimated the start of combustion timing by the pressure and temperature at the injection timing based on the characteristics of autoignition. The widely used ignition delay relationships in autoignition is the equation (5.2.20) [49] where τ_{id} is the ignition delay, E_A is an activation energy for the autoignition, $\tilde{R}$ is the universal gas constant, and A and n are the constants.

$$\tau_{\mathrm{id}} = Ap^{-n}\exp(\frac{E_A}{\tilde{R}T}) \tag{5.2.20}$$

The ignition delay models including the equation (5.2.20) did not consider the oxygen concentration in the pilot burned zone that was important concept in multiple injection engines. The ignition delay model developed by Lee et al. [139]

applied the swirl factor to consider the oxygen concentration in the pilot burned zone. The concept was that the entrained unburned gas into the pilot burned zone was proportional with the multiplication of swirl ratio, the separation time of pilot and main injection, and engine speed. The atomization and vaporization effects was also considered as the rail pressure and hole size of the injector. The equation (5.2.21) shows the ignition delay model [139] used in this study where A, x_n were the coefficients, m_{pilot} is the pilot injection quantity and P_{rail} is the injection pressure.

$$Ignition\ \ delay = A \times \rho_{SOI}^{x_1} \times exp\left(\frac{2100}{T_{SOI}}\right) \times O_{2,SOI}^{x_2} \times m_{pilot}^{x_3} \times \left(\frac{P_{rail}}{hole\ \ size}\right)^{x_4} \quad (5.2.21)$$

The thermodynamic properties used in the ignition delay model were represented based on the fuel injection timing. However, the injection parameters except the mass of fuel were not presented in the combustion design method. The start of combustion and combustion duration were determined by the function that expressed mass fraction burned. Therefore, it was established the inverse calculation method to predict the injection point from the parameters and thermodynamic properties at the start of the combustion. The oxygen concentration at the start of the combustion was the same with that at the injection timing. The density (ρ_{SOI}) and temperature (T_{SOI}) at the injection timing was calculated by the equations (5.2.22) and (5.2.23). The mass of the in-cylinder mixture at the two points was the same, so the densities could be expressed in terms of their relationship with volume. The temperature at the injection timing was derived from the polytropic process.

$$\rho_{SOI} = \rho_{SOC} \frac{V_{SOC}}{V_{SOI}} \quad (5.2.22)$$

$$T_{SOI} = T_{SOC}\left(\frac{V_{SOI}}{V_{SOC}}\right)^{1-n}$$

(5.2.23)

The equation (5.2.4) was derived by substitution of the equations (5.2.22) and (5.2.23) into the equation (5.2.21). The ignition delay model modified with the thermodynamic properties at the start of combustion and the unknown parameter was only the volume at the injection timing. To find the injection timing from the modified ignition delay model, the ignition delay candidates at each crank angle before the start of combustion and the ignition delay values from the model by using the volume at each crank angle were compared. The point where the two values met could be determined as the injection timing. The schematic principle of the above process is shown in Figure 5.2.10.

$$ID = A \times \left(\rho_{SOC} \times \frac{V_{SOC}}{V_{SOI}}\right)^{x_1} \times exp\left(\frac{2100}{T_{SOC}} \times \left(\frac{V_{SOC}}{V_{SOI}}\right)^{1-n}\right) \times O_{2,SOC}^{x_2} \times m_{pilot}^{x_3} \times \left(\frac{P_{rail}}{hole\ size}\right)^{x_4}$$

(5.2.24)

The injection timing from the modified ignition delay model was estimated about main injection and pilot injection. The application of the model at each injection had difference in the terms of the pilot injection quantity (m_{pilot}) and the oxygen concentration ($O_{2,SOC}$). When applying the model for pilot injection, the pilot injection quantity term was ignored because there was no preceding fuel injection and combustion. In the case of the oxygen concentration, average oxygen concentration was used for pilot injection, and the oxygen concentration in pilot burned zone was used for main injection. Figure 5.2.11 and Figure 5.2.12 show the estimated results of the ignition delay and injection timing from the modified ignition delay model using parameters of SOC conditions.

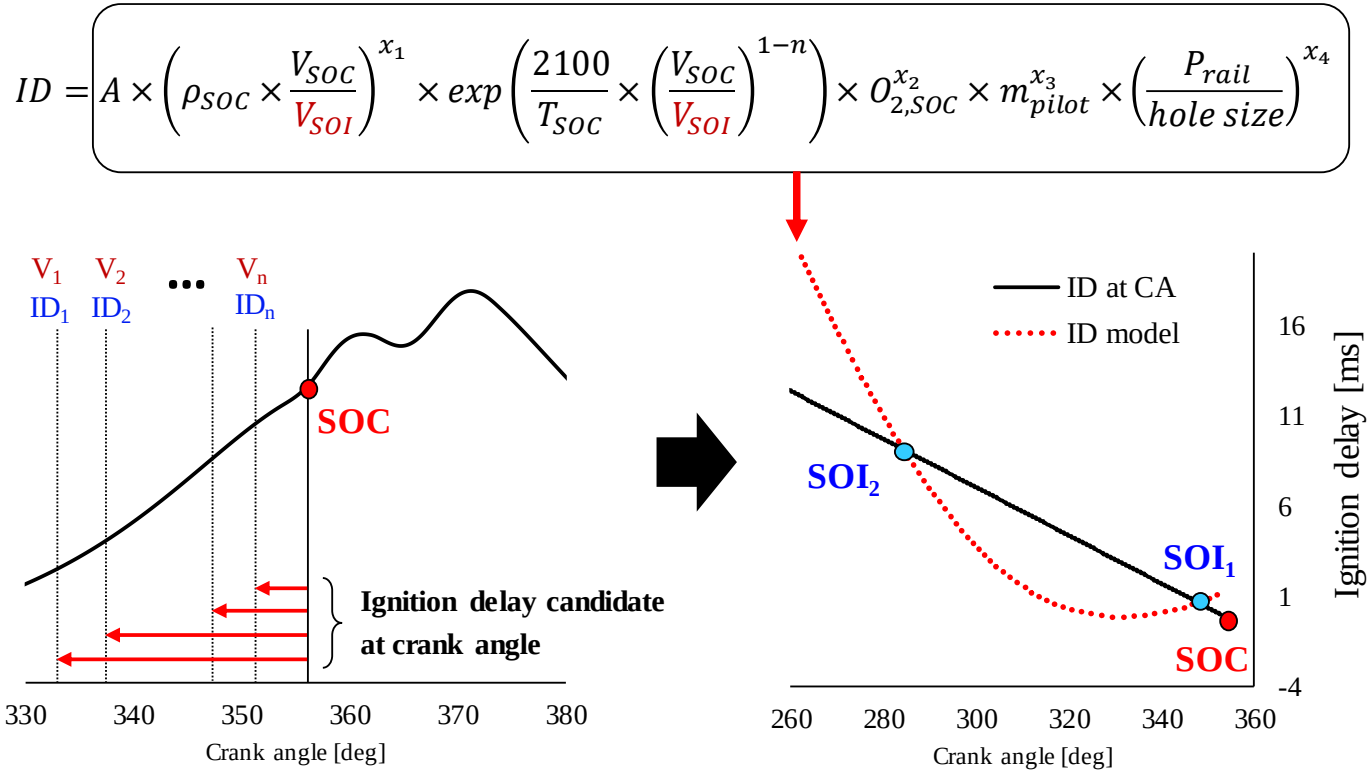

Figure 5.2.10 Schematic process to calculate the injection timing from the modified ignition delay model

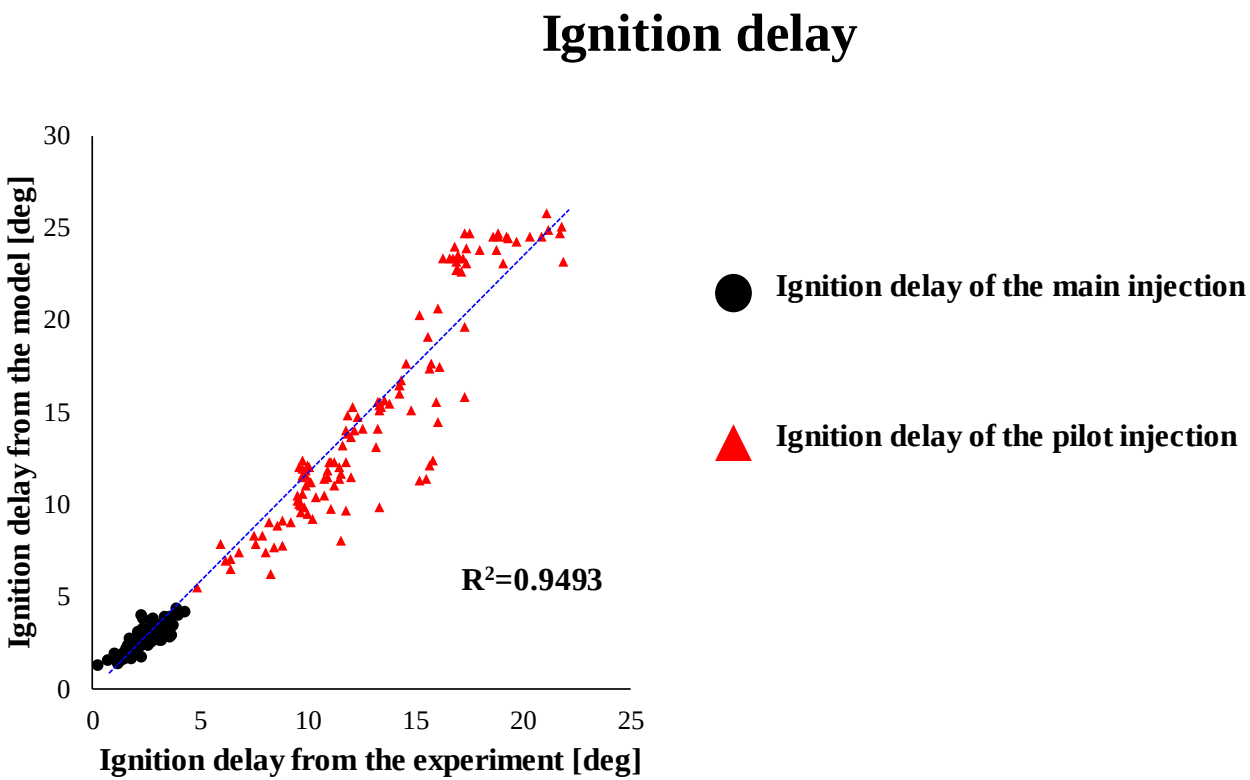

Figure 5.2.11 Estimated ignition delay from the modified ignition delay model

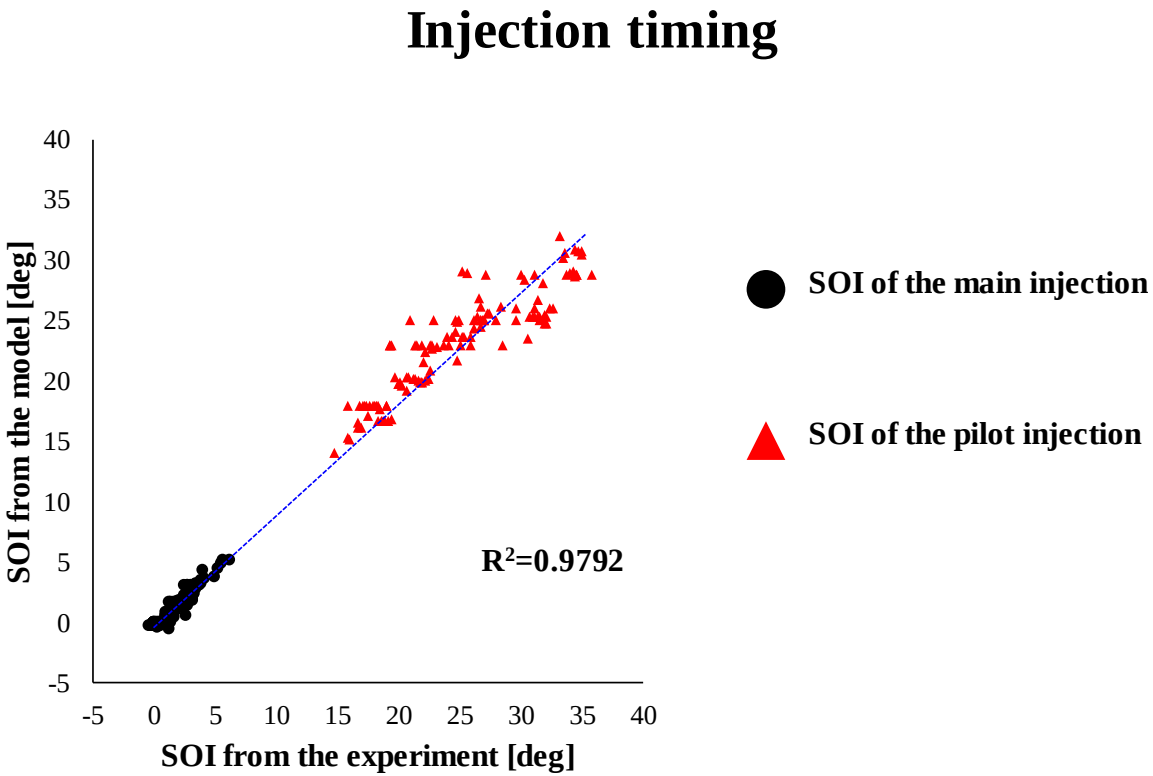

Figure 5.2.12 Estimated injection timing from the modified ignition delay model

5.3 Optimization Methodology

As a final step in the combustion design, the optimization was conducted to derive combustion phases with target performance. The variables subject to optimization were the coefficients used in determining mass fraction burned, intake pressure and lambda. The MATLAB was used for optimization. All processes were coded for the combustion design, such as the previously described combustion pressure construction, IMEP calculation, combustion noise index calculation, and the emission models for each iteration sequence during the optimization.

5.3.1 Optimization algorithms

The optimization algorithm provides specific principles and methods for finding optimization variables with minimum objective functions. The optimization algorithms used in the combustion design were a minimum of constrained nonlinear multivariable function (interior-point) and particle swarm optimization.

The interior-point method is one of the most widely used algorithms in optimization studies. The algorithm solved a sequence of approximate minimization problems. During the iteration, the algorithm directs the objective function to a feasible region and optimizes it using the conjugate gradient to minimize. The algorithm uses the gradient during the iteration to find optimized solution, it is easy to find local optimized point and highly sensitive to initial values. Therefore, in order to obtain a good optimal value, it is necessary to

intuitively grasp the determination range of optimization variables when determining the initial value. On the other hand, due to the low load of calculations, the convergence takes a short time. In this study, a minimum of constrained nonlinear multivariable function (interior-point) was used when the mass fraction burned was determined by Wiebe function. Wiebe function had many parameters and specific boundary for appropriate combustion phase. When the mass fraction burned was defined by Wiebe function, the interior-point algorithm allowed convergence results to be sensitive to initial values but with a physics-based combustion form in boundary conditions and constraints.

The particle swarm optimization is based on the algorithm suggested by Kennedy and Eberhart [140]. The particle swarm optimization begins by creating initial particles in space within boundary conditions and determining initial velocity. The objective function values are calculated at each location of the initial particle and the optimal point is determined. In the next iteration, the location and velocity in the next step are determined by considering the location and objective performance of the neighbors based on the current speed and location. The performance at the determined location is evaluated and conducted iteration through a series of processes to find the optimal point. Figure 5.3.1 shows the particles of lambda and intake pressure during the optimization using PSO. The PSO optimizes by distributing particles in space within boundary conditions of optimization variables. Therefore, the PSO does not specify an initial value. The algorithm has less risk of finding local minimum, but has larger computation load. In the combustion design, the PSO was used to optimize the combustion determined from the various MFB functions. The other MFB functions had lower coefficient than Wiebe function for determining the shape and there was no intuition for initial values because they were not physically known and experimentally uncertain to implement.

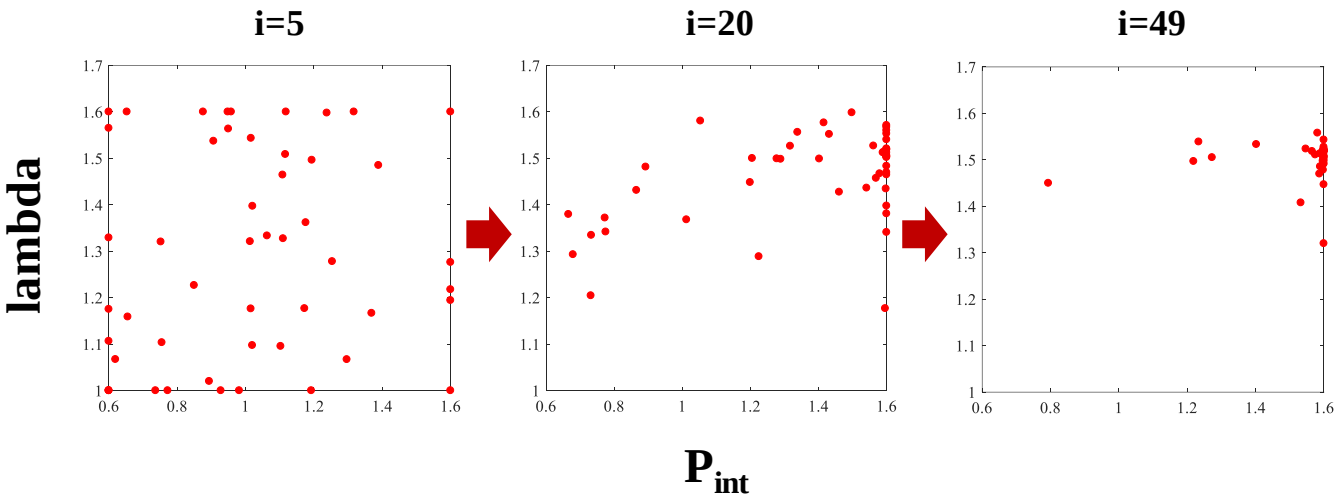

Figure 5.3.1 The particles positions of intake pressure and lambda using particle swarm optimization.

5.3.2 Boundary conditions and constraints

In the optimization of nonlinear programming solver, the problem is defined as the equation (5.3.1).

$$\min_{x} f(x) \text{ such that } \begin{cases} A \cdot x \leq b \\ Aeq \cdot x = beq \\ c(x) \leq 0 \\ ceq(x) = 0 \\ lb \leq x \leq ub \end{cases} \tag{5.3.1}$$

where x is the solution of optimization parameter, $f(x)$ is the objective function, lb and ub are the boundary conditions, and A, Aeq, b, beq, c and ceq are the matrices and vectors for constraints.

The A and b are linear inequality constraints. Linear inequality constraints decided the inequality relationship between the parameters. The optimization using Wiebe function had the linear inequality constraints as shown in the equations (5.3.2) – (5.3.5) that represented the order of pilot and main injections, and the pilot fuel injection quantity limit. The constraints of the equations (5.3.2) – (5.3.5) helped efficient iteration of variables.

$$\theta_{0,p} - \theta_{0,m1} \leq 0 \tag{5.3.2}$$

$$\theta_{0,m1} - \theta_{0,m2} \leq 0 \tag{5.3.3}$$

$$Q_{total,p} - Q_{total,m1} \leq 0 \tag{5.3.4}$$

$$Q_{total,p} - Q_{total,m2} \leq \ 0$$

(5.3.5)

The Aeq and beq are the constraints for linear equality constraints. Similar with inequality constraints, linear equality constraints determined the equality correlation of the parameters. There was a one linear equality constraint for the optimization that the sum of the heat of each MFB function was equal to the calculated heat output from the fuel injection quantity. At one operation point, the total fuel injection quantity was fixed as a constant, but during the optimization, each injection quantity was determined by this equality condition. The equation (5.3.6) shows the linear equality constraint used in the optimization.

$$Q_{total,p} + Q_{total,m1} + Q_{total,m2} = Q_{total}$$

(5.3.6)

The c and ceq are the nonlinear inequality and equality constraints. The constraints that are hard to express with linear equations are determined by nonlinear constraints. In this study, the EGR rate was determined from the intake pressure and lambda, so it was impossible to designate the parameter for constraint and determine the boundary condition using lb and ub. In terms of the limitation of the difference between intake pressure and exhaust pressure, and the geometric characteristics of intake and exhaust paths, the EGR rate was limited. It was decided not to exceed 15% higher from the base EGR rate through the nonlinear inequality constraint. The equation (5.3.7) shows the nonlinear constraint for EGR rate.

$$\frac{\frac{m_{cyl}}{1000} \times \frac{1}{M_{fuel}} - \lambda\gamma\left(M_{O_2} + \psi M_{N_2}\right)}{\left(\gamma(\lambda-1)M_{O_2} + \gamma\lambda\psi M_{N_2} + xM_{CO_2} + \frac{y}{2}\ M_{H_2O}\right) + \frac{m_{cyl}}{1000} \times \frac{1}{M_{fuel}} - \lambda\gamma\left(M_{O_2} + \psi M_{N_2}\right)} \leq EGR_{base} + 15\%$$

(5.3.7)

Constraints were needed to optimization for desired process of iteration in the appropriate range of parameters. However, the optimization using the PSO as optimization algorithm was impossible to set constraint. To apply the constraint in the optimization, the constraints were augmented in the objective function as a penalty function. The augmented constraint was the limitation of EGR rate.

The lb and ub are the boundary conditions for the optimization variables. The parameters for the MFB from Wiebe function was determined as the wider range of the representative conventional combustion. The accumulative heat release from the pilot injection was limited to the half of total heat. The upper boundary condition for intake pressure was also limited to not exceed 0.5 bar higher than the base intake pressure. In the optimization process using the PSO as optimization algorithm, the linear equality constraint for the total heat was impossible, so the parameter r was added that meant the ratio of heat from the pilot injection of the total heat and the upper boundary for the r was set to 0.5. Table 5.3.1 and Table 5.3.2 show the lower and upper boundary conditions for the optimization using Wiebe function and polynomial function.

Table 5.3.1 The lower and upper boundary conditions for the optimization variables using Wiebe function

Parameters	a_p	m_p	$\theta_{0,p}$	$\Delta\theta_p$	$Q_{total,p}$	a_{m1}	m_{m1}	$\theta_{0,m1}$	$\Delta\theta_{m1}$	$Q_{total,m1}$
lb	0.1	0.01	-30	0.2	0	0.1	0.01	-20	0.2	0
ub	50	5	20	60	$\frac{Q_{total}}{2}$	50	5	20	80	Q_{total}

Parameters	a_{m2}	m_{m2}	$\theta_{0,m2}$	$\Delta\theta_{m2}$	$Q_{total,m2}$	P_{in}	λ
lb	0.1	0.01	-10	0.2	0	0.6	1
ub	50	5	50	100	0	Base+0.5	2

Table 5.3.2 The lower and upper boundary conditions for the optimization variables using polynomial function

Parameters	a_p	$\theta_{0,p}$	$\Delta\theta_p$	$\boldsymbol{Q_{total,p}}$	a_m	$\theta_{0,m}$	$\Delta\theta_m$	$\boldsymbol{Q_{total,m}}$	**r**	$\mathbf{P_{in}}$	**λ**
$\boldsymbol{lb}$	0.1	-30	3	0	0.1	-10	3	0	0.01	0.5	1
$\boldsymbol{ub}$	2	40	50	$\frac{\boldsymbol{Q_{total}}}{\mathbf{2}}$	2	40	80	$\boldsymbol{Q_{total}}$	0.5	Base+ 0.5	2

5.3.3 Determination of the objective function

5.3.3.1 Base form of the objective function

In the optimization process, iterations were conducted based on the direction of minimizing objective function. Objective function represents the performances of each subjective performance as a one index. The optimization designer sets the criteria on the performances to optimize. In this study, the subject performances were IMEP for thermal efficiency, CNI for combustion noise, NOx and soot emissions. The base objective function has a form of the equation (5.3.8).

$$J = \left(c_{imep}\frac{imep_{target} - imep}{imep_{target}}\right)^2 + \left(c_{CNI}(CNI_{target} - CNI)\right)^2 + \left(c_{NOx}\frac{NOx_{target} - NOx}{NOx_{target}}\right)^2 + \left(c_{Soot}(Soot_{target} - Soot)\right)^2 \quad (5.3.8)$$

where $\boldsymbol{J}$ is the performance index and $\boldsymbol{c_{imep}}$, $\boldsymbol{c_{CNI}}$, $\boldsymbol{c_{NOx}}$ and $\boldsymbol{c_{soot}}$ are the scale factors for each performance. The target of performance is the input for desired performance

Among the four performances in the equation (5.3.8), IMEP and NOx were normalized by the target value because these performances had the large scale differences by engine operating range. The principle of optimization by the objective function was that the closer the performance from designed combustion approached the target value, the closer the calculated objective function value became to zero, as shown in Figure 5.3.2. The scale factors were determined in the criteria of the lower and upper boundary for the performances. Based on the performance value obtained in the base experiment, the boundaries for the marginal gain of each performance that could be obtained as a result of

optimization and determined the scale factors so that the difference between the target and base performances at the boundary points could be normalized by -1 at lower boundary and 1 at upper boundary. Table 5.3.3 – Table 5.3.6 show the criteria of each performance and the boundary performances at two operation appoints that have representative different scale. The determined scale factors for IMEP, CNI, NOx and soot emissions were shown in Table 5.3.7.

The objective function suggested in this section optimizes the combustion that had performances close to the desired performances. If the combustion was designed by specifying target performances, the desired performance could have been derived, but there could be potential gain. The objective function needed to be modified for finding a point where performances were maximized.

5.3.3.2 Objective functions for various design concept

The objective function was modified to maximize specific performance. Target performances were thermal efficiency, NOx and soot emissions. The principle was that, instead of a form that allowed convergence to target performance, the output was located alone in the denominator or numerator, so that the value of the performance function decreased as the performance improved. Figure 5.3.3 shows the form of objective functions according to the target performance. Figure 5.3.4 shows the tendency of the performance index by changed term. In the case of performance maximization term, the target value was meaningless in itself and used for normalization purpose. The scale factors were used as the same to the base objective function that the difference in the performance index at the lower and upper boundaries was two.

In general, the combustion noise was not a priority of calibration target because noise was kept below a certain level, maximizing thermal efficiency or

exhaust emissions. If noise performance was to be a priority, the same method could be used. In this study, noise was not used as a target to maximize performance, but the limiting function was used to prevent noise from being determined above a certain level. Figure 5.3.5 shows the applied mechanism of limiting function. The liming function did not affect the performance index below the baseline limit, but penalized it by adding a large performance index above the limit.

Table 5.3.3 The lower and upper boundary for determining the scale factor of IMEP

IMEP [bar]		Lower limit	Target (base)	Upper limit
Criterion		-6%	0	+6%
Operating area	1500 rpm, BMEP 4 bar	4.87	5.18	5.49
	2000 rpm, BMEP 10 bar	21.35	22.71	24.07

Table 5.3.4 The lower and upper boundary for determining the scale factor of CNI

CNI [dB]		Lower limit	Target (base)	Upper limit
Criterion		-6	0	6
Operating area	1500 rpm, BMEP 4 bar	168.0	174.0	180.0
	2000 rpm, BMEP 10 bar	174.9	180.9	186.9

Table 5.3.5 The lower and upper boundary for determining the scale factor of NOx emission

NOx [ppm]		Lower limit	Target (base)	Upper limit
Criterion		-90%	0	90%
Operating area	1500 rpm, BMEP 4 bar	6.4	64.1	121.9
	2000 rpm, BMEP 10 bar	52.6	526.3	999.9

Table 5.3.6 The lower and upper boundary for determining the scale factor of soot emission

Soot [FSN]		Lower limit	Target (base)	Upper limit
Criterion		-1.5	0	1.5
Operating area	1500 rpm, BMEP 4 bar	0.023	1.523	3.023
	2000 rpm, BMEP 10 bar	0	0.558	2.058

Table 5.3.7 The scale factors for subject performances

IMEP	**Noise**	**NOx**	**Soot**
c_{imep}	c_{CNI}	c_{NOx}	c_{soot}
16.67	0.17	1.11	0.67

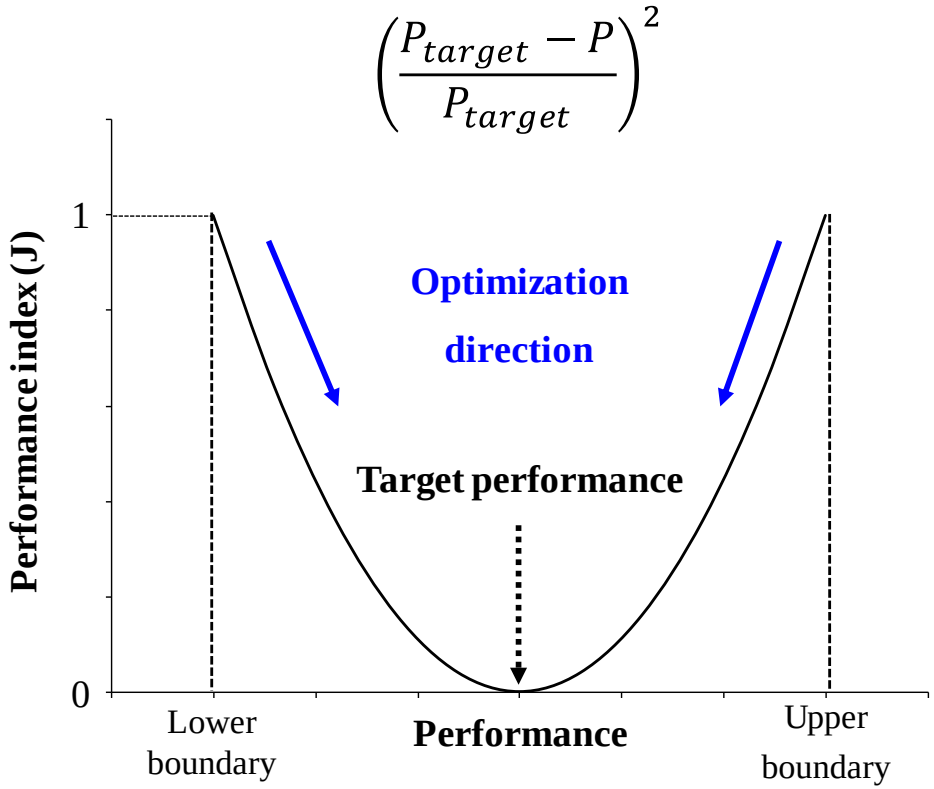

Figure 5.3.2 The performance index by the difference of target performance (base form)

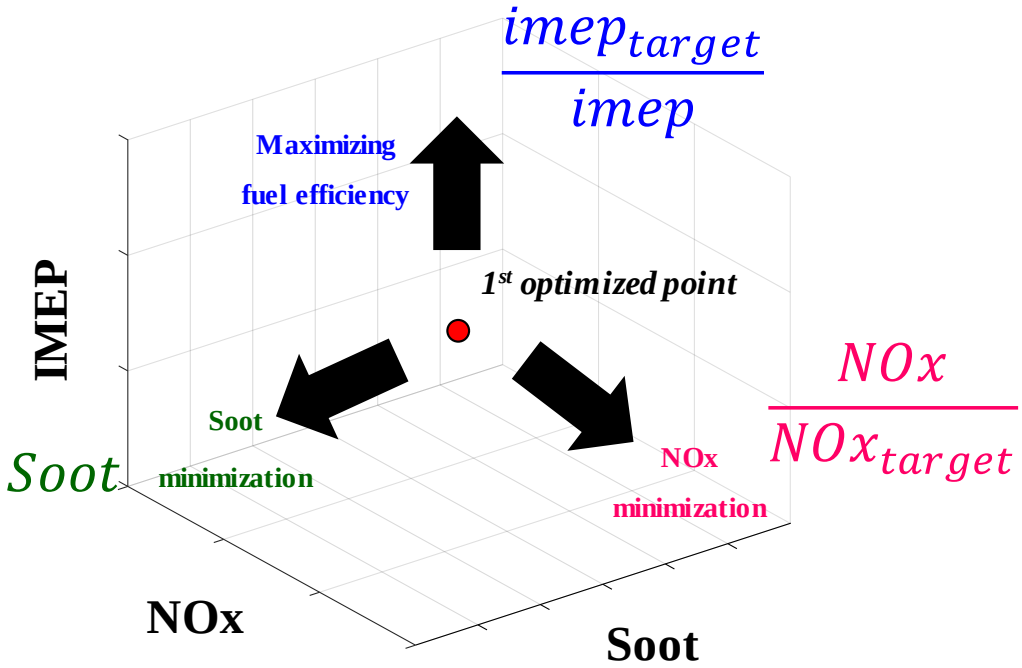

Figure 5.3.3 Schematic graph of objective functions for various design concepts

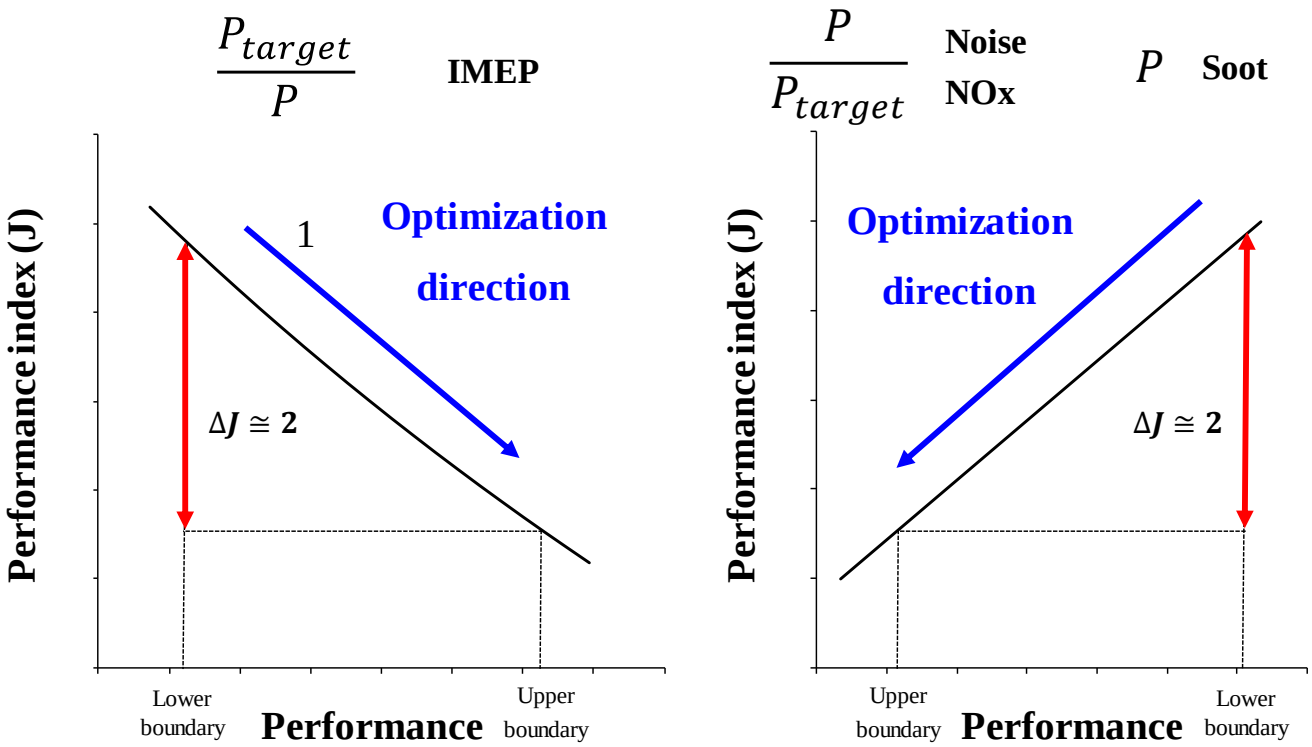

Figure 5.3.4 The performance index by the difference of performance (various design concept)

$$if\ Noise \geq Noise_{limit} \rightarrow J + 100$$
$$Noise < Noise_{limit} \rightarrow J + 0$$

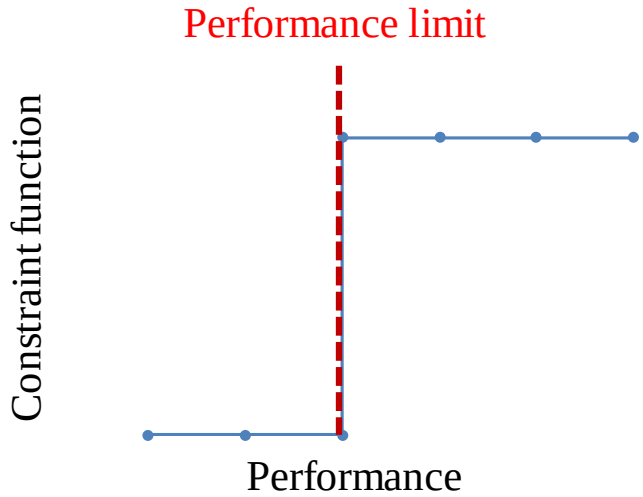

Figure 5.3.5 The objective function modification – Performance limits function

Chapter 6. Results of Combustion Design

6.1 Results from Base Objective Function

In this section, the results of the combustion design using Wiebe function for the constructing MFB with base objective function were presented. The operating points were 1500 rpm, BMEP 4 bar representing low load and 2000 rpm, BMEP 8 bar for high load.

6.1.1 Low load: 1500 rpm, BMEP 4 bar

The results from base experiment was used as reference performances that IMEP of 5.18 bar, CNI of 174 dB, 64 ppm and 1.52 FSN of NOx and soot emissions. The target values were determined in terms of thermal efficiency improvement, emissions reduction, and optimal set. Figure 6.1.1 shows the results of thermal efficiency improvement. The target value of IMEP was set to 5.4 bar that was a 4.2% improved result compared to the base. The target values of CNI and NOx emission were set to higher than base results for giving a wide range of thermal efficiency improvement. Except for soot emission, all the other performances were close to the target. Heat release rate showed higher peak and shorter combustion duration than that of experiment. It was due to peak pressure and heat release rate approaching top dead center (TDC) as optimization result for high thermal efficiency. Also, soot emission benefited from the combustion with low soot emission. NOx emission was largely formed by increased combustion temperature with high peak pressure, even though the EGR rate increased over the experimental value (43.2%).

The result of combustion design for low emission was shown in Figure 6.1.2. The target performance was set to IMEP and CNI similar to experimental value, and NOx and soot emissions with high reduction rate. The EGR rate was increased to 52.9% and the intake pressure was 0.78 bar. The low intake pressure and high EGR rate mainly affected NOx reduction with maintaining similar thermal efficiency level. In the emission reduction case, the performances The designed combustion performances were all similar to the target values. In terms of combustion phase, the peaks of pressure and HRR were lower than experiment and thermal efficiency improvement case, but the combustion duration was also shorter. Figure 6.1.3 shows the results of combustion design with optimal performance target. The target values were set to improve performances except noise. The target noise was set to be 1 dB higher than the experimental value to increase the margin of overall performance improvement. Fuel efficiency, noise and NOx emission results were similar to the target value, with low soot emission. The combustion phase featured a combination of thermal efficiency improvements and emission reduction cases. The EGR rate and intake pressure were higher than other cases, and the pilot combustion was merged to the first main combustion. Although the maximum pressure was high, due to the high EGR, NOx emission was able to be reduced by 38% compared to base condition.

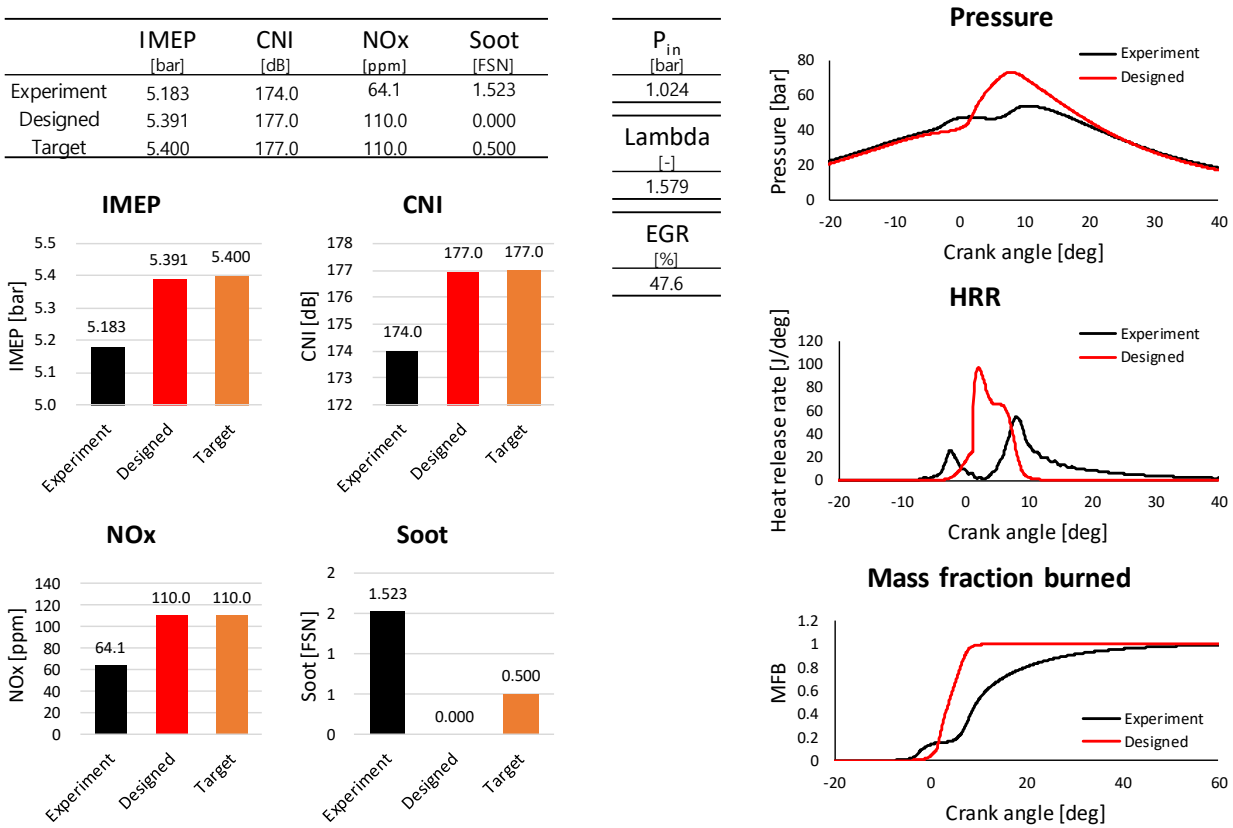

Figure 6.1.1 The combustion design results of thermal efficiency improvement with the base objective function at 1500 rpm, BMEP 4 bar

	IMEP [bar]	CNI [dB]	NOx [ppm]	Soot [FSN]
Experiment	5.183	174.0	64.1	1.520
Designed	5.201	175.0	2.9	0.465
Target	5.200	175.0	10.0	0.500

P_{in} [bar]
0.782

Lambda [-]
1.115

EGR [%]
52.9

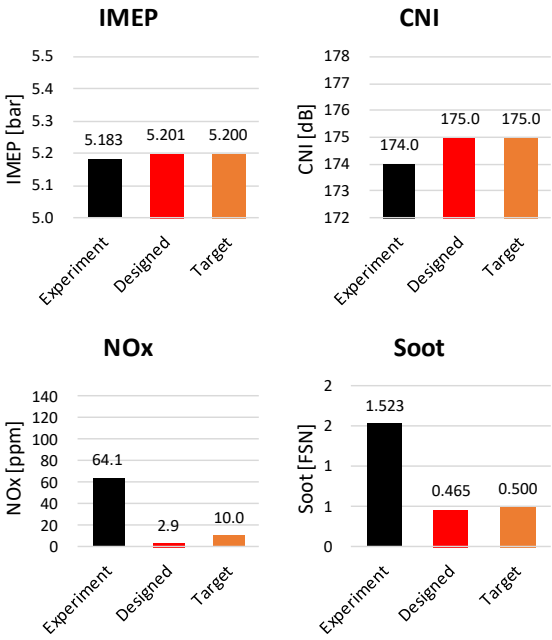

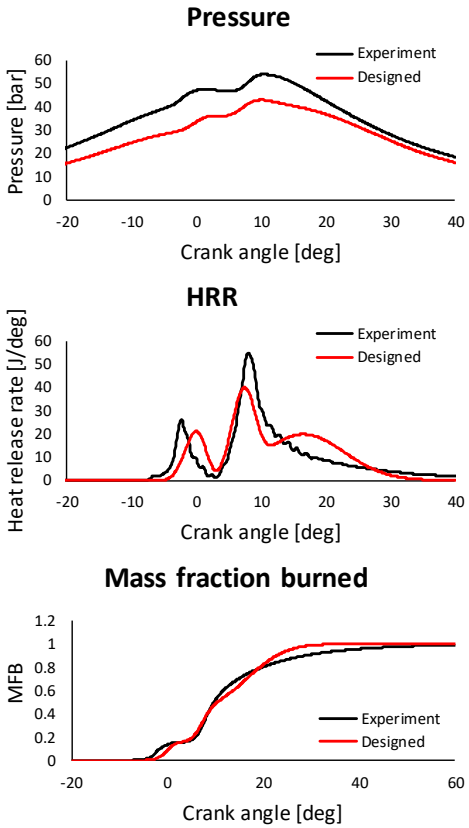

Figure 6.1.2 The combustion design results of emissions reduction with the base objective function at 1500 rpm, BMEP 4 bar

	IMEP [bar]	CNI [dB]	NOx [ppm]	Soot [FSN]
Experiment	5.183	174.0	64.1	1.523
Designed	5.264	175.0	39.5	0.016
Target	5.250	175.0	40.0	0.500

P_{in} [bar]
1.229

Lambda [-]
1.604

EGR [%]
56.3

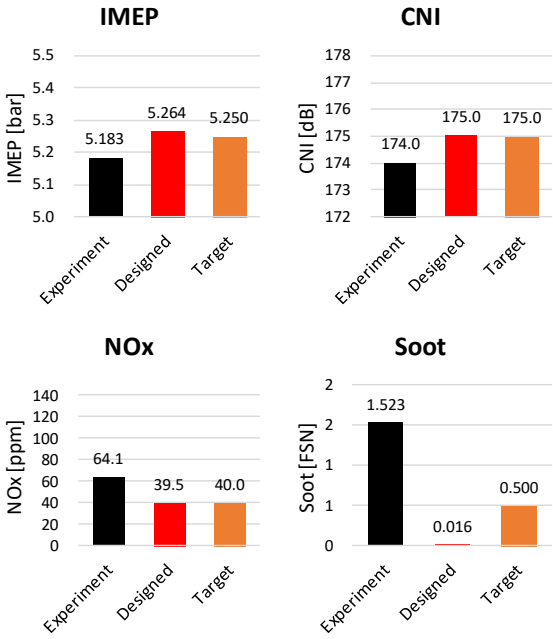

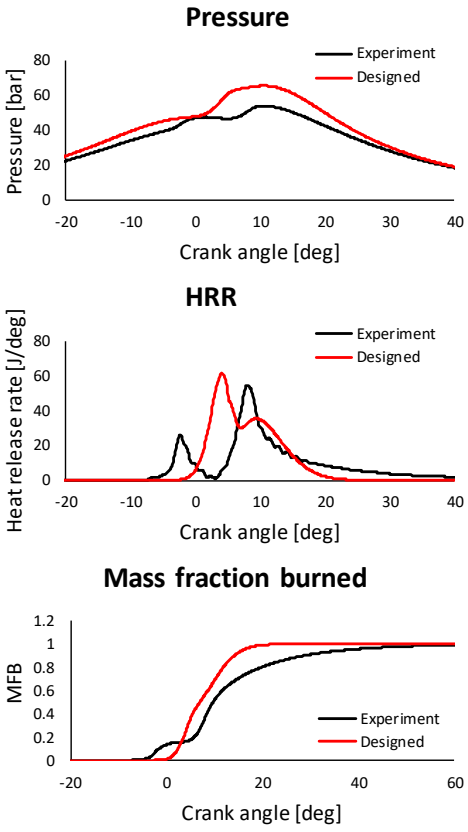

Figure 6.1.3 The combustion design results of optimal set with the base objective function at 1500 rpm, BMEP 4 bar

6.1.2 High load: 2000 rpm, BMEP 8 bar

The combustion design concept was also determined by improving thermal efficiency, reducing emissions, and optimal set in 2000 rpm, BMEP 8 bar. The results of thermal efficiency improvement case are shown in Figure 6.1.4. The target for IMEP was set to improve 7.6% and the target for NOx was also set to increase to 93.6% for margin of thermal efficiency improvement. IMEP of designed combustion was improved by 6% to 10.1 bar, but it did not reach the target. On the other hand, NOx and noise showed deterioration beyond target. This result implied that the target performance values were set beyond the performance limits at the operating point. Combustion pressure and heat release rate were similar to those at low load, with peak pressure and heat release rate advancing closer to TDC and intake pressure higher than the experimental value. Soot emission also showed similar tendency that low emission due to short combustion duration. The EGR rate was 14.1% higher than the experiment, but the effects of increased intake pressure and maximum pressure were more dominant, resulting in a significant increase in NOx emission.

In the emission reduction case, the performances showed similar results to the target performance values except soot with lower results. The results are shown in Figure 6.1.5. As the intake pressure was 0.35 bar lower than the experimental value, lambda became rich. The combustion pressure was lower than the experimental value due to the low intake pressure, which helped significantly reduce NOx with a high EGR rate. Heat release rate in main combustion showed to maintain a similar level to the peak heat release rate of approximately 15 degrees, indicating that the combustion rate of the fuel was maintained at a similar rate in that combustion duration. Although it was uncertain that the rate of

combustion maintained constant, it proposed a combustion strategy that could help reduce emissions while preventing loss of thermal efficiency.

Figure 6.1.6 shows the results of combustion design with optimal target values. The target IMEP was set to improve 3.4% by experiment IMEP and NOx emission was set to reduce 35.5% by experiment NOx emission. The designed combustion showed 4.8% improved IMEP and 32.1% decreased NOx emission with low soot emission. CNI was increased 2.4 dB. These results showed that thermal efficiency improved 1.2% less compared to thermal efficiency improvement case, but NOx emission was inversely reduced. From the result, it was suggested that although NOx emission was bound to increase at the limit level of the improvement range of thermal efficiency, a small reduction in the improvement margin in thermal efficiency could achieve a more optimized level overall.

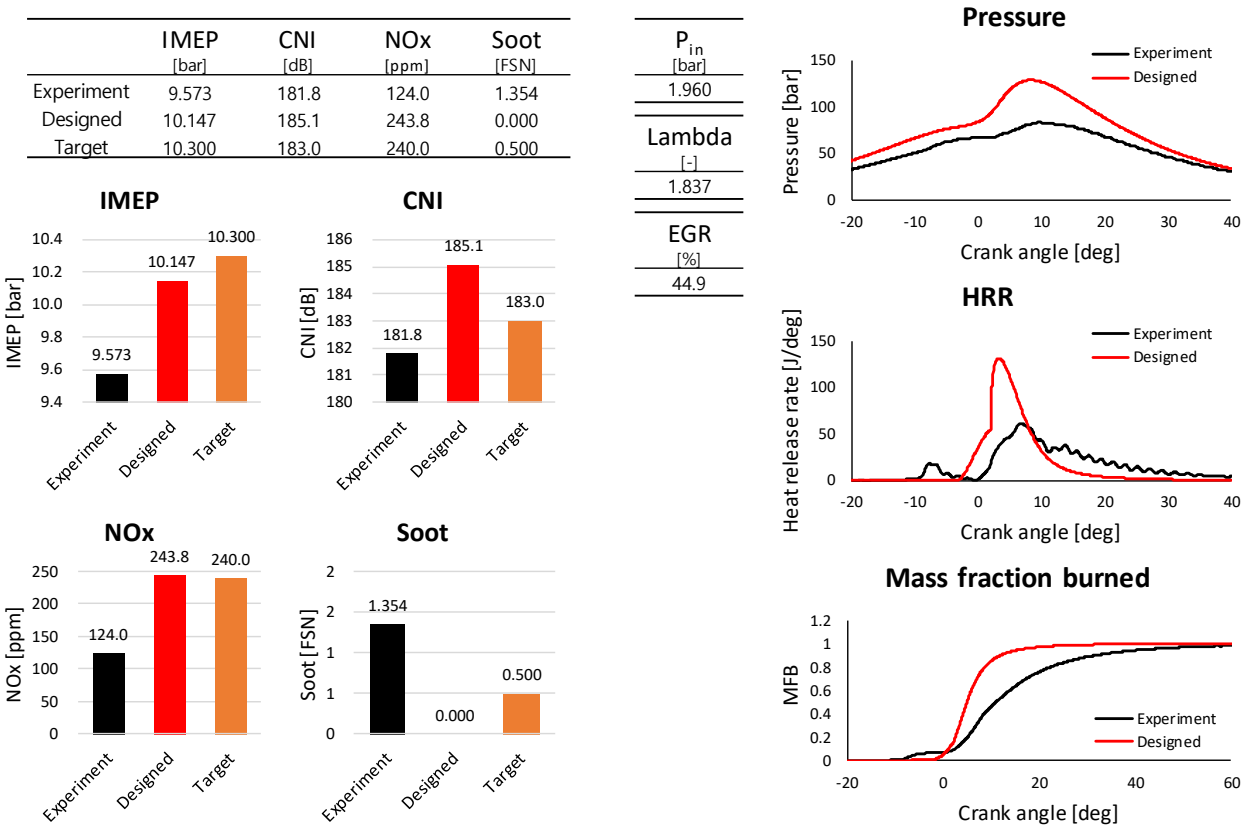

Figure 6.1.4 The combustion design results of thermal efficiency improvement with the base objective function at 2000 rpm, BMEP 8bar

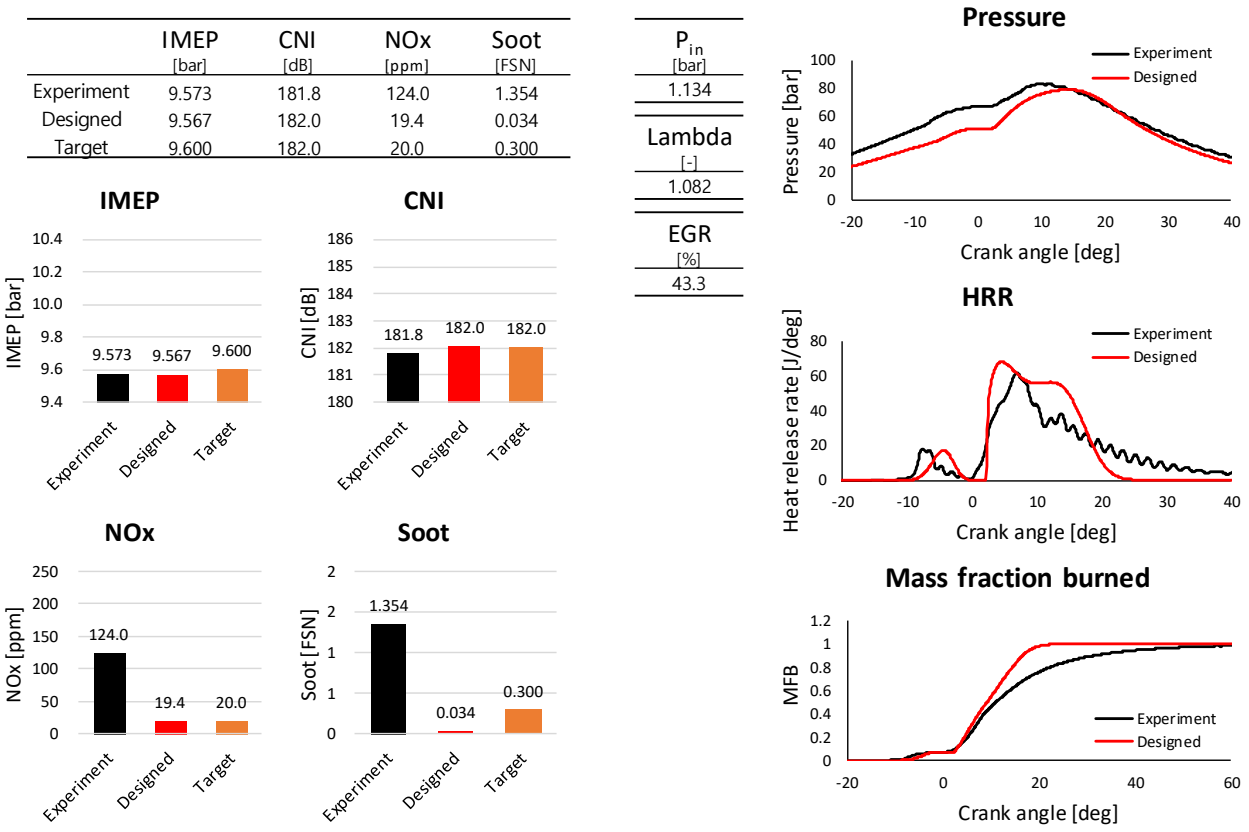

Figure 6.1.5 The combustion design results of emissions reduction with the base objective function at 2000 rpm, BMEP 8bar

	IMEP [bar]	CNI [dB]	NOx [ppm]	Soot [FSN]
Experiment	9.573	181.8	124.0	1.354
Designed	10.037	184.2	84.2	0.000
Target	9.900	183.0	80.0	0.500

P_{in} [bar]
1.418

Lambda [-]
1.353

EGR [%]
43.5

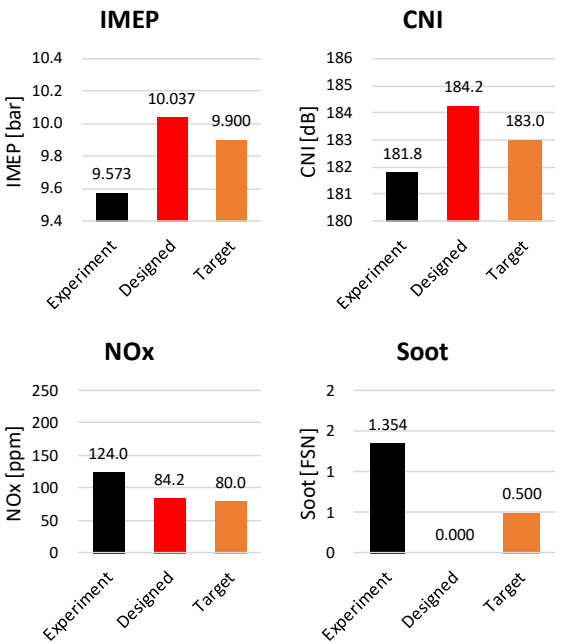

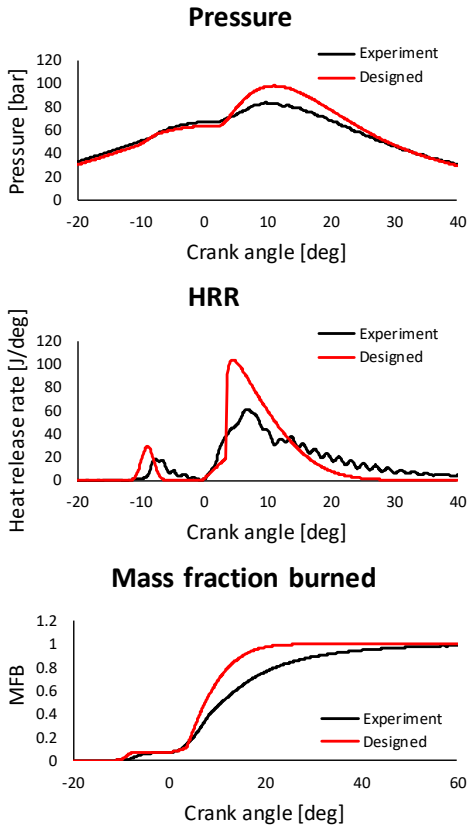

Figure 6.1.6 The combustion design results of optimal set with the base objective function at 2000 rpm, BMEP 8bar

6.2 Results by various design concept

In the combustion design applying objective functions for various design concept, it was established that design concept to the desired combustion performance rather than targeting specific performance value to maximize performance. The first design concept for each performance at 1500 rpm, BMEP 4 bar was assumed as follow:

- Maximization of IMEP
- CNI does not exceed 4 dB by experimental value.
- NOx emission below 40 ppm
- Soot emission less than 0.6 FSN

The sequence and results of the combustion design sequence to satisfy the above concepts are shown in Figure 6.2.1. As a first step, the optimization using the modified objective function was conducted to maximize IMEP. The noise criterion was penalized to prevent it from exceeding the level set in terms of limitation. The result of first optimization showed similar values with the target performance except for IMEP. IMEP result was 5.33 bar less than the target of 5.4 bar. It was considered that the results had maximized thermal efficiency gains at the targets, and conducted a second optimization to evaluate the possibility of further NOx reduction. The second optimization used the modified objective function to minimize NOx emission. The NOx result of second optimization was 6 ppm that reduced significantly, but IMEP was decreased simultaneously. Since the benefits of thermal efficiency had reached limit, it was confirmed that additional NOx reduction required the loss of thermal efficiency. In a third step, it was evaluated that the optimization potential using the base objective function.

The target performance except NOx emission based on the result of first optimization and the target NOx emission was set to decreased value. The result from the third optimization were showed similar tendency to increase in thermal efficiency and decrease in NOx emission. Combining the results during the optimization process, all of them reduced NOx compared to base experimental value and improved thermal efficiency as shown in Figure 6.2.2. In the optimization step the soot results remained low and the trade-off relationship was shown between IMEP and NOx emission. According to the initial design concept, the result of first optimization, which had a 2.9% thermal efficiency improvement while satisfying the emission level, was determined as optimal combustion.

The design concept at 2000 rpm, BMEP 8 bar was established as follow:

- Improvement of IMEP by 3% or more
- CNI does not exceed 4 dB by experimental value.
- Minimization of NOx emission
- Soot emission less than 0.54 FSN

The results and process in the combustion design were shown in Figure 6.2.3. The NOx emission was set to minimize and it was optimized with the modified objective function by minimizing NOx emission. Target performances were set to 3.4% improvement of IMEP, same level of CNI, and decreased soot level in first optimization. The target NOx emission was 60% reduced value but it was meaningless in the NOx minimization process. The noise criterion was also applied in the form of constraint function. The NOx result from the designed combustion was 11 ppm and soot emission also showed low level of 0.12 FSN. However, since the improvement rate of thermal efficiency was insufficient for the desired thermal efficiency as 2.5%, a margin on NOx for further improvement

of thermal efficiency was set as 30 ppm that was 75.8% reduced value. The second optimization with the modified objective function for maximizing thermal efficiency was conducted. The result of second step showed 5.16% increased thermal efficiency result compared with the experimental IMEP. The NOx also remained at set value about 32.4 ppm, but the soot emission was increased to 0.53 FSN. The third optimization was conducted by changing the objective function to the minimization form of soot emission under equivalent conditions to evaluate the potential for further soot reduction although the soot result from the second step satisfied the requirements. Low soot result was derived through the third step optimization but IMEP decreased to 9.82 bar. Similar to the low load case, three factors of IMEP, NOx and soot emissions showed trade-off relationship at the boundary performance level. Figure 6.2.4 shows the results of combustion design under the design concept. The most appropriate result for the design intention could be determined as a result of step 2 with the highest thermal efficiency while satisfying the exhaust emission criteria.

According to the methods introduced in this section, the combustion design with the modification of the objective function by design intention could find optimal combustion that met specific criteria. In addition to the two design concepts presented in this section, the combustion design methodology can apply various performances criteria by utilizing a limit function and modification to maximize target performance.

Step 1.

$$min.\ J = \left(c_{imep2} \times \frac{imep_{target}}{imep}\right) + \left(c_{CNI} \times (CNI_{target} - CNI)\right)^2 + \left(c_{NOx} \times \frac{NOx_{target} - NOx}{NOx_{target}}\right)^2 + \left(c_{Soot} \times (Soot_{target} - Soot)\right)^2 + f_{constraint}(CNI < 178)$$

	IMEP	CNI	NOx	Soot
Experiment	5.183	174	64.13	1.52

	IMEP	CNI	NOx	Soot
Target	5.400	176.0	40.0	0.500
Designed	5.333	175.2	39.3	0.140

Step 2.

$$min.\ J = \left(c_{imep2} \times \frac{imep_{target} - imep}{imep_{target}}\right)^2 + \left(c_{CNI} \times (CNI_{target} - CNI)\right)^2 + \left(c_{NOx} \times \frac{NOx}{NOx_{target}}\right) + \left(c_{Soot} \times (Soot_{target} - Soot)\right)^2 + f_{constraint}(CNI < 178)$$

	IMEP	CNI	NOx	Soot
Target	5.333	175.2	30.0	0.140
Designed	5.216	175.2	5.9	0.080

Step 3.

$$min.\ J = \left(c_{imep2} \times \frac{imep_{target} - imep}{imep_{target}}\right)^2 + \left(c_{CNI} \times (CNI_{target} - CNI)\right)^2 + \left(c_{NOx} \times \frac{NOx_{target} - NOx}{NOx_{target}}\right)^2 + \left(c_{Soot} \times (Soot_{target} - Soot)\right)^2 + f_{constraint}(CNI < 178)$$

	IMEP	CNI	NOx	Soot
Target	5.333	175.2	20.0	0.140
Designed	5.284	175.4	20.4	0.010

Figure 6.2.1 The optimization steps to satisfy combustion design concept at 1500 rpm, BMEP 4 bar

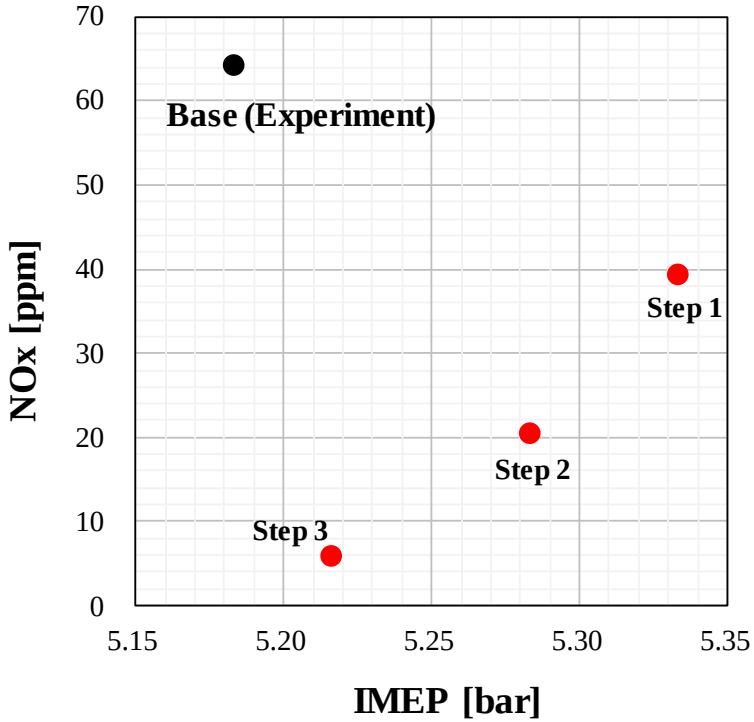

Figure 6.2.2 Trade-off relationship between IMEP and NOx emission in the optimization step at 1500 rpm, BMEP 4 bar

	IMEP	CNI	NOx	Soot
Experiment	9.573	181.8	124.0	1.354

Step 1.

$$min.\ J = \left(c_{imep2} \times \frac{imep_{target} - imep}{imep_{target}}\right)^2 + \left(c_{CNI} \times (CNI_{target} - CNI)\right)^2$$
$$+ \left(c_{NOx} \times \frac{NOx}{NOx_{target}}\right) + \left(c_{Soot} \times (Soot_{target} - Soot)\right)^2 + f_{constraint}(CNI < 185.8)$$

	IMEP	CNI	NOx	Soot
Target	9.900	182.0	49.6	0.500
Designed	9.813	180.2	10.6	0.116

Step 2.

$$min.\ J = \left(c_{imep2} \times \frac{imep_{target}}{imep}\right) + \left(c_{CNI} \times (CNI_{target} - CNI)\right)^2$$
$$+ \left(c_{NOx} \times \frac{NOx_{target} - NOx}{NOx_{target}}\right)^2 + \left(c_{Soot} \times (Soot_{target} - Soot)\right)^2 + f_{constraint}(CNI < 185.8)$$

	IMEP	CNI	NOx	Soot
Target	9.900	180.2	30.0	0.116
Designed	10.067	183.1	32.4	0.530

Step 3.

$$min.\ J = \left(c_{imep2} \times \frac{imep_{target} - imep}{imep_{target}}\right)^2 + \left(c_{CNI} \times (CNI_{target} - CNI)\right)^2$$
$$+ \left(c_{NOx} \times \frac{NOx_{target} - NOx}{NOx_{target}}\right)^2 + \left(c_{Soot} \times (Soot)\right) + f_{constraint}(CNI < 185.8)$$

	IMEP	CNI	NOx	Soot
Target	10.067	183.1	32.4	0.300
Designed	9.822	185.8	29.59	0.001

Figure 6.2.3 The optimization steps to satisfy combustion design concept at 2000 rpm, BMEP 8 bar

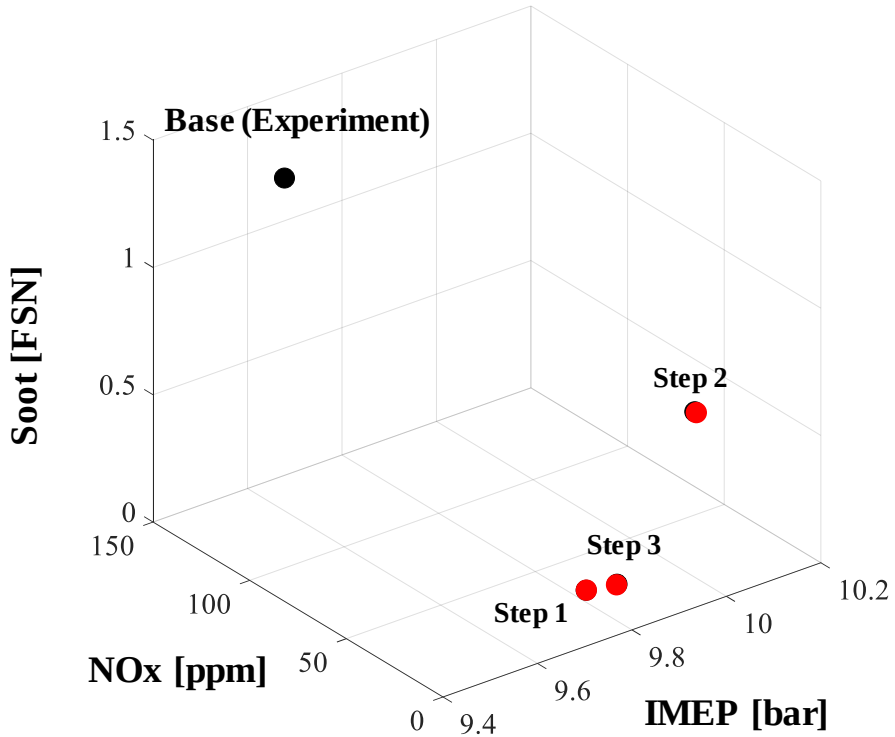

Figure 6.2.4 The optimization results during the combustion design at 2000 rpm, BMEP 8bar

6.3 Results Using Polynomial Function as MFB

In this section, the combustion design was performed by representing MFB as a polynomial function in 1500 rpm and BMEP 4 bar region. The PSO method was used as optimization algorithm. The objective function was used with a modified form to maximize thermal efficiency, and the target performance applied the same value as the targets used in finding the optimal set in Section 6.1.1. Two polynomial functions representing pilot and main combustion were used to build the MFB. The function that was earlier than the start of combustion meant pilot combustion and the total heat of the pilot combustion was limited at the half of the total heat. In addition, the constraint of EGR rate was removed for the wide variety of combustion phases and combustion conditions. In a polynomial, since the shape of the graph changes with respect to the value of a, so the combustion design was performed by dividing it into two cases, less than one and more than one.

Figure 6.3.1 shows the combustion design results in the case that a was less than one. IMEP increased by 20.1% as a result of the combustion design, and NOx and soot emissions were also reduced by 88.1% and 44.7%, respectively, resulting in an overall increase of performance. The improvement rate of IMEP was difficult to show in the conventional engine development or calibration processes. It was confirmed that the combustion phase approached an ideal combustion cycle. Due to the high intake pressure and advanced combustion phase, the adiabatic temperature would be higher than the experimental value, but NOx emission showed below 10 ppm because of extremely high EGR rate. Noise was deteriorated to 177.9 dB by the high pressure rise rate. The results from the case of a above one showed similar thermal efficiency as shown in Figure 6.3.2. Although the shape of heat release rate was different with the case of a less than

one, the pressure and heat release rate were advanced and focused near TDC. Figure 6.3.3 shows the PV diagram with the experimental data and the results from combustion design using polynomial functions. Compared to the results from the cases of Wiebe function, the increase in thermal efficiency was greater. The fuel burned at high intake pressure and the combustion speed was fast around TDC, making it closer to ideal combustion cycle. On the other hand, NOx emission was reduced by excessive EGR rate, which was expected to result in higher NOx emission from high pressure when using EGR rate in typical level. Despite excessive EGR rate, soot emission was able to be reduced due to short combustion duration.

Representing the MFB as a polynomial function does not result in a physically reasonable combustion phase. However, this attempt is meaningful not in terms of evaluating physical feasibility, but in an attempt to take a new approach to the characteristics of combustion.

	IMEP [bar]	CNI [dB]	NOx [ppm]	Soot [FSN]
Experiment	5.183	174.0	64.1	1.523
Designed	6.223	177.9	7.6	0.840
Target	5.400	175.0	40.0	0.500

P_{in} [bar]
1.6

Lambda [-]
1.52

EGR [%]
70.5

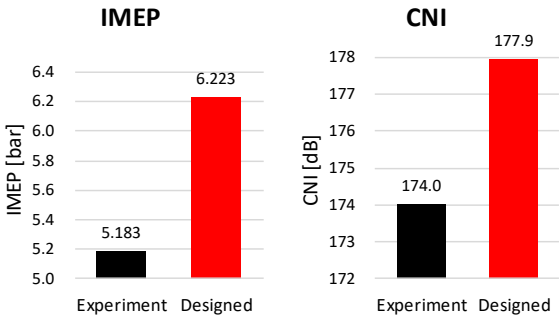

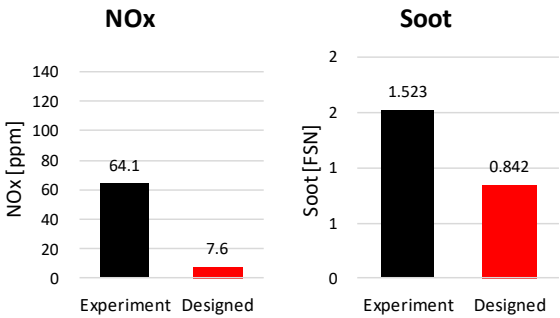

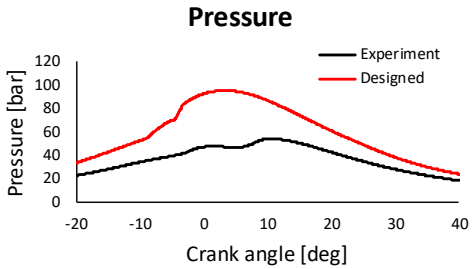

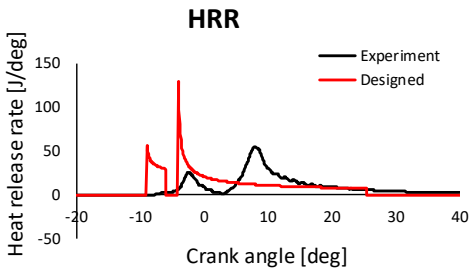

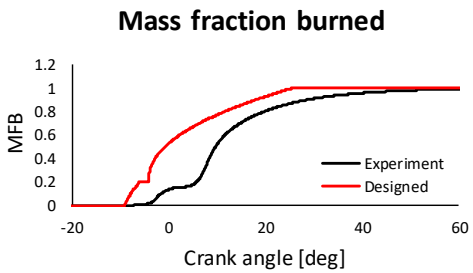

Figure 6.3.1 The combustion design result by using the polynomial function as MFB ($a < 1$)

	IMEP [bar]	CNI [dB]	NOx [ppm]	Soot [FSN]
Experiment	5.183	174.0	64.1	1.523
Designed	6.376	176.4	43.7	0.001
Target	5.400	175.0	40.0	0.500

P_{in} [bar]
1.578

Lambda [-]
1.778

EGR [%]
64.3

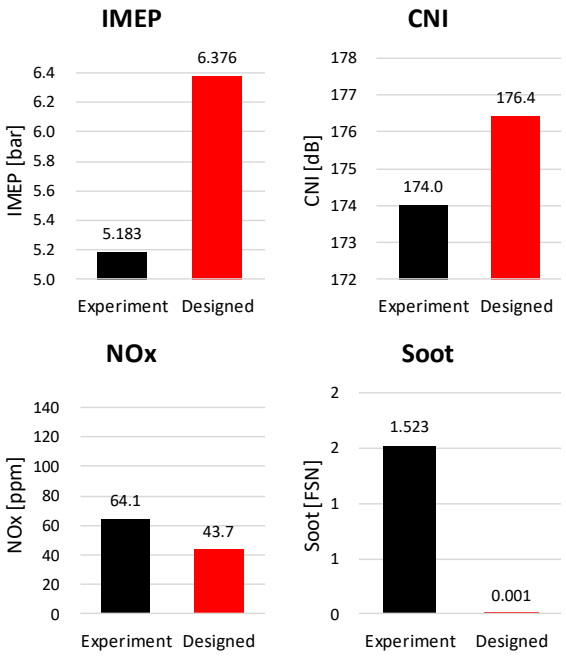

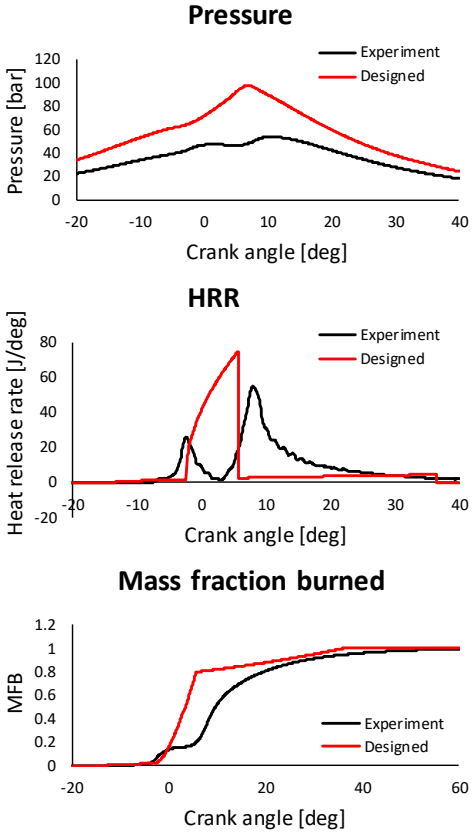

Figure 6.3.2 The combustion design result by using the polynomial function as MFB ($a \geq 1$)

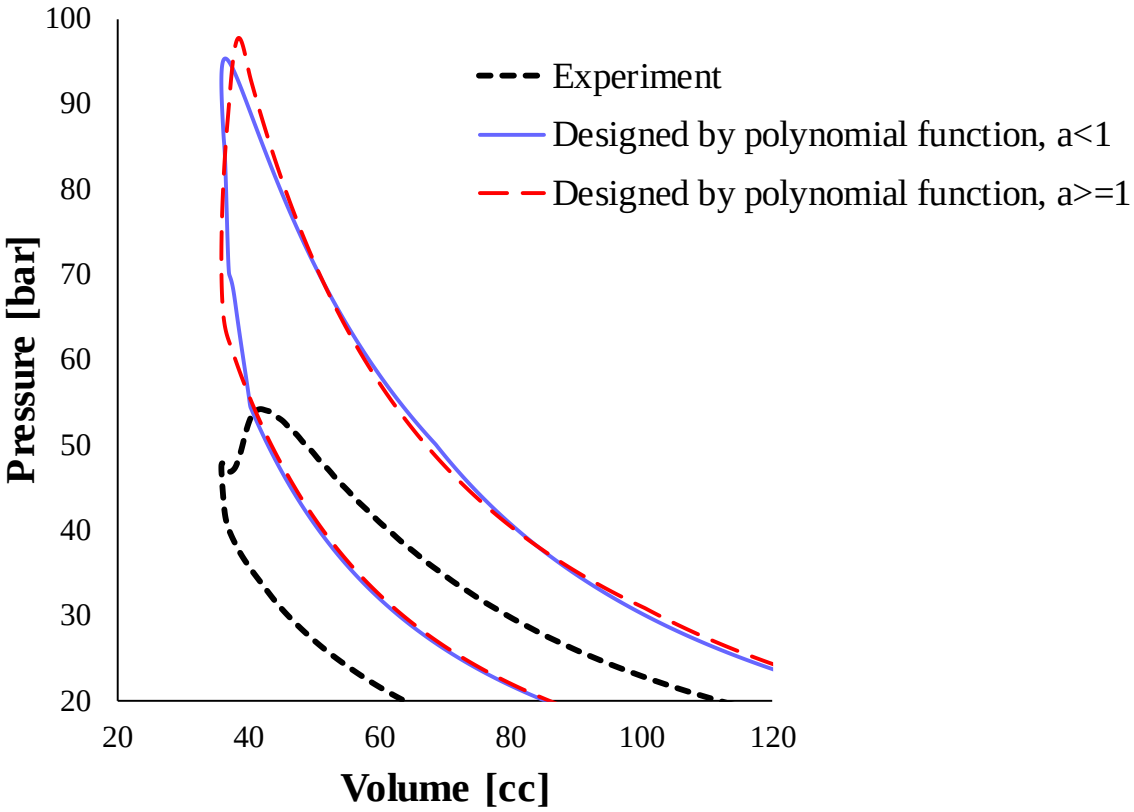

Figure 6.3.3 The PV diagram from the experiment and combustion design using polynomial functions

6.4 Application of Combustion Design to WLTP

6.4.1 Combustion design at steady points in WLTP operating area

Based on WTLP data acquired through experiment, the combustion design methodology was applied. At first, during the WLTP test, the design target operating region of the engine was selected and the combustion design was applied to each point. Figure 6.4.1 shows the engine operation area during WLTP and selected optimization steady points. The 46 points were selected that were able to cover operation region during the WLTP. Validation of the combustion model underlying the combustion design methodology was carried out in the selected area. At each point, the combustion pressure acquired from the experiment was expressed as a Wiebe function, and then the models for each performance were calculated from the base engine parameters and the Wiebe function were evaluated for correlation with the experimental value.

Figure 6.4.2 and Figure 6.4.3 show correlations of the results from combustion models for each performance with experimental values. IMEP and NOx emission showed good relationship that had above 0.9 R-squared values. CNI from the noise estimation was affected by the noise at acquired in-cylinder pressure. The soot emission from the model contained the error from the estimated injection timing. Despite these error factors, each model showed a good relationship at steady points. The coefficients and engine parameters that expressed the in-cylinder pressure from the experiment were used as the initial conditions in the optimization process.

In the optimization process, the base form of objective function was used to avoid a divergence of optimization results. The performance targets at each steady points were determined based on the results from the experiment. Although it was used only for normalization purposes in objective function, desired thermal efficiency was determined targets of 2 to 7% increase depending on the operating area. Similar to the target of thermal efficiency, NOx reduction target was set as a target of 20 to 50%, which was different depending on the operating area. Fuel efficiency and NOx emission had a decreased ratio of improvement in high load area above BMEP 10 bar. In this case, determining the degree improvement were decreased because the optimization results did not reach the target. Noise target was determined as an increase of 1 dB compared to CNI from the base experiment. Instead of determining the target CNI in low noise level, the upper limit constraint function of noise was removed to further improve thermal efficiency even if the deterioration of noise was significant in area of less thermal efficiency improvement. The target for soot emission was determined on the criterion of 60% reduction.

Figure 6.4.4 and Figure 6.4.5 show the combustion design result at the steady points expressed in the map. The maximum IMEP improvement was 17.5% at 1500 rpm, BMEP 6bar. The low thermal efficiency increase effect in high load conditions compared to low load region. In the graph, the brighter in operation area, the more improved thermal efficiency. Averaged thermal efficiency improvement rate was 5.15% in overall design points. Noise deteriorated in all areas, with only 0.88 dB worsening in 2000 rpm, BMEP 4 bar, while 12.9 dB worsening in 1750 rpm, BMEP 12 bar. At 1750 rpm, BMEP 12bar case, the thermal efficiency improvement effect was higher than that of the nearby area, but the noise deteriorated further. The maximum reduction rate of NOx emission was 84.5% at 1750 rpm, BMEP 8 bar. Overall, the greater the increase in thermal efficiency, the smaller the reduction rate in NOx emission. Overall design points

showed an average reduction rate of 43.3%. In terms of the reduction rates of soot emission, largely reduced region of more than 99% were dominant across the entire operation area.

Figure 6.4.6 to Figure 6.4.8 show the results of combustion phase at three points 1750 rpm, BMEP 8bar, 2000 rpm, BMEP 6 bar, and 2250 rpm, BMEP 8 bar. In 1750 rpm, BMEP 8bar case, the NOx reduction rate showed the maximum reduction rate of the total designed points. 2000 rpm, BMEP 6 bar case showed unusual shape of the heat release rate that had three peaks. The designed combustion high thermal efficiency improvement and NOx reduction rate with low level of soot emission. The maximum pressure point that caused by the last combustion of the distributed main injection quantity had small area of NOx formation and low adiabatic temperature with low intake pressure. The heat release rate of 2250 rpm, BMEP 8bar case showed similar shape with the heat release rate of the emission reduction design result at 2000 rpm, BMEP 8bar in section 6.1.1. The peak pressure was low while maintaining a high level of heat release rate to achieve emission reduction.

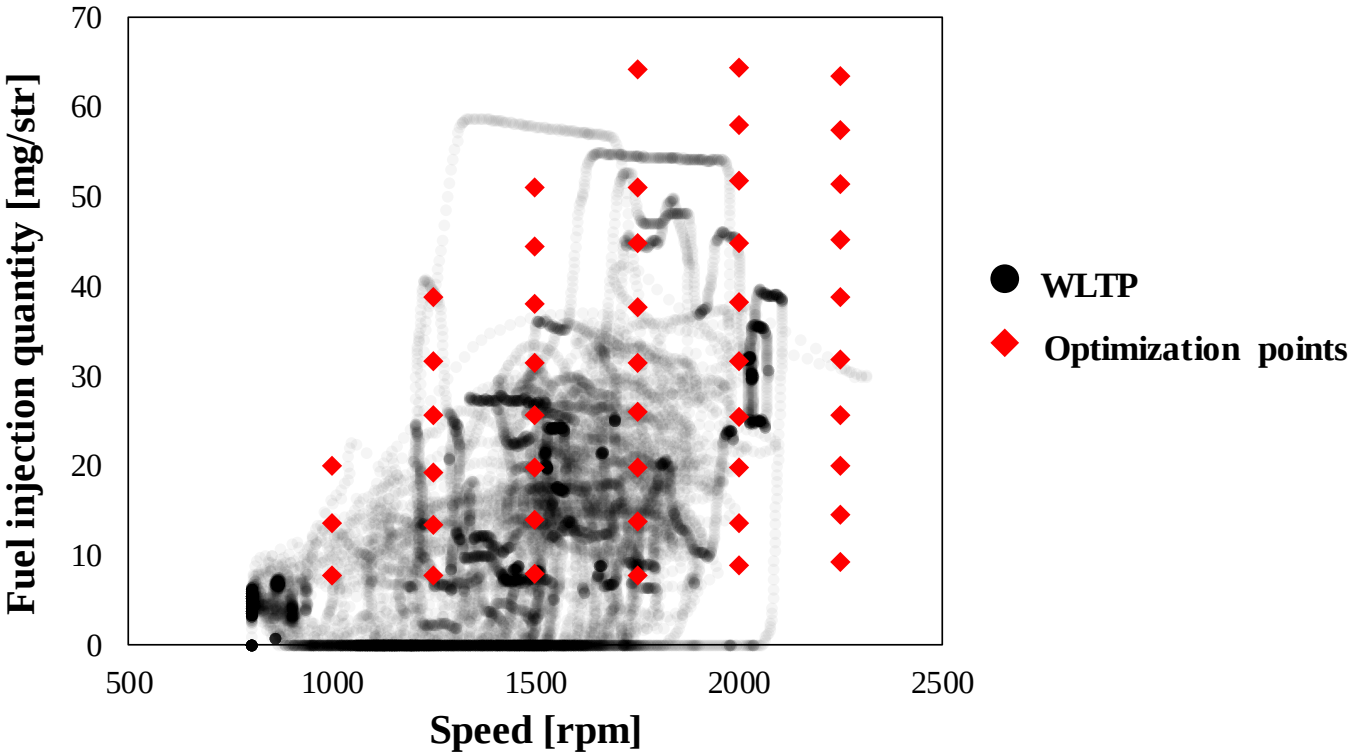

Figure 6.4.1 Operating area during WLTP and optimization points

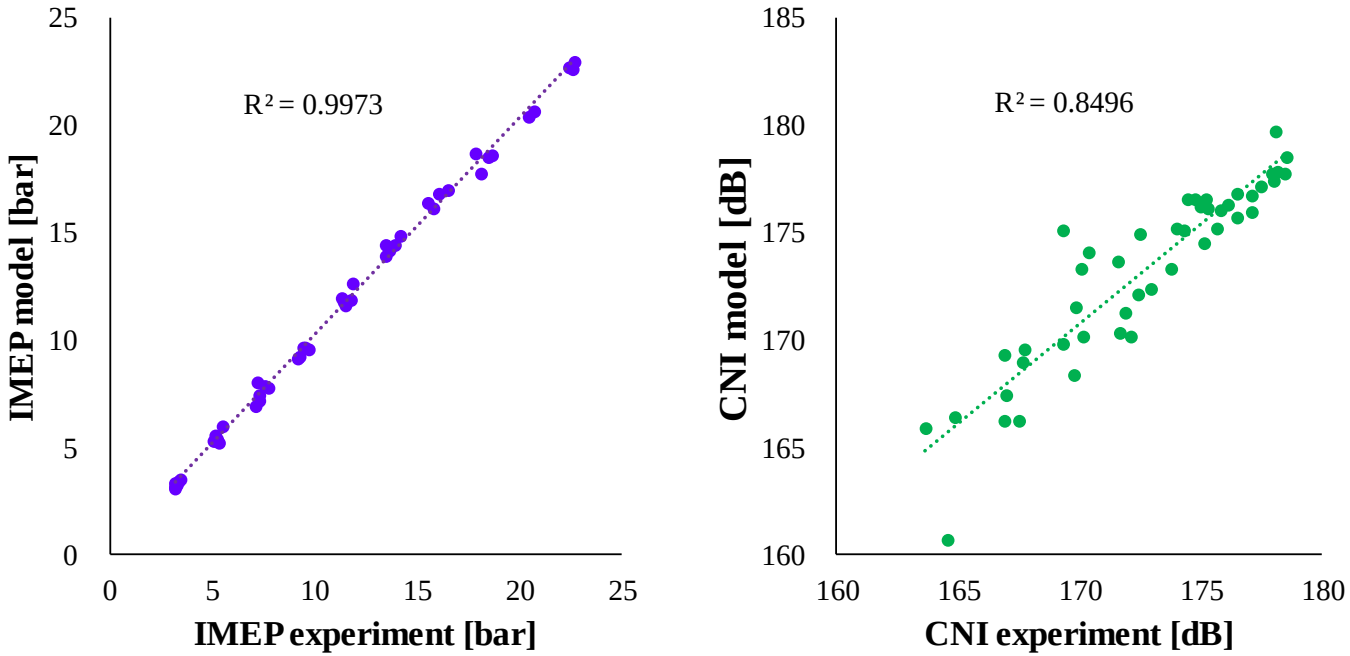

Figure 6.4.2 The models validation using Wiebe function in steady points: IMEP and CNI models

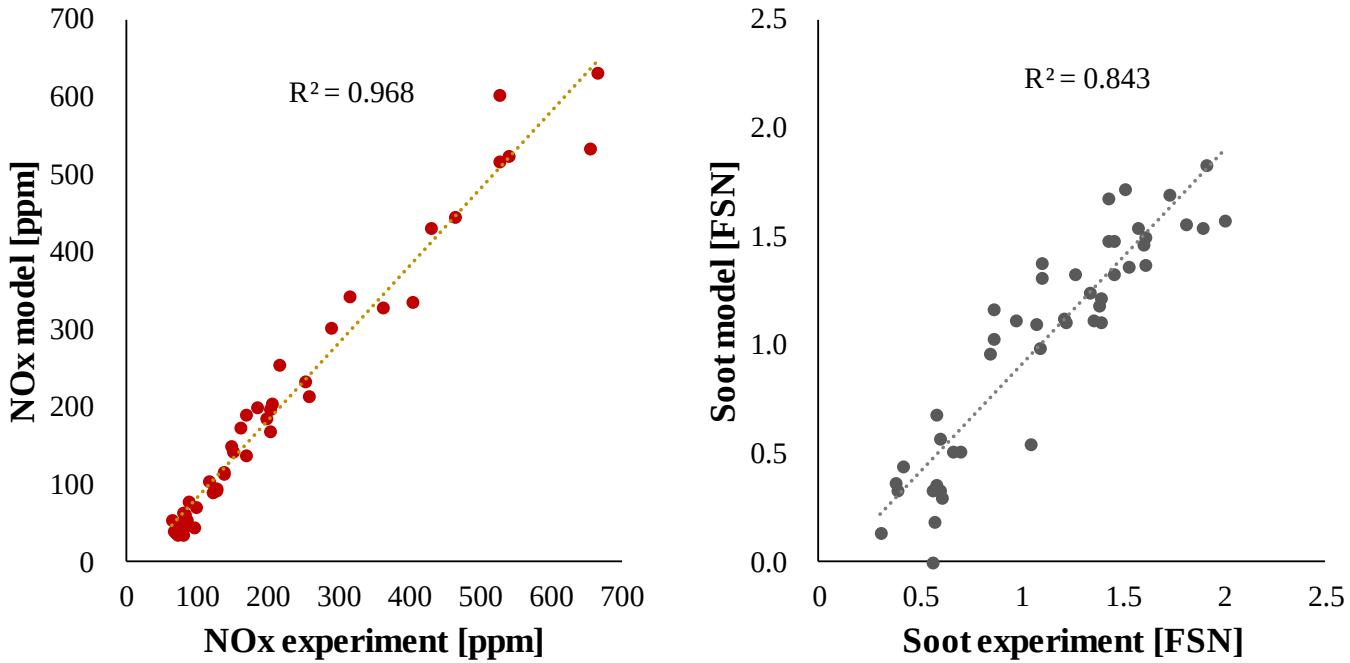

Figure 6.4.3 The models validation using Wiebe function in steady points: NOx and soot models

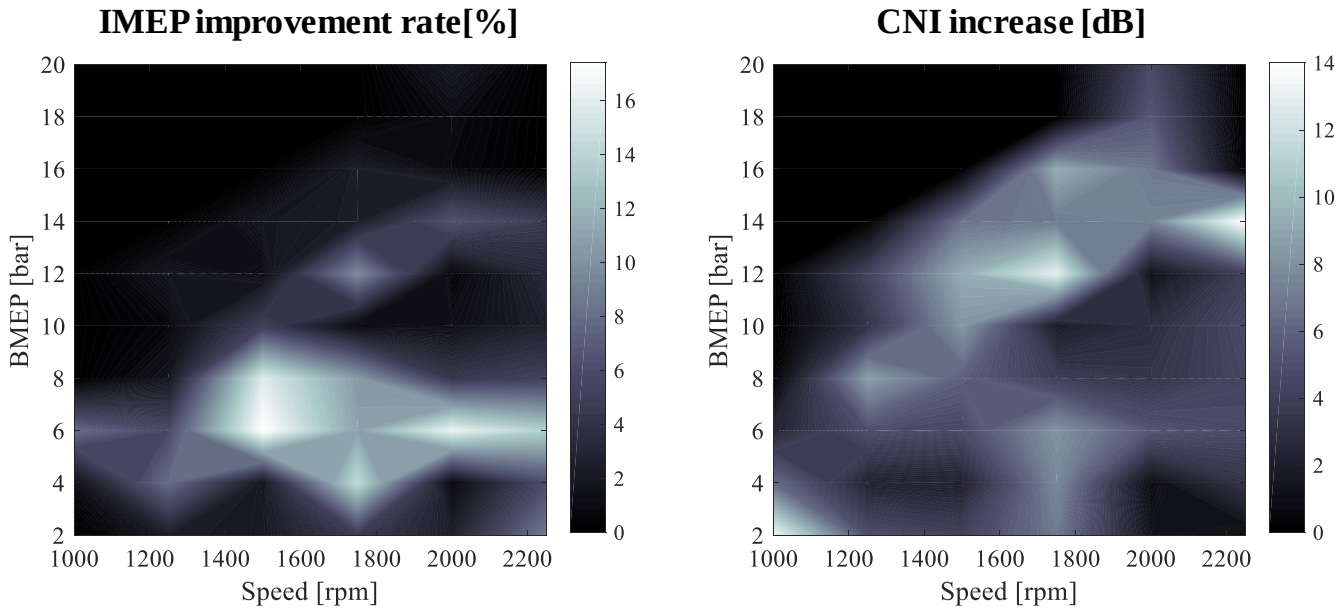

Figure 6.4.4 The combustion design results at steady state points for WLTP application: IMEP improvement rate and CNI increase

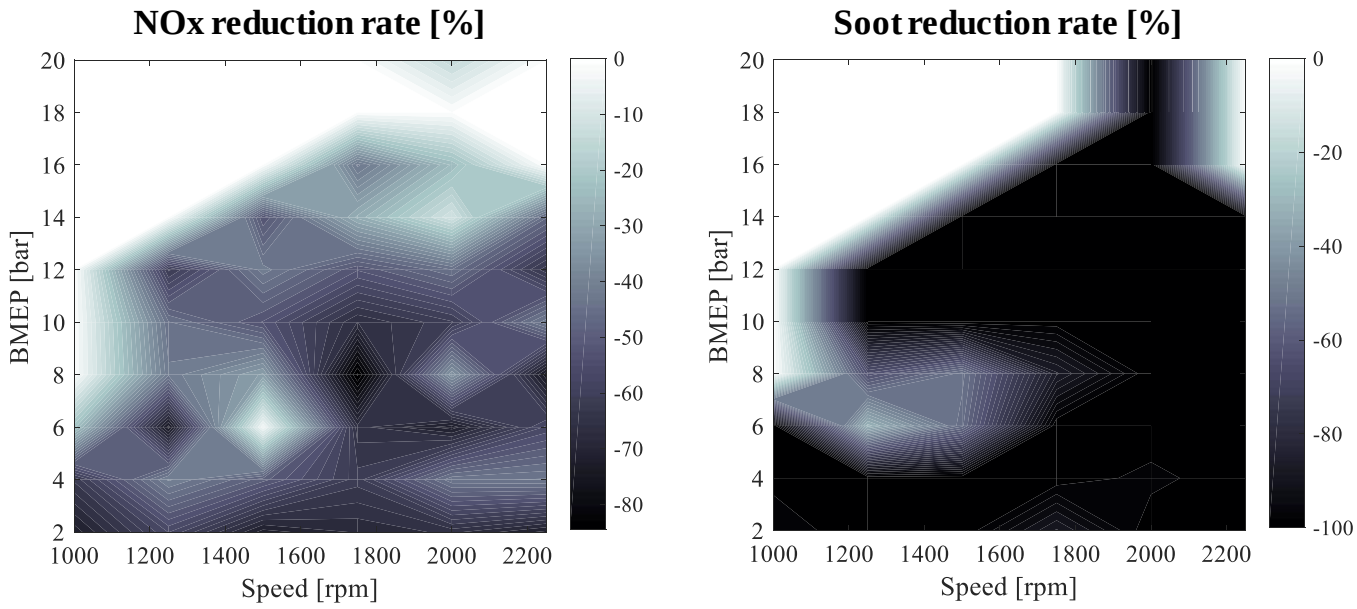

Figure 6.4.5 The combustion design results at steady state points for WLTP application: NOx and soot reduction rate

	IMEP [bar]	CNI [dB]	NOx [ppm]	Soot [FSN]
Experiment	9.476	180.4	116.6	1.606
Designed	10.466	180.0	18.1	0.231

P_{in} [bar]
1.01

Lambda [-]
1.02

EGR [%]
36.6

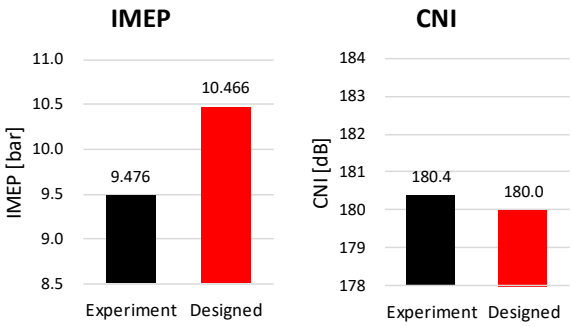

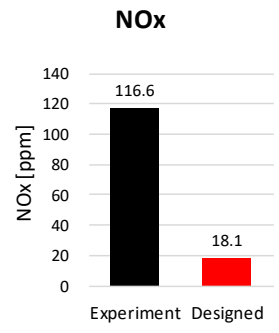

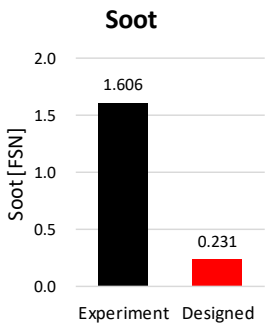

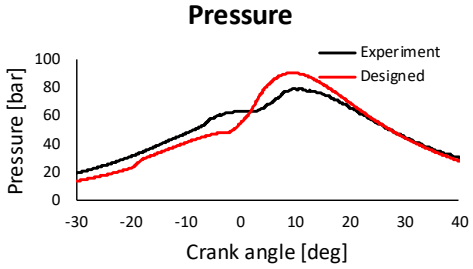

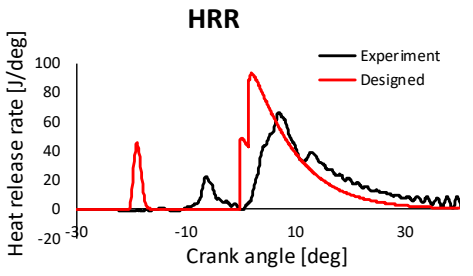

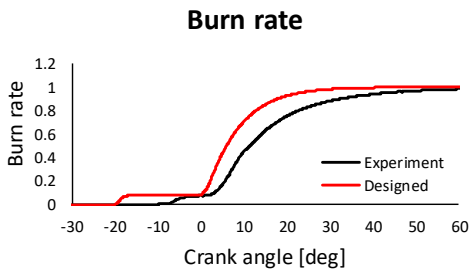

Figure 6.4.6 The combustion design result for WLTP application at 1750 rpm, BMEP 8 bar

	IMEP [bar]	CNI [dB]	NOx [ppm]	Soot [FSN]
Experiment	7.553	181.8	97.2	1.067
Designed	8.783	183.3	28.1	0.000

P_{in} [bar]
0.78

Lambda [-]
1.07

EGR [%]
36.5

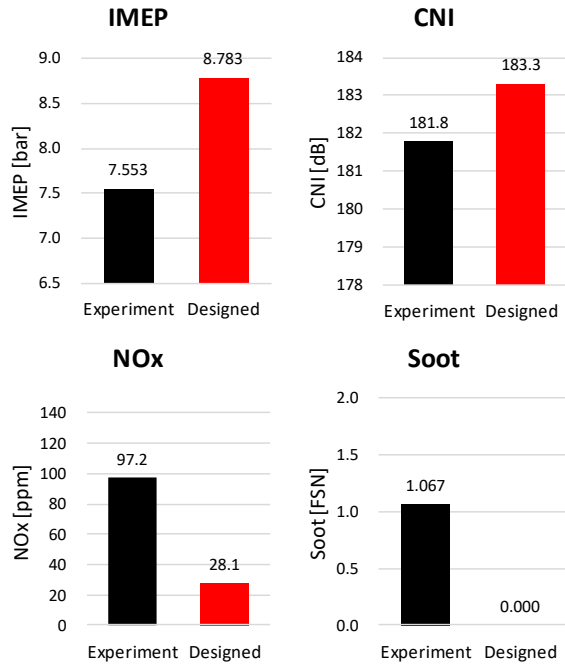

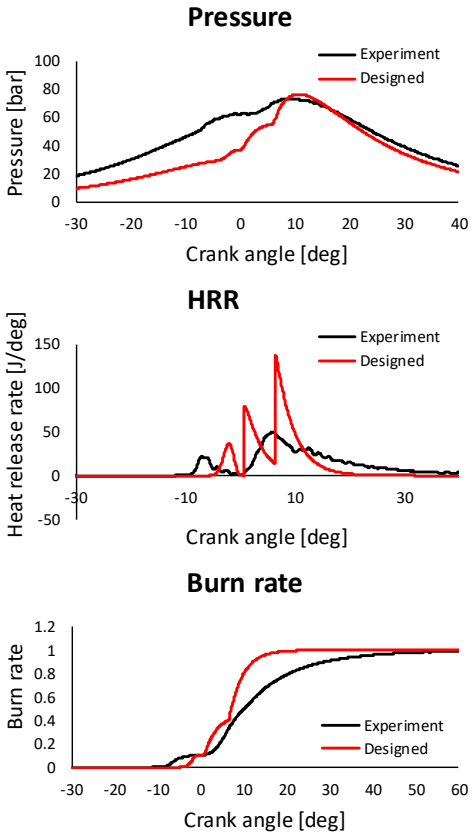

Figure 6.4.7 The combustion design result for WLTP application at 2000 rpm, BMEP 6 bar

	IMEP [bar]	CNI [dB]	NOx [ppm]	Soot [FSN]
Experiment	9.703	182.6	125.1	1.093
Designed	10.195	183.0	33.2	0.004

P_{in} [bar]
1.13

Lambda [-]
1.13

EGR [%]
40.1

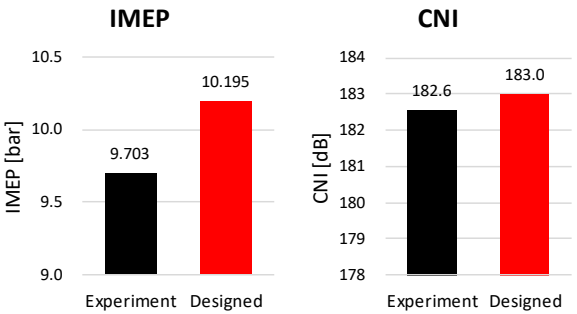

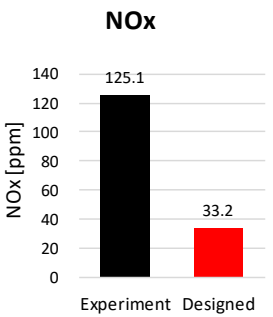

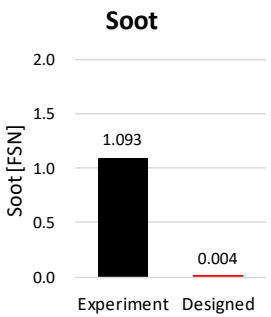

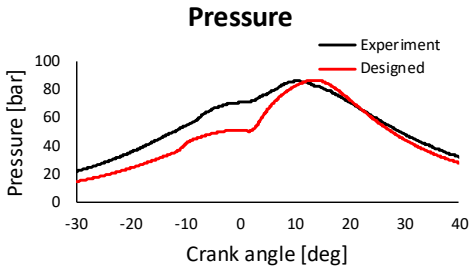

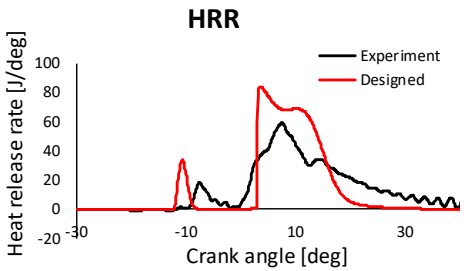

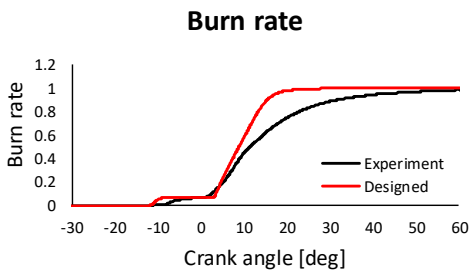

Figure 6.4.8 The combustion design result for WLTP application at 2250 rpm, BMEP 8 bar

6.4.2 Results of an application to WLTP

From the combustion design results at steady point in WLTP, the coefficients for Wiebe function, intake pressure and lambda were determined, and the parameters were modeled by speed and fuel injection quantity. Based on the experiment result of fuel injection quantity and speed at each cycle of WLTP, the parameters for combustion model were derived as an output of the parameter models. In this process, fuel injection quantity was derived that had the same IMEP with that of base condition. The fuel consumption, NOx and soot reduction rate were assessed by phase and entire cycle when the engine operated with designed combustion. The results for each performance and comparison with the experimental data are shown in Figure 6.4.9 to Figure 6.4.11.

The fuel mass consumption decreased by 4.7% compared to the base when calculated as average in total phase. Among the phases, the fuel mass decreased the most in phase 3 to 5.0%. In phase 3, there were the dominant area of BMEP 6 to 8 bar that had the high thermal efficiency improvement rate. The NOx emission from the combustion design showed 44.7% of reduction rate in entire test cycle. Compared to phase 1 and 2, which were dominated by low load region, the reduction rate of NOx decreased as it moved into the area with high load. In phase 4, the NOx reduction rate showed 36.5% because the NOx reduction effect was reduced at high load above BMEP 14 bar as a result of steady optimization. In terms of soot emission, the total reduction rate of soot was 60.7%. In the steady results, the reduction rate of soot emission exceeded 90% in most areas, but the WLTP application results were less than that. The designed combustion of steady points varied in shape unlike conventional diesel combustion. When applying the result of combustion design at steady state to WLTP, fuel injection quantity and speed were used to derive parameters that determined combustion. In this process,

the transition of the combustion phase between the steady points could lead undesired combustion shape. The soot estimation model used combustion characteristics such as combustion temperature and duration, and injection parameters at injection timing. The soot reduction effect could be decreased by the mismatch of above parameters due to transition of combustion phase. Nevertheless, soot emission showed prominent reduction.

Fuel mass [mg/str]	Phase1	Phase2	Phase3	Phase4	Total
Experiment	0.032	0.046	0.059	0.094	0.056
Designed	0.031	0.044	0.056	0.090	0.054
Improve rate [%]	-3.61	-4.46	-5.00	-4.95	-4.65

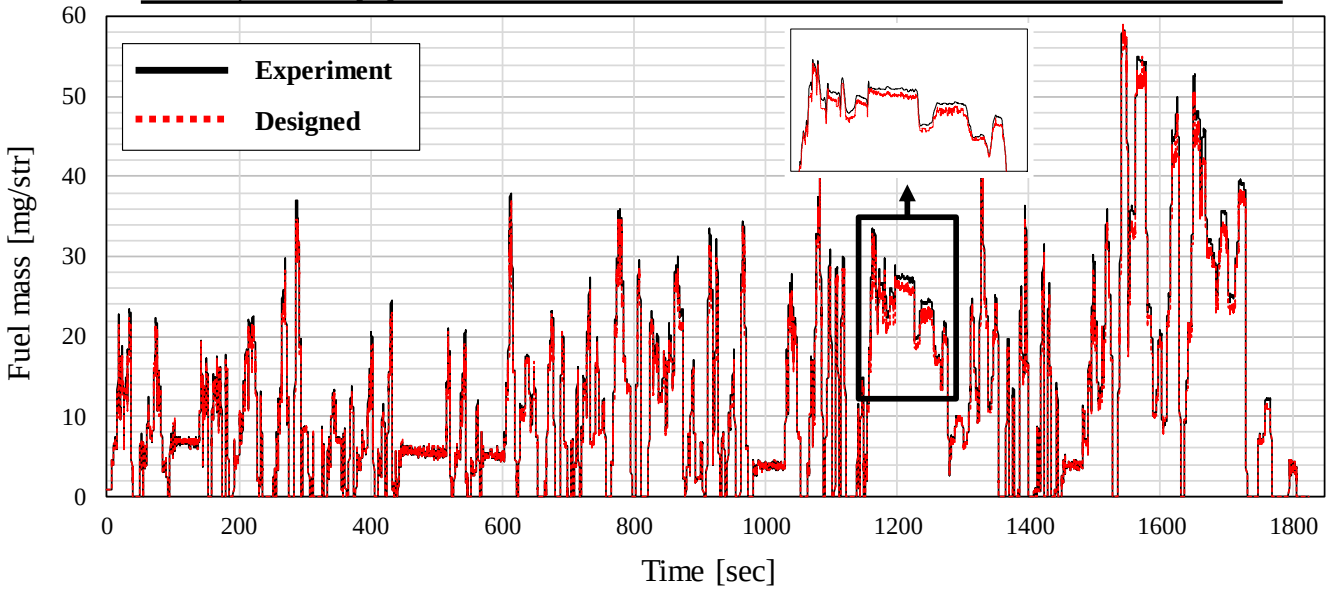

Figure 6.4.9 The fuel consumption result of combustion design application to WLTP

NOx [g]	Phase1	Phase2	Phase3	Phase4	Total
Experiment	1.041	1.181	1.869	2.963	7.054
Designed	0.541	0.559	0.915	1.882	3.898
Reduction rate [%]	-48.00	-52.63	-51.03	-36.49	-44.74

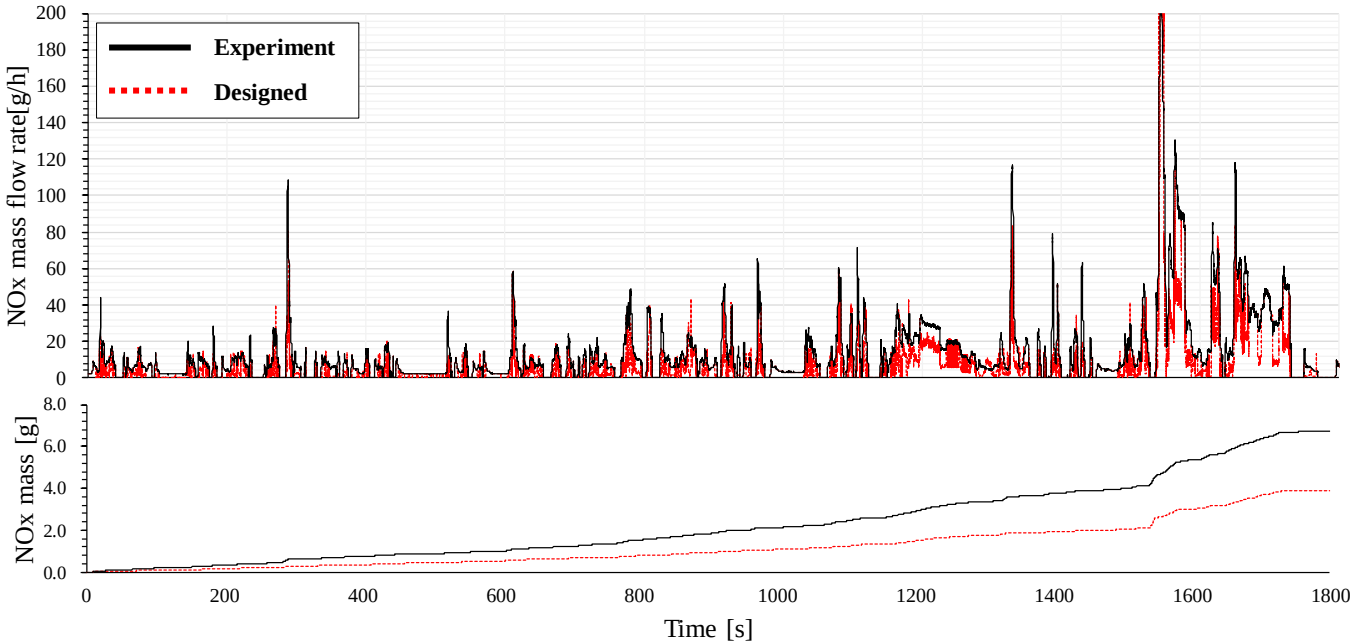

Figure 6.4.10 The NOx emission result of combustion design application to WLTP

Soot [g]	Phase1	Phase2	Phase3	Phase4	Total
Experiment	0.116	0.134	0.175	0.250	0.676
Designed	0.059	0.058	0.086	0.062	0.265
Reduction rate [%]	-48.91	-56.88	-50.76	-75.10	-60.73

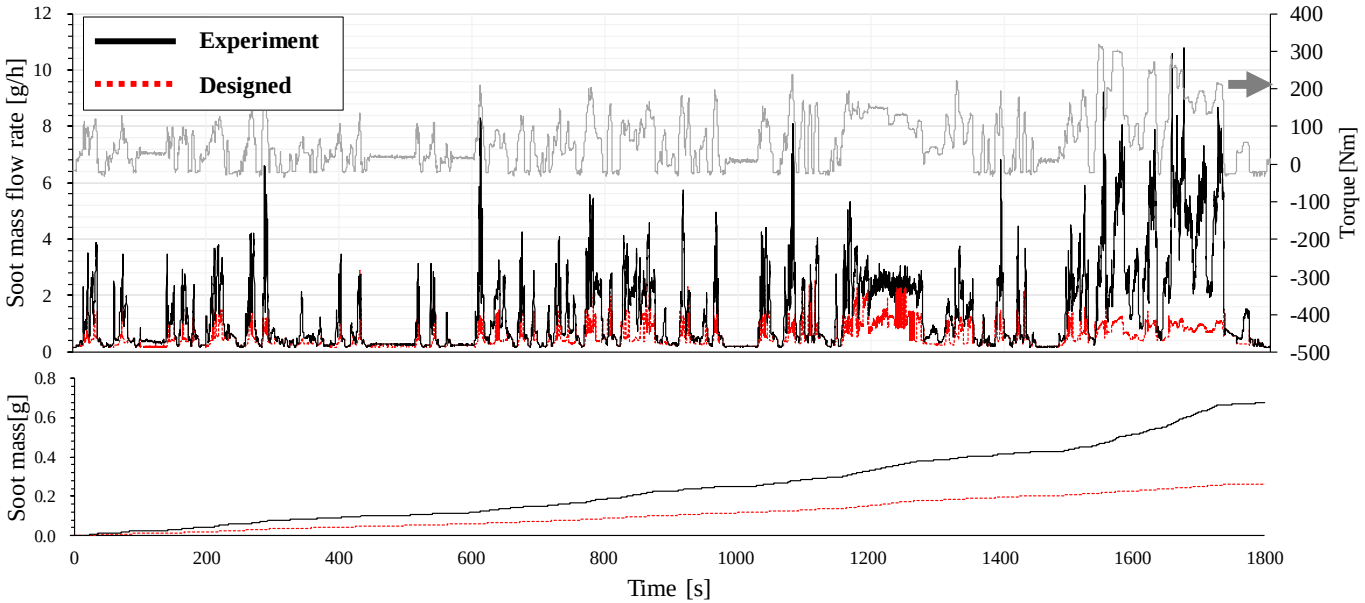

Figure 6.4.11 The soot emission result of combustion design application to WLTP

Chapter 7. Conclusions

In this study, the combustion design methodology was developed with 0-D models to derive the combustion that had desired performance of thermal efficiency, combustion noise, NOx and soot emissions. For the soot estimation, the semi-empirical 0-D soot model developed in this study was used. As part of the combustion design methodology, the simulation sequence for calculating thermodynamic properties and constructing combustion pressure was developed. Optimization methodology including the optimization algorithms, boundary conditions and constraints, and the objective function was provided for optimization sequence in the combustion design method.

The engine test was conducted in base condition, EGR swing, intake temperature and coolant temperature swing conditions. The soot emission results in different environmental conditions was used to develop the robust soot model construction. The two main factors of the soot deterioration with intake temperature increase were decrease in the ignition delay and lift-off length. The results of base condition experiment were used as initial conditions for optimization and criteria for target performance setting.

The simplified spray model was established to develop the 0-D soot models that was used in the combustion design method. The equivalence ratio at the lift-off length can be considered as representative index for the degree of air entrained in the fuel jet and mixing degree. The simplified spray model used lift-off length equation suggested by Siebers [87]. The scaling law for liquid length developed using the idealized spray model by Siebers [75]. In the process of derivation of the scaling law for liquid length, the mass flow ratio of the fuel and the ambient gas was calculated by Cantera that was a 0-D chemical simulation tool. The basic form of the laminar flame speed equation was developed by Kim [126]. When the laminar

flame speed was used in the lift-off length calculation, the laminar flame speed needed to be considered for the effect of diluents differently with the basis equation. The laminar flame speed increased with oxygen concentration and other gases (CO_2, N_2 and H_2O) decreased because of the chemical effect and thermal effect. By using the gas composition ratio, the heat capacity ratio of oxygen in the ambient gas was calculated to consider the diluents effect. The volume fraction of oxygen which showed good correlation with the heat capacity ratio was used in diluents effect term. The thermal diffusivity was calculated by using Cantera with the gas composition, temperature and pressure at the fuel injection timing. By using the above parameters, the lift-off length could be obtained. The equivalence ratio at the lift-off length from the simplified spray model was validated with the experimental data from engine combustion network and showed 0.9548 of R-squared value. Based on the scaling law of liquid length, the liquid fuel penetration length was calculated numerically. Also, the relationships for the fuel and air mixture distribution could be derived. By the substitution of the lift-off length into the relationships, the equivalence ratio at the lift-off length was obtained. The equivalence ratio used as the main factor in the 0-D soot formation model.

The 0-D soot model was developed by cooperative research with Youngbok Lee [124]. Developed soot model consisted of the soot formation model and soot oxidation model. The soot formation model was established with the fuel injection quantity as a factor representing the amount of precursor underlying the soot formation, the equivalence ratio at the lift-off length as a representative factor for the mixing degree, and the MFB 5 to 90 for the duration of soot formation. The soot oxidation model used the oxidation rate developed by Nagle and Strickland-Constable [89, 90] and heat flux compensation term to consider the heat transfer from the cylinder wall. The developed 0-D semi-empirical model was validated with the test engine cases including environmental condition and EGR swing cases. In the total cases, the model showed 0.901 of R-squared value.

Other performances, thermal efficiency, combustion noise and NOx emission in the combustion design method were evaluated by other 0-D models. IMEP was used as the indicator of thermal efficiency. The combustion noise index developed by Jung et al. [122] was used as the index for the combustion noise. The CNI showed better correlation with the measured noise than the maximum pressure rise rate. The index was calculated by the in-cylinder pressure interpreted as frequency domain via FFT and the sum of the 1 – 3.15 kHz range of the third octave band level. The 0-D NOx model developed by Lee et al. [67, 123] was used for the NOx estimation. The model based on the extended Zeldovich mechanism and the maximum NO formation rate as representing factor of the NO formation. The adiabatic temperature was calculated for the maximum temperature and the spatial concentration correction was applied in the model.

The concept of combustion design method suggested the new process for engine and combustion development. The combustion phase and parameters were derived as the output through the combustion design process from the desired performance, thermal efficiency, combustion noise, NOx and soot emissions, as the input. The parameters for constructing in-cylinder pressure were intake pressure, lambda and the mass faction burned. The MFB was determined by using Wiebe function and polynomial function as new approach to combustion phase. The total heat during the cycle was calculated by the difference between the gross heat release and a heat loss. A heat loss was modeled by speed and fuel injection quantity that were determined in the initial step of combustion design. From the MFB and total heat, the heat release rate was derived. The mass of in-cylinder air and EGR rate were calculated from intake pressure, temperature, lambda, that were determined as initial conditions, and the chemical reaction equation. The gas compositions during the combustion were calculated for calculation of polytropic index and other thermodynamic parameters. Polytropic index by the gas composition, intake temperature and pressure was calculated based on the

estimation method developed by Lee and Min [68]. The in-cylinder pressure in compression stroke was calculated by polytropic process with the estimated polytropic index. In the combustion duration, the combustion pressure was constructed by solving the differential equation of the heat release rate with the pressure. In expansion stroke, the in-cylinder pressure was also calculated by polytropic process. The timing of pilot and main injection used in the NOx and soot model were calculated reversely by using the ignition delay model developed by [139]. IMEP, CNI, NOx and soot emissions were calculated from the thermodynamic parameters and combustion pressure by using the 0-D models.

In the optimization process, the optimization algorithms used in the combustion design method were a minimum of constrained nonlinear multivariable function (interior-point) for Wiebe function and particle swarm optimization for polynomial function. The boundary conditions and constraints were determined for efficient iteration in optimization process. The base form of objective function for optimization allowed to find specific combustion of desired performance that was used as input. The objective functions for various design concepts were used in maximizing target performance. The limit function determined the performance limit.

The results of combustion design using Wiebe function for the MFB and base objective function were presented at low load (1500 rpm, BMEP 4 bar) and high load (2000 rpm, BMEP 8 bar). In each operation point, the desired performance was determined in terms of thermal efficiency improvement, emission reduction, and optimal sets. The performance of output combustion well followed the target performance except soot emission with different combustion shape. The combustion design using the modified objective function were performed in assumption of the specific design concepts. The results were considered to show the maximum combustion performance in the operating point with the trade-off

relationship between the performance index. The combustion design results using polynomial function as the MFB suggested the potential for performance improvements that were hard to achieve in conventional engine calibration or development process, with new combustion patterns different from existing combustion shape. The combustion design method was applied to WLTP by designing the steady points in WLTP operation region. The fuel consumption during WLTP improved by 4.7% compared to experimental result. The NOx and soot emissions showed 44.7% and 60.7% of reduction rates.

This research includes the combustion design methodology by using 0-D models for thermal efficiency, combustion noise, NOx and soot emissions. From the results, the 0-D combustion simulation and optimization method that derive the combustion of desired performance are provided. This study can present combustion shape with desired or optimized performance in combination with thermodynamic conditions, suggesting the development process different from existing research methods of engine and combustion strategies for target combustion.

Bibliography

1. Jonson JE, Borken-Kleefeld J, Simpson D, et al. Impact of excess NOx emissions from diesel cars on air quality, public health and eutrophication in Europe. *Environmental Research Letters* 2017; 12: 094017.

2. Anenberg SC, Miller J, Minjares R, et al. Impacts and mitigation of excess diesel-related NOx emissions in 11 major vehicle markets. *Nature* 2017; 545: 467-471.

3. Chossière GP, Malina R, Ashok A, et al. Public health impacts of excess NOx emissions from Volkswagen diesel passenger vehicles in Germany. *Environmental Research Letters* 2017; 12: 034014.

4. Seagrave J, McDonald JD, Gigliotti AP, et al. Mutagenicity and in vivo toxicity of combined particulate and semivolatile organic fractions of gasoline and diesel engine emissions. *Toxicological Sciences* 2002; 70: 212-226.

5. Kim K-H, Kabir E and Kabir S. A review on the human health impact of airborne particulate matter. *Environment international* 2015; 74: 136-143.

6. Weiss M, Bonnel P, Hummel R, et al. Analyzing on-road emissions of light-duty vehicles with Portable Emission Measurement Systems (PEMS)(EUR24697 EN). *Brussels, European Commission* 2011.

7. Weiss M, Bonnel P, Kühlwein J, et al. Will Euro 6 reduce the NOx emissions of new diesel cars?–Insights from on-road tests with Portable Emissions Measurement Systems (PEMS). *Atmospheric Environment* 2012; 62: 657-665.

8. Kwon S, Park Y, Park J, et al. Characteristics of on-road NOx emissions from Euro 6 light-duty diesel vehicles using a portable emissions measurement system. *Science of the Total Environment* 2017; 576: 70-77.

9. Triantafyllopoulos G, Katsaounis D, Karamitros D, et al. Experimental assessment of the potential to decrease diesel NOx emissions beyond minimum requirements for Euro 6 Real Drive Emissions (RDE) compliance. *Science of the Total Environment* 2018; 618: 1400-1407.

10. Ramos A, Muñoz J, Andrés F, et al. NOx emissions from diesel light duty vehicle tested under NEDC and real-word driving conditions. *Transportation Research Part D: Transport and Environment* 2018; 63: 37-48.

11. Clairotte M, Valverde V, Bonnel P, et al. Joint Research Centre, 2017 Light-Duty Vehicles Emissions Testing. *Publications Office of the European Union: Luxembourg* 2018.

12. Cha J, Lee J and Chon MS. Evaluation of real driving emissions for Euro 6 light-duty diesel vehicles equipped with LNT and SCR on domestic sales in Korea. *Atmospheric Environment* 2019; 196: 133-142.

13. Luján JM, Bermúdez V, Dolz V, et al. An assessment of the real-world driving gaseous emissions from a Euro 6 light-duty diesel vehicle using a portable emissions measurement system (PEMS). *Atmospheric Environment* 2018; 174: 112-121.

14. Automotive D. Worldwide Emissions Standards-Passenger Cars and Light Duty Vehicles. *Delphi Automotive LLP*; 5725: 48098-42815.

15. Maurer M, Holler P, Zarl S, et al. *Investigations of Lean NOx Trap (LNT) Regeneration Strategies for Diesel Engines*. Report no. 0148-7191, 2017. SAE Technical Paper.

16. DiGiulio CD, Pihl JA, Choi J-S, et al. NH3 formation over a lean NOX trap (LNT) system: Effects of lean/rich cycle timing and temperature. *Applied Catalysis B: Environmental* 2014; 147: 698-710.

17. Parks J, West B, Swartz M, et al. *Characterization of lean NOx trap catalysts with in-cylinder regeneration strategies*. Report no. 0148-7191, 2008. SAE Technical Paper.

18. West B, Huff S, Parks J, et al. Assessing reductant chemistry during in-cylinder regeneration of diesel lean NOx traps. *SAE transactions* 2004: 1975-1985.

19. Myung C-L, Jang W, Kwon S, et al. Evaluation of the real-time de-NOx performance characteristics of a LNT-equipped Euro-6 diesel passenger car with various vehicle emissions certification cycles. *Energy* 2017; 132: 356-369.

20. Ko J, Myung C-L and Park S. Impacts of ambient temperature, DPF regeneration, and traffic congestion on NOx emissions from a Euro 6-compliant diesel vehicle equipped with an LNT under real-world driving conditions. *Atmospheric environment* 2019; 200: 1-14.

21. Ko J, Jin D, Jang W, et al. Comparative investigation of NOx emission characteristics from a Euro 6-compliant diesel passenger car over the NEDC and WLTC at various ambient temperatures. *Applied energy* 2017; 187: 652-662.

22. Damma D, Ettireddy PR, Reddy BM, et al. A review of low temperature NH3-SCR for removal of NOx. *Catalysts* 2019; 9: 349.

23. Forzatti P. Present status and perspectives in de-NOx SCR catalysis. *Applied catalysis A: general* 2001; 222: 221-236.

24. Thirupathi B and Smirniotis PG. Nickel-doped Mn/TiO2 as an efficient catalyst for the low-temperature SCR of NO with NH3: Catalytic evaluation and characterizations. *Journal of Catalysis* 2012; 288: 74-83.

25. Chen L, Si Z, Wu X, et al. DRIFT study of CuO–CeO2–TiO2 mixed oxides for NO x reduction with NH3 at Low temperatures. *ACS applied materials & interfaces* 2014; 6: 8134-8145.

26. Chen M, Yang J, Liu Y, et al. TiO 2 interpenetrating networks decorated with SnO 2 nanocrystals: enhanced activity of selective catalytic reduction of NO with NH 3. *Journal of Materials Chemistry A* 2015; 3: 1405-1409.

27. Cavataio G, Girard J, Patterson JE, et al. *Laboratory testing of urea-SCR formulations to meet tier 2 bin 5 emissions*. Report no. 0148-7191, 2007. SAE Technical Paper.

28. Ura JA, Girard J, Cavataio G, et al. *Cold start performance and enhanced thermal durability of vanadium SCR catalysts*. Report no. 0148-7191, 2009. SAE Technical Paper.

29. Ettireddy PR, Kotrba A, Boningari T, et al. *Low temperature SCR catalysts optimized for cold-start and low-load engine exhaust conditions*. Report no. 0148-7191, 2015. SAE Technical Paper.

30. Mollenhauer K, Tschöke H and Johnson KG. *Handbook of diesel engines*. Springer Berlin, 2010.

31. Holzman DC. Vehicle motion alarms: necessity, noise pollution, or both? : National Institute of Environmental Health Sciences, 2011.

32. Stansfeld S, Haines M and Brown B. Noise and health in the urban environment. *Reviews on environmental health* 2000; 15: 43-82.

33. Stansfeld SA and Matheson MP. Noise pollution: non-auditory effects on health. *British medical bulletin* 2003; 68: 243-257.

34. Berglund B, Lindvall T, Schwela DH, et al. Guidelines for community noise. 1999.

35. Loss NIH. Dangerous decibels focuses on noise-induced hearing loss. See http://www. dangerousdecibels. org/education/information-center …, 2015.

36. Tousignant T, Wellmann T, Govindswamy K, et al. *Application of combustion sound level (CSL) analysis for powertrain*. Report no. 0148-7191, 2009. SAE Technical Paper.

37. Flotho A and Spessert B. Geräuschminderung an direkteinspritzenden Dieselmotoren. *Automobil-Industrie* 1988; 3: 88.

38. Ghojel J. Review of the development and applications of the Wiebe function: a tribute to the contribution of Ivan Wiebe to engine research. *International Journal of Engine Research* 2010; 11: 297-312.

39. Shen M, Tuner M, Johansson B, et al. *Effects of EGR and intake pressure on PPC of conventional diesel, gasoline and ethanol in a heavy duty diesel engine*. Report no. 0148-7191, 2013. SAE Technical Paper.

40. Lee J, Chu S, Cha J, et al. Effect of the diesel injection strategy on the combustion and emissions of propane/diesel dual fuel premixed charge compression ignition engines. *Energy* 2015; 93: 1041-1052.

41. Zheng Z, Yue L, Liu H, et al. Effect of two-stage injection on combustion and emissions under high EGR rate on a diesel engine by fueling blends of diesel/gasoline, diesel/n-butanol, diesel/gasoline/n-butanol and pure diesel. *Energy Conversion and Management* 2015; 90: 1-11.

42. Liu H, Wang Z, Li B, et al. Exploiting new combustion regime using multiple premixed compression ignition (MPCI) fueled with gasoline/diesel/PODE (GDP). *Fuel* 2016; 186: 639-647.

43. Chu S, Lee J, Kang J, et al. High load expansion with low emissions and the pressure rise rate by dual-fuel combustion. *Applied Thermal Engineering* 2018; 144: 437-443.

44. Beidl CV and Stücklschwaiger W. Application of the AVL-annoyance index for engine noise quality development. *Acta acustica united with acustica* 1997; 83: 789-795.

45. Payri F, Broatch A, Tormos B, et al. New methodology for in-cylinder pressure analysis in direct injection diesel engines—application to combustion noise. *Measurement Science and Technology* 2005; 16: 540.

46. Chiatti G, Chiavola O, Palmieri F, et al. Diagnostic methodology for internal combustion diesel engines via noise radiation. *Energy Conversion and Management* 2015; 89: 34-42.

47. Henein NA. Analysis of pollutant formation and control and fuel economy in diesel engines. *Energy and Combustion Science* 1979: 283-325.

48. Miller JA and Bowman CT. Mechanism and modeling of nitrogen chemistry in combustion. *Progress in energy and combustion science* 1989; 15: 287-338.

49. Heywood JB. *Internal combustion engine fundamentals*. McGraw-Hill Education, 2018.

50. Lavoie GA, Heywood JB and Keck JC. Experimental and theoretical study of nitric oxide formation in internal combustion engines. *Combustion science and technology* 1970; 1: 313-326.

51. Bowman CT. Kinetics of pollutant formation and destruction in combustion. *Progress in energy and combustion science* 1975; 1: 33-45.

52. Hiroyasu H, Kadota T and Arai M. Development and use of a spray combustion modeling to predict diesel engine efficiency and pollutant emissions: Part 1 combustion modeling. *Bulletin of JSME* 1983; 26: 569-575.

53. Zeldovich I, Barenblatt GI, Librovich V, et al. Mathematical theory of combustion and explosions. 1985.

54. Kyriakides S, Dent J and Mehta P. Phenomenological diesel combustion model including smoke and NO emission. *SAE transactions* 1986: 477-502.

55. Bazari Z. A DI diesel combustion and emission predictive capability for use in cycle simulation. *SAE transactions* 1992: 747-770.

56. Andersson M, Johansson B, Hultqvist A, et al. A predictive real time NOx model for conventional and partially premixed diesel combustion. *SAE Transactions* 2006: 863-872.

57. Ericson C, Westerberg B, Andersson M, et al. *Modelling diesel engine combustion and NOx formation for model based control and simulation of engine and exhaust aftertreatment systems*. Report no. 0148-7191, 2006. SAE Technical Paper.

58. Arrègle J, López JJ, Guardiola C, et al. *Sensitivity study of a NOx estimation model for on-board applications*. Report no. 0148-7191, 2008. SAE Technical Paper.

59. Scappin F, Stefansson SH, Haglind F, et al. Validation of a zero-dimensional model for prediction of NOx and engine performance for electronically controlled marine two-stroke diesel engines. *Applied Thermal Engineering* 2012; 37: 344-352.

60. Asprion J, Chinellato O and Guzzella L. A fast and accurate physics-based model for the NOx emissions of Diesel engines. *Applied energy* 2013; 103: 221-233.

61. Quérel C, Grondin O and Letellier C. *A semi-physical NOx model for diesel engine control*. Report no. 0148-7191, 2013. SAE Technical Paper.

62. Quérel C, Grondin O and Letellier C. Semi-physical mean-value NOx model for diesel engine control. *Control Engineering Practice* 2015; 40: 27-44.

63. Guardiola C, Martín J, Pla B, et al. Cycle by cycle NOx model for diesel engine control. *Applied Thermal Engineering* 2017; 110: 1011-1020.

64. d'Ambrosio S, Finesso R, Fu L, et al. A control-oriented real-time semi-empirical model for the prediction of NOx emissions in diesel engines. *Applied Energy* 2014; 130: 265-279.

65. Finesso R and Spessa E. A real time zero-dimensional diagnostic model for the calculation of in-cylinder temperatures, HRR and nitrogen oxides in diesel engines. *Energy conversion and management* 2014; 79: 498-510.

66. Lee S, Lee Y, Han K, et al. *Virtual NOx sensor for transient operation in light-duty diesel engine*. Report no. 0148-7191, 2016. SAE Technical Paper.

67. Lee S, Lee Y, Kim G, et al. Development of a real-time virtual nitric oxide sensor for light-duty diesel engines. *Energies* 2017; 10: 284.

68. Lee Y and Min K. Estimation of the polytropic index for in-cylinder pressure prediction in engines. *Applied Thermal Engineering* 2019; 158: 113703.

69. Tao F, Golovitchev VI and Chomiak J. A phenomenological model for the prediction of soot formation in diesel spray combustion. *Combustion and Flame* 2004; 136: 270-282.

70. Argachoy C and Pimenta A. Phenomenological model of particulate matter emission from direct injection diesel engines. *Journal of the Brazilian Society of Mechanical Sciences and Engineering* 2005; 27: 266-273.

71. Kong S-C, Sun Y and Rietz RD. Modeling diesel spray flame liftoff, sooting tendency, and NO x emissions using detailed chemistry with phenomenological soot model. 2007.

72. Tao F, Reitz RD, Foster DE, et al. Nine-step phenomenological diesel soot model validated over a wide range of engine conditions. *International Journal of Thermal Sciences* 2009; 48: 1223-1234.

73. Naber JD and Siebers DL. Effects of gas density and vaporization on penetration and dispersion of diesel sprays. *SAE transactions* 1996: 82-111.

74. Dec JE. A conceptual model of DL diesel combustion based on laser-sheet imaging. *SAE transactions* 1997: 1319-1348.

75. Siebers DL. Scaling liquid-phase fuel penetration in diesel sprays based on mixing-limited vaporization. *SAE transactions* 1999: 703-728.

76. Higgins B and Siebers D. Measurement of the flame lift-off location on DI diesel sprays using OH chemiluminescence. *SAE Transactions* 2001: 739-753.

77. Siebers D, Higgins B and Pickett L. Flame lift-off on direct-injection diesel fuel jets: oxygen concentration effects. *Sae Transactions* 2002: 1490-1509.

78. Pickett LM, Siebers DL and Idicheria CA. Relationship between ignition processes and the lift-off length of diesel fuel jets. *SAE transactions* 2005: 1714-1731.

79. Musculus MP and Kattke K. Entrainment waves in diesel jets. *SAE International Journal of Engines* 2009; 2: 1170-1193.

80. Wakuri Y, Fujii M, Amitani T, et al. Studies on the penetration of fuel spray in a diesel engine. *Bulletin of JSME* 1960; 3: 123-130.

81. Siebers DL. Liquid-phase fuel penetration in diesel sprays. *SAE transactions* 1998: 1205-1227.

82. Kalaghatigi G. Lift-off heights and visible lengths of vertical turbulent jet diffusion flames in still air. *Combustion Science and Technology* 1984; 41: 17.

83. Peters N. Turbulent combustion. IOP Publishing, 2001.

84. Siebers D and Higgins B. Flame lift-off on direct-injection diesel sprays under quiescent conditions. *SAE Transactions* 2001: 400-421.

85. Pickett LM and Siebers DL. Soot in diesel fuel jets: effects of ambient temperature, ambient density, and injection pressure. *Combustion and Flame* 2004; 138: 114-135.

86. Pickett LM and Siebers DL. Soot formation in diesel fuel jets near the lift-off length. *International Journal of Engine Research* 2006; 7: 103-130.

87. Siebers DD. Unpublished Notes. *Sandia National Laboratory* 2002.

88. Hiroyasu H and Kadota T. Models for combustion and formation of nitric oxide and soot in direct injection diesel engines. *SAE transactions* 1976: 513-526.

89. Nagle J. Oxidation of carbon between 1000-2000°C. In: *Proceedings of Fifth Carbon Conference, London, England, 1962* 1962.

90. Walls J and Strickland-Constable R. Oxidation of carbon between 1000–2400 C. *Carbon* 1964; 1: 333-338.

91. Vishwanathan G and Reitz RD. Development of a practical soot modeling approach and its application to low-temperature diesel combustion. *Combustion Science and Technology* 2010; 182: 1050-1082.

92. Ibrahim F, Mahmood WMFW, Abdullah S, et al. *Comparison of Simple and Detailed Soot Models in the Study of Soot Formation in a Compression Ignition Diesel Engine*. Report no. 0148-7191, 2017. SAE Technical Paper.

93. Dempsey A, Seiler P, Svensson K, et al. Evaluation of the two-step Hiroyasu soot model over a broad range of diesel combustion systems. *SAE technical paper* 2018: 01-0242.

94. Çebi EC, Rottenkolber G and Uyar E. *In-cylinder pressure based real-time estimation of engine-out particulate matter emissions of a diesel engine*. Report no. 0148-7191, 2011. SAE Technical Paper.

95. Steuer J, Mladek M, Dengler C, et al. Flexible engine control system for the development of innovative combustion processes. *ATZelektronik worldwide* 2009; 4: 22-26.

96. Finesso R, Misul D and Spessa E. Development and validation of a semi-empirical model for the estimation of particulate matter in diesel engines. *Energy conversion and management* 2014; 84: 374-389.

97. Hanson R, Curran S, Wagner R, et al. Piston bowl optimization for RCCI combustion in a light-duty multi-cylinder engine. *SAE International Journal of Engines* 2012; 5: 286-299.

98. Wang B, Li T, Ge L, et al. Optimization of combustion chamber geometry for natural gas engines with diesel micro-pilot-induced ignition. *Energy conversion and management* 2016; 122: 552-563.

99. Li B, Liu H, Yu L, et al. Optimization of piston bowl and valve system in compression ignition engine fueled with gasoline/diesel/polyoxymethylene dimethyl ethers for high efficiency. *International Journal of Engine Research* 2021; 22: 468-478.

100. Brooks T, Lumsden G and Blaxill H. *Improving base engine calibrations for diesel vehicles through the use of DoE and optimization techniques*. Report no. 0148-7191, 2005. SAE Technical Paper.

101. Castagné M, Bentolila Y, Chaudoye F, et al. Comparison of engine calibration methods based on design of experiments (DoE). *Oil & Gas Science and Technology-Revue de l'IFP* 2008; 63: 563-582.

102. Beatrice C, Napolitano P and Guido C. Injection parameter optimization by DoE of a light-duty diesel engine fed by Bio-ethanol/RME/diesel blend. *Applied energy* 2014; 113: 373-384.

103. Millo F, Arya P and Mallamo F. Optimization of automotive diesel engine calibration using genetic algorithm techniques. *Energy* 2018; 158: 807-819.

104. Liu J, Ma B and Zhao H. Combustion parameters optimization of a diesel/natural gas dual fuel engine using genetic algorithm. *Fuel* 2020; 260: 116365.

105. Ge H-W, Shi Y, Reitz RD, et al. Optimization of a HSDI diesel engine for passenger cars using a multi-objective genetic algorithm and multi-dimensional modeling. *SAE International Journal of Engines* 2009; 2: 691-713.

106. Ge H-W, Shi Y, Reitz RD, et al. *Heavy-duty diesel combustion optimization using multi-objective genetic algorithm and multi-dimensional modeling*. Report no. 0148-7191, 2009. SAE Technical Paper.

107. Smallbone A, Bhave A, Hillman M, et al. *Virtual performance and emissions mapping for diesel engine design optimization*. Report no. 0148-7191, 2013. SAE Technical Paper.

108. Xu G, Jia M, Li Y, et al. Multi-objective optimization of the combustion of a heavy-duty diesel engine with low temperature combustion under a wide load range:(I) Computational method and optimization results. *Energy* 2017; 126: 707-719.

109. Senecal P, Montgomery D and Reitz R. A methodology for engine design using multi-dimensional modelling and genetic algorithms with validation through experiments. *International Journal of Engine Research* 2000; 1: 229-248.

110. Senecal PK, Pomraning E and Richards K. *Multi-mode genetic algorithm optimization of combustion chamber geometry for low emissions*. Report no. 0148-7191, 2002. SAE Technical Paper.

111. Liu Y and Reitz RD. *Optimizing HSDI diesel combustion and emissions using multiple injection strategies*. Report no. 0148-7191, 2005. SAE Technical paper.

112. Sun Y and Reitz RD. *Modeling diesel engine NOx and soot reduction with optimized two-stage combustion*. Report no. 0148-7191, 2006. SAE Technical Paper.

113. Shi Y and Reitz RD. Optimization study of the effects of bowl geometry, spray targeting, and swirl ratio for a heavy-duty diesel engine operated at low and high load. *International Journal of Engine Research* 2008; 9: 325-346.

114. Kamaltdinov V, Markov V and Lysov I. Determining Parameters of Double-Wiebe Function for Simulation of Combustion Process in Overload Diesel Engine with Common Rail Fuel Feed System. In: *IOP Conference Series: Materials Science and Engineering* 2018, p.022053. IOP Publishing.

115. Liu J and Dumitrescu CE. Single and double Wiebe function combustion model for a heavy-duty diesel engine retrofitted to natural-gas spark-ignition. *Applied energy* 2019; 248: 95-103.

116. Shibata G, Ogawa H, Amanuma Y, et al. Optimization of multiple heat releases in pre-mixed diesel engine combustion for high thermal efficiency and low combustion noise by a genetic-based algorithm method. *International journal of engine research* 2019; 20: 540-554.

117. Liu J and Dumitrescu CE. Improved thermodynamic model for lean natural gas spark ignition in a diesel engine using a triple Wiebe function. *Journal of Energy Resources Technology* 2020; 142.

118. Loganathan S, Manohar RM, Thamaraikannan R, et al. *Direct injection diesel engine rate of heat release prediction using universal load correction factor in double Wiebe function for performance simulation*. Report no. 0148-7191, 2012. SAE Technical Paper.

119. Liu L, Horibe N and Ishiyama T. Combustion modelling for a diesel engine with multi-stage injection using a stochastic combustion model. *Proceedings of the Institution of Mechanical Engineers, Part D: Journal of Automobile Engineering* 2014; 228: 518-534.

120. Shibata G, Ishi K, Ushijima H, et al. *Optimization of heat release shape and the connecting rod crank radius ratio for low engine noise and high thermal efficiency of premixed diesel engine combustion*. Report no. 0148-7191, 2015. SAE Technical Paper.

121. Franken T and Mauss F. *Development of methodology for predictive diesel combustion simulation using 0D stochastic reactor model*. Report no. 0148-7191, 2016. SAE Technical Paper.

122. Jung I, Jin J, So H, et al. An advanced method for developing combustion noise through the analysis of diesel combustion. *SAE International Journal of Engines* 2013; 6: 1379-1385.

123. Lee S. *Modeling of a real-time virtual pressure and NOx sensnor for light-duty diesel engines*. Seoul National University, 2017.

124. Lee Y. *Development of Virtual NOx and Soot Models for Diesel Engines*. Seoul National University, 2021.

125. Lakshminarayanan P and Aswin S. *Estimation of particulate matter from smoke, oil consumption and fuel sulphur*. Report no. 0148-7191, 2017. SAE Technical Paper.

126. Kim J. *Development of combustion and soot emission models for direct-injection spark-ignition engines*. Seoul National University, Seoul, 2017.

127. Metghalchi M and Keck JC. Burning velocities of mixtures of air with methanol, isooctane, and indolene at high pressure and temperature. *Combustion and flame* 1982; 48: 191-210.

128. Galmiche B, Halter F, Foucher F, et al. Effects of dilution on laminar burning velocity of premixed methane/air flames. *Energy & Fuels* 2011; 25: 948-954.

129. Zhou J, Cordier M, Mounaïm-Rousselle C, et al. Experimental estimate of the laminar burning velocity of iso-octane in oxygen-enriched and CO2-diluted air. *Combustion and Flame* 2011; 158: 2375-2383.

130. Chen Z, Tang C, Fu J, et al. Experimental and numerical investigation on diluted DME flames: Thermal and chemical kinetic effects on laminar flame speeds. *Fuel* 2012; 102: 567-573.

131. Rhodes DB and Keck JC. Laminar burning speed measurements of indolene-air-diluent mixtures at high pressures and temperatures. *SAE Transactions* 1985: 23-35.

132. Zhao F, Yu W, Pei Y, et al. Influence factor of diesel soot formation in diesel engine combustion predicted by multistep soot model with highlight in soot surface activity. *Chinese science bulletin* 2014; 59: 1176-1186.

133. Angelberger C, Poinsot T and Delhay B. *Improving near-wall combustion and wall heat transfer modeling in SI engine computations*. Report no. 0148-7191, 1997. SAE Technical Paper.

134. Jung I, Jin J, Lee D, et al. *Closed-loop control method for monitoring and improving the diesel combustion noise*. Report no. 0148-7191, 2016. SAE Technical Paper.

135. Park W, Lee J, Min K, et al. Prediction of real-time NO based on the in-cylinder pressure in Diesel engines. *Proceedings of the Combustion Institute* 2013; 34: 3075-3082.

136. Desantes J, Galindo J, Guardiola C, et al. Air mass flow estimation in turbocharged diesel engines from in-cylinder pressure measurement. *Experimental Thermal and Fluid Science* 2010; 34: 37-47.

137. Arsie I, Di Leo R, Pianese C, et al. Estimation of in-cylinder mass and AFR by cylinder pressure measurement in automotive Diesel engines. *IFAC Proceedings Volumes* 2014; 47: 11836-11841.

138. Kim G. *Numerical analysis on the characteristics of NOx and PM emissions using multiple injection strategies in diesel engines*. Seoul National University, 2018.

139. Lee Y, Lee S and Min K. *Ignition Delay Model of Multiple Injections in CI Engines*. Report no. 0148-7191, 2019. SAE Technical Paper.

140. Kennedy J and Eberhart R. Particle swarm optimization. In: *Proceedings of ICNN'95-international conference on neural networks* 1995, pp.1942-1948. IEEE.

국 문 초 록

최근 내연기관 성능향상을 위한 연구는 연비, 배출량, 소음, 진동 등의 측면에 초점이 맞춰지고 있다. 연비는 지구온난화에 영향을 준 이산화탄소 배출 감소와 관련이 있다. 또한, 디젤 연소로 인한 질소산화물과 그을음 배출은 인간의 건강에 해로우며 생명까지도 위협한다. 배기 가스의 유해성은 많은 나라들의 정부들로 하여금 차량 배출 규제를 엄격하게 만들도록 동기를 부여하고 있다. 최근에는 실험실의 인증치와 도로의 실제 배출량 수준 간의 차이를 고려해 Real-driving emissions 규제가 시행됐다. 소음 공해는 또한 인간과 공중 보건 문제의 관점에서 중요한 주제이다. 엔진에서 발생하는 연소 소음은 엔진 변수 및 연소 특성에 의해 영향을 받는 실린더 압력 배출에 따라 달라진다. 적절한 분사 전략 또는 연소 형태는 원하는 연소 소음 수준을 만족하도록 최적화할 수 있다.

엔진 개발 과정 중에 연비, 배기 배출물 및 소음의 각 성능을 최적화하기 위한 많은 노력과 시간이 소모된다. 최적의 성능을 얻으려면 연소 및 엔진 작동 변수를 최적화하기 위해 많은 실험이 필요하다. 실험 없이 엔진 성능을 최적화하기 위해 전산유체역학 시뮬레이션을 수행하려면 높은 계산 비용이 필요하다. 따라서, 계산 비용이 낮은 0-D 연소 최적화 방법론을 개발하는 것이 중요하다. 이전 연구들에 의한 0-D 연소 최적화 방법은 분사 전략 또는 엔진 변수를 최적화했다. 결과로 도출되는 연소는 기존 연소 형상의 범위 내에 있으며 연소 형상의 다양성 측면에서 실험적으로 변수를 최적화하는 방법과 다를 바

없다. 본 연구에서는 원하는 성능을 입력으로, 최적 연소 및 연소 변수를 출력으로 도출되는 연소 디자인 방법론을 개발하였다.

첫 번째 단계로 엔진 실험을 수행하여 베이스 조건, EGR 스윙, 흡기 온도 및 냉각수 온도 스윙 조건에서의 연비 및 배기 배출의 기본 성능을 평가하였다. 이 결과는 연소 디자인에 활용되는 0-D soot 모델 수립과 최적화 과정에서 초기 조건으로 사용되었다. Soot 생성 모델은 lift-off length에서 당량비를 계산하는 단순화된 스프레이 모델을 기반으로 했다. Lift-off length에서의 당량비는 그을음 형성 모델의 주요 요인 중 하나로 사용되었다. 연소 디자인 과정에서 IMEP는 연비를 대변하는 인자로 사용되었다. 연소 소음 평가에는 연소 소음 지수가 사용되었다. NOx 배출량 예측에는 이전 연구로부터 개발된 0-D NOx 모델이 적용되었다.

연소 디자인 방법론에서, 실린더 내 압력 계산에 필요한 변수는 흡기 압력, 람다 및 질량 연소율이었다. 질량 연소율은 기존에 널리 사용되는 위베 함수와 연소상에 대한 새로운 접근법으로 다항식 함수를 사용하여 결정되었다. 실린더 내 공기의 질량과 EGR율은 초기 조건으로 결정된 흡기 압력, 온도, 람다 및 화학 반응 방정식으로 계산되었다. 연소 중의 기체 조성비는 polytropic 지수 및 여러 열역학적 변수의 계산을 위해 계산되었다. 실린더 내 압력은 polytropic 과정과 열 발생률으로 계산되었다. 최적화 과정에서 연소 디자인 방법에 사용된 최적화 알고리즘은 제한된 비선형 다변량 함수(Interior-point 기법)와 입자 군집 최적화의 최소값이었다. 경계 조건과 제약 조건은 최적화 과정의 효율적인 iteration을 위해 결정되었다. 최적화를 위한 목적 함수의 기

본 형태는 입력으로 사용된 원하는 성능을 가지는 특정한 연소를 찾을 수 있게 했다. 목표 성능을 최대화하는 다양한 디자인 목적에 따라 목표 함수는 변형되어 사용되었다.

연소 디자인의 결과는 다양한 운전 영역에서 MFB와 목적 함수에 따라 연구되었다. WLTP 운전 영역에서 정상 상태 연소들을 디자인하여 연소 디자인 방법론을 WLTP에 적용하였다. 적용 결과, WLTP 중 연료 소모량은 4.7% 감소되었다. NOx와 soot 배출은 각각 44.7%와 60.7%의 감소율을 보였다. 본 연구에서는 원하는 성능의 연소를 도출하는 0-D 연소 시뮬레이션 및 최적화 방법을 제공하였다. 이 연구는 원하는 성능 혹은 최적화된 성능을 가지는 연소상을 열역학적인 조건들과 함께 제시할 수 있어 이를 바탕으로 기존의 연구 방법과 다른 목표 연소를 구현하기 위한 엔진과 연소 전략 개발 방향을 제시할 수 있다.

주요어: 연소 디자인 방법론, 엔진 연소 최적화, 0-D 연소 시뮬레이션, 0-D soot 모델, 스프레이 모델, 디젤 엔진

학 번: 2015-20744